

Vitaliy Pipich

Ordering Transition and Critical Phenomena
in a three Component Polymer Mixture of
A/B Homopolymers and
a A-B Diblockcopolymer

2003

Physikalische Chemie

**Ordering Transition and Critical Phenomena
in a three Component Polymer Mixture of
A/B Homopolymers and
a A-B Diblockcopolymer**

Inaugural-Dissertation
zur Erlangung des Doktorgrades der Naturwissenschaften
im Fachbereich Chemie und Pharmazie
der Mathematisch-Naturwissenschaftlichen Fakultät
der Westfälischen Wilhelms-Universität Münster

vorgelegt von
Vitaliy Pipich
aus Chmelnytskyi, Ukraine

- 2003 -

Dekan:	Prof. Dr. Jens Leker
Erster Gutachter:	Prof. Dr. Dieter Richter
Zweiter Gutachter:	Prof. Dr. Andreas Heuer
Tag der mündlichen Prüfungen:	26.03, 30.03, 06.04.2004
Tag der Promotion:	30.04.2004

Contents

1	Introduction	1
2	Theory	5
2.1	Ginzburg-Landau-Wilson Hamiltonian	5
2.2	Mean Field Phase Diagram of A/B/A-B Blends	10
2.3	Polymer Blends: A/B	13
2.3.1	Thermodynamics of Polymer Blends: Critical Behavior – Flory-Huggins Theory	13
2.3.2	Effect of Thermal Fluctuations: A/B blends	15
2.3.3	Belyakov-Kiselev Crossover Model	16
2.4	Diblock Copolymer Melts	17
2.4.1	Thermodynamics of Block Copolymers	17
2.4.2	RPA: A-B melts	17
2.4.3	Effect of Thermal Fluctuations: A-B melts	18
2.5	A/B/A-B	19
2.5.1	RPA of the Ternary A/B/A-B System	19
2.5.2	Effect of Thermal Fluctuations:A/B/A-B	21
2.5.3	Scaling Behavior	24
2.6	Polymeric Microemulsion	26
3	Experimental	29
3.1	Sample	29

3.1.1	Polymer Synthesis and Characterization	29
3.1.2	Sample Preparation	31
3.1.3	Thermostat	32
3.2	Small Angle Neutron Scattering	34
3.2.1	Basics of Small Angle Neutron Scattering	34
3.2.2	Raw Data Reduction	36
3.2.3	Dead Time Effect	37
3.2.4	Resolution Function	38
4	Experimental results	41
4.1	Phase Diagram	41
4.1.1	Lifshitz Line	41
4.1.2	Disorder Line	46
4.1.3	Microemulsion Phases	47
4.1.4	Temperature Induced Disorder–Microemulsion Transition .	49
4.1.5	Lamellar - Bicontinuous Microemulsion Transition	52
4.1.6	Order-Disorder Transition of the Diblock Copolymer melt	53
4.1.7	Ordering Transition in A/B/A-B Blend	53
4.1.8	Phase Diagram in Different Contrasts	55
4.2	Critical Exponents and Crossover	59
4.2.1	Ising Critical Behavior	59
4.2.2	Lifshitz Critical Behavior	64
4.2.3	Reentrance Behavior and Double Critical Point	66
4.3	Role of the Diblock Copolymer	68
5	Interpretation of the Data	73
5.1	$S(Q)$ and $S(Q^*)$ below the LL ($\Phi < \Phi_{LL}$)	73
5.2	$S(Q)$ and $S(Q^*)$ beyond the LL ($\Phi > \Phi_{LL}$)	76
5.3	$S(Q)$ and $S(0)$ near the LL	79

<i>CONTENTS</i>	iii
6 Discussion	83
6.1 Critical Exponents: Critical Path	83
6.2 Disordered and Microemulsion Lifshitz Line. Bicontinuous and Droplet Microemulsion	86
6.3 G_i and Microemulsion channel	87
6.4 Flory-Huggins Parameter	88
7 Conclusions	91
List of Figures	96
List of Tables	100
Bibliography	102
Acknowledgments	109
CV(Lebenslauf)	111

Chapter 1

Introduction

Phase separation and critical anomalies of thermal composition fluctuations in binary polymer blends are well-known universal phenomena which have been intensively explored both from a theoretical and experimental point of view [1]. Usually, the critical behavior of thermal fluctuations is discussed in terms of universality classes and the crossover between them. Each universality class is characterized by a set of unique critical exponents describing thermodynamic parameters as the correlation length and susceptibility by scaling laws. At temperatures far from the critical point thermal fluctuations become very weak that they can be handled theoretically as individual fluctuation modes within the so-called Gaussian approximation. The critical exponents are in most cases identical to those of the mean field case so that one usually identifies this regime as fulfilling the mean field approximation.

Approaching the critical point fluctuations become stronger and non-linear effects become apparent indicating a crossover to a different fluctuation dominated universality class. In the case of binary polymer blends one gets the crossover to the universality class of the 3D-Ising model [2,3]. Such a crossover is estimated by a Ginzburg criterion [3, 4] delivering a Ginzburg number G_i , representing a reduced temperature which for binary polymer blends is proportional to N^{-1} , N being degree of polymerization. The Ginzburg number determines the temperature interval of strong thermal fluctuations around the critical point. Such a universal Ginzburg criterion is only valid for incompressible polymer blends [1,5]. The crossover behavior of the susceptibility and correlation length from mean field to 3D-Ising critical behavior can be described by crossover models [6, 7].

The critical behavior of polymer blends can be quite differently influenced by the microstructure of the polymer, by external pressure fields, and additives as solvent molecules [8,9,10]. So, the covalent binding of two homopolymers to a diblock copolymer leads to a crossover from 3D-Ising to the Brasovskii universality class which shows much stronger fluctuation effects [11,12] and a Ginzburg number G_i , being proportional to $N^{-1/2}$. One consequence for symmetric diblock

copolymers is a characteristic change of the disorder-order phase transition from second-order to weak first-order. Another situation appears in the presence of a third component which could affect the critical behavior due to fluctuations of density. Fisher's renormalized Ising model describes such an "impurity" effect by increasing the Ising critical exponents by a factor of $1/(1-(\alpha))$ [13,14]. Here, α is the critical exponent of the specific heat of the Ising system. In other cases, structural changes of the polymers or external pressure fields influence "non-universal" critical parameters as the critical temperature T_C and the Ginzburg number Gi . So, pressure usually leads to a reduced Ginzburg number [9,10].

In this study small angle neutron scattering (SANS) studies on a binary A,B homopolymer mixture of critical composition mixed with a symmetric A-B diblock copolymer are presented. These A-B diblock copolymers act as surfactant molecules reducing the surface energy and thereby leading to an improved miscibility and to stronger thermal fluctuations. But, as homopolymer blends and diblock copolymers obey different universality classes blending leads to new phenomena as the universality class of the isotropic Lifshitz case and to microemulsion phases. Mean field theory predicts a Lifshitz critical point and in some cases even a Lifshitz tricritical point [15] with the critical exponents $\gamma = 1$ and $\nu = 1/4$ of susceptibility and correlation length, respectively. Those mean field critical exponents were observed in such a system of rather large polymer mass [16]. Another related study on a mixture of significantly reduced polymer mass gave a sharp transition with increasing diblock content from 3D-Ising ($\gamma = 1.24$, $\nu = 0.63$) to the isotropic Lifshitz critical exponents of ($\gamma = 1.62$ and $\nu = 0.9$) [17,18]. These studies have shown that thermal composition fluctuations play an important role in the range of the Lifshitz universality class. Due to the vanishing surface energy which acts as a restoring force for the fluctuations and leads to a scaling behavior of Ginzburg number according to $N^{-2/3}$ [15]. These strong fluctuations are responsible for several deviations from the mean field predicted phase behavior: (1) No Lifshitz critical point is observed and a microemulsion channel appears between the two-phase and lamellar phase regimes [19]; (2) the Lifshitz Line shows a non-monotonic temperature dependence [18].

The present studies were mainly focused on the regime of the Lifshitz critical behavior. We made new observations from which we hope to further clarify the phase behavior, especially in this range. So, within a narrow range of diblock concentration between 6 and 12% a closed-loop two-phase regime terminated by a double critical point and a droplet and bicontinuous microemulsion phase was observed. The border line, where the correlations of the bicontinuous microemulsion phase becomes visible, appears as the lower temperature continuation of the Lifshitz line.

Samples with three different scattering contrasts were explored in order to better understand the behavior of the diblock copolymer. This was done by measuring the fluctuations between all the A and B monomers, irrespectively, whether they originate from the homopolymer or the block copolymer (bulk con-

trast); from one block of the diblock copolymer (block contrast) and in the other case only from the middle part of the diblock copolymer (film contrast). In neutron scattering such conditions of changing contrast are relatively easily achieved from the exchange of hydrogen and deuterium during the synthesis of the polymers.

Chapter 2

Theory

2.1 Ginzburg-Landau-Wilson Hamiltonian

We investigated a ternary polymer mixture consisting of a binary polymer blend of Polybutadiene (PB) and Polystyrene (PS) of critical composition and of the corresponding symmetrical PB-PS diblock copolymer of varying concentrations. In order to get the ordering phase transitions of the blend and the diblockcopolymer in the same temperature range the molar volume of the diblock copolymer was about six times larger than those of the homopolymers. In order to measure the “component” fluctuations with a strong scattering contrast, for most of SANS studies, the PB and PS were deuterated and protonated, respectively (so-called “bulk” contrast). Thermal composition fluctuations with respect to the total monomer fractions correspond to a scalar ($n = 1$) order parameter represented by the local concentration of the PB or PS component $\Phi = \Phi(x)$. The common Landau expansion describes the basic thermodynamic features sufficiently well within mean field approximation of those systems near their consolute line according to the Hamiltonian [20, 21],

$$H = \frac{1}{2} \int d^d x \left(c_2 (\vec{\nabla} \Phi)^2 + c_4 (\vec{\nabla} \Phi)^4 + r \Phi^2 + u \Phi^4 + u_6 \Phi^6 \right). \quad (2.1)$$

An ordinary critical point (for example a demixing point) occurs when the susceptibility r becomes zero, and the other parameters are positive. An ordinary tricritical point (when three phases coexist) occurs when $r = 0$ and $u = 0$, with the other parameters positive. At a Lifshitz critical point, $r = c_2 = 0$ and similarly at a Lifshitz tricritical point, $r = u = c_2 = 0$, with all the other parameters positive.

A Lifshitz critical point and a Lifshitz line generally appear in those systems with competing tendencies for phase separation into bulk and spatially modulated phases. When the appropriate parameter controlling the relative strength of the two tendencies is varied along the critical line of phase transitions a special

Table 2.1: *Mean field definitions of characteristic points. The parameters of the second column will be defined later.*

Type of CP	Hamiltonian parameters	Structure Factors parameters
Critical Solution Point	$r^{-1} = 0$	$S^{-1}(0) = 0$
Lifshitz Point	$c_2 = 0$	$L_2 = 0$
Lifshitz Critical Point	$r^{-1} = 0$ $c_2 = 0$	$S^{-1}(0) = 0$ $L_2 = 0$
Tricritical Lifshitz Critical Point	$r^{-1} = 0$ $c_2 = 0$ $u = 0$	$S^{-1}(0) = 0$ $L_2 = 0$

multi-critical point occurs at which the character of phase separation undergoes a change from bulk phase separation to the phase separation into a spatially modulated phase. The Lifshitz point is known to exist in magnetic systems [21, 22, 23, 24], liquid crystals [25], polyelectrolytes [26, 27], oil/ water/surfactant mixtures [28], random block-copolymers [29, 30], and mixtures of homopolymers and diblock copolymers [15, 31]. In the paper by Kudlay and Semenov in ref. [32] a theoretical description of the behavior of the Lifshitz line with varying temperature is developed and it was shown that the wave vector dependence of the fluctuation corrections is responsible for the experimentally observable non-linearity of the Lifshitz line.

Homopolymer blends are sufficiently well described by the Hamiltonian with $c_4 = 0$ and $u_6 = 0$ (Φ^4 model). A third component can influence on the Hamiltonian by reducing the u-parameter.

A principal effect of an (A-B) diblock copolymer dissolved in an (A/B) homopolymer blend is the reduction of the surface energy which according to the Hamiltonian, in Eq. 2.1, is described by a reduction of the parameter c_2 . This parameter is positive at low copolymer content, becomes zero at the concentration of the Lifshitz line, and negative for larger copolymer content. The Hamiltonian accounts for the composition fluctuations in the homogeneous (disordered) one-phase regime. The composition fluctuations are described by the structure factor $S(Q)$, Q being the momentum transfer, and is measured directly in a scattering experiment ($Q = \frac{4\pi}{\lambda} \sin \Theta$, where λ and Θ is the wavelength of the used radiation and the half of the scattering angle, respectively).

Positive c_2 -values demonstrate the characteristic behavior of polymer blends; $S(Q)$ is maximum at $Q = 0$, and the susceptibility, r^{-1} , is correspondingly given

by $S(Q = 0)$,

$$r^{-1} = S(0). \quad (2.2)$$

At the critical temperature T_c of macrophase separation the susceptibility diverges and the inverse susceptibility $S^{-1}(0)$ becomes zero. For negative c_2 -values the structure factor, $S(Q)$, has the basic characteristics of block copolymer melts, the maximum value of $S(Q)$ appears at a finite Q -value, $Q = Q^*$. The susceptibility is then given by the structure factor at this Q^* -value. According to the mean field theory of symmetric copolymers additives, the susceptibility $S(Q^*)$ diverges at the order-disorder critical point, and orders on a mesoscopic length scale beyond through microphase separation.

In mean field approximation the inverse structure factor $S^{-1}(Q)$ can be expanded into powers of Q^2 . Considering the decrease of the surface energy with increasing copolymer content the structure factor can be described by [15]

$$S^{-1}(Q) = S^{-1}(0) + L_2 Q^2 + L_4 Q^4, \quad (2.3)$$

where the coefficients L_2 and L_4 are proportional to the c_2 and c_4 terms in the Hamiltonian Eq. 2.1, respectively.

The structure factor of a binary polymer blend demonstrates a Q^{-2} scaling dependence, described by an Ornstein-Zernike approach, which is equivalent to Eq. 2.3 with $L_4=0$. As diblock copolymer additives lead to a decrease of the role of the c_2 -term in the Hamiltonian the c_4 -term becomes visible and dominant as well as the L_4 -term in the structure factor; the disappearance of the c_2 term leads to a characteristic Lifshitz Q^{-4} behavior of the structure factor. In case of equal molecular volumes of homopolymers and diblock copolymers mean field theory predicts the existence of a tricritical Lifshitz point, where c_2 , u and r^{-1} become zero.

Symmetric diblock copolymers modulate homopolymers on the local length scale like a surfactant does in a water-oil microemulsion. In analogy between water-oil microemulsions and homopolymer - diblock copolymer blends within mean field approximation both systems are characterized by the same structure factor Eq. 2.3. In order to explain the broad single peak profile of SANS patterns from oil-water microemulsion structures, Teubner and Strey [33] proposed a simple function derived from the phenomenological Ginzburg-Landau free energy functional (compare with given Hamiltonian in Fig. 2.1). The microemulsion structure is characterized by an alternative distribution of water and oil domains, for which they introduced the following spatial correlation function,

$$g(r) \sim \exp\left(-\frac{r}{\xi_{TS}}\right) \left[\frac{1}{\lambda_{TS}} \sin\left(\frac{2\pi r}{\lambda_{TS}}\right) \right], \quad (2.4)$$

where the domain periodicity λ_{TS} and the correlation length ξ_{TS} are the two relevant static length scales. The parameters λ_{TS} and ξ_{TS} are expressed in terms

of the structure factor parameters of Eq. 2.3 as

$$\lambda_{TS} = 2\pi \left[\frac{1}{2} \left(\sqrt{\frac{S^{-1}(0)}{L_4}} - \frac{L_2}{2L_4} \right) \right]^{-1/2}, \quad (2.5)$$

$$\xi_{TS} = \left[\frac{1}{2} \left(\sqrt{\frac{S^{-1}(0)}{L_4}} + \frac{L_2}{2L_4} \right) \right]^{-1/2}. \quad (2.6)$$

In the limit $\lambda_{TS} \rightarrow \infty$ the correlation function Eq. 2.4 demonstrates an exponential decay as binary blends. On the other hand, a periodic structure of the ordered lamellar phase is described by Eq. 2.4 in the limit of $\xi_{TS} \rightarrow \infty$. In mean field approximation the disorder-order transition has second order characteristics, and thus the correlation length diverges at a order-disorder phase boundary.

In order to estimate the size distribution of the PB and PS domains it seems to be useful to use a disorder parameter $D_m = \lambda_{TS}/(2\pi\xi_{TS})$ as proposed in Ref. [34]. The disorder parameter allows to make a definition of some phase lines

$$D_m = \frac{\lambda_{TS}}{2\pi\xi_{TS}} = \begin{cases} = \infty & \text{at the disorder line} \\ = 1 & \text{at the Lifshitz line} \\ = 0 & \text{at the lamellar phase boundary} \end{cases}$$

Table 2.1 summarizes the characteristic lines and points of this system in mean field approximation.

Strey et al. [35, 36, 37] have further classified the differently structured fluids in the disordered phase of the oil/water/surfactant system by defining the amphiphilicity factor, f_a , in terms of the structure factor parameters Eq. 2.3 as

$$f_a = \frac{L_2}{\sqrt{4S^{-1}(0)L_4}}, \quad (2.7)$$

and extending the Teubner-Strey model over all ranges of amphiphilicity. For strong amphiphilicity with $f_a < -1$, the microemulsion phase is unstable with respect to the lamellar phase. With slightly less amphiphilicity, $-1 < f_a < 0$, a strongly structured, “good” microemulsion phase results. The real “amphiphilicity” of systems increases as f_a decreases. One distinguishing characteristics of a “good” microemulsion is the tendency to create a large interface area due to a vanishing or negative microscopic surface tension. This corresponds to a negative value of L_2 , and thus negative f_a . The line $f_a = 0$ is the Lifshitz line of the microemulsion (μLL). A further decrease in amphiphilicity, $0 < f_a < 1$, results in a “poor” microemulsion. Here, the correlation function $g(r)$ is still oscillatory, but interfacial correlations no longer dominate the scattering and the structure factor peak occurs at zero wave vector. Finally, for $f_a > 1$, the fluid has no structure and $g(r)$ is no longer oscillatory. The boundaries between these classifications do not correspond to thermodynamic transitions, but are simply demarcations

between differently structured fluids. The (water/water) Lifshitz line is defined by $L_2 = 0$, and marks the boundary between "good" and "poor" microemulsions. The disorder line at $f_a = 1$ signifies the transition from correlated to uncorrelated interfaces.

2.2 Mean Field Phase Diagram of A/B/A-B Blends

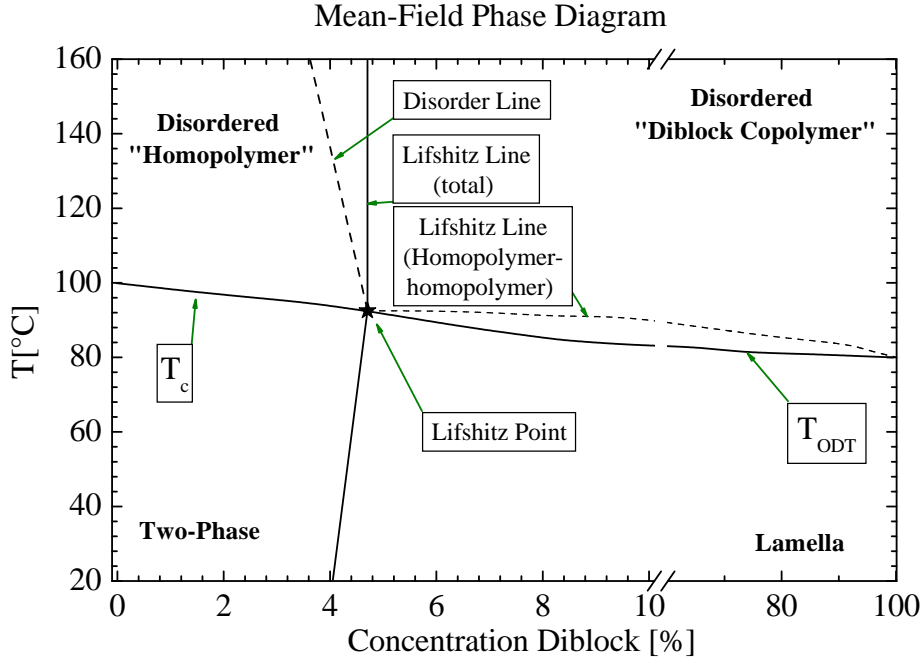


Figure 2.1: *Phase diagram of the ternary mixture at equal concentrations of A and B homopolymers as obtained from mean field theory. At low temperatures there exists a two-phase coexistence between A-rich and B-rich phases at low copolymer concentrations, a lamellar phase at high concentrations. The Lifshitz line divides the disordered phase to “homopolymer-like” and “copolymer-like” ranges.*

Ternary mixtures of two partially incompatible homopolymers and a diblock copolymer are in some respects similar to mixtures of oil, water, and amphiphile. But the copolymer is generally not so efficient as a solubilizer of the homopolymers as an amphiphile is for oil and water, because the homopolymer-homopolymer Lifshitz line is far from the total Lifshitz line [15].

Mean field theory can predict the phase diagram for symmetric ternary systems. The schematic phase diagram of A/B/A-B blends are shown in Fig. 2.1.

In the paper [15] the concept of disorder lines and Lifshitz lines was exploited from a theoretical point of view for ternary polymer system:

- The disorder line (DL) of the system is the locus of points at which the correlation function (Eq. 2.4) no longer decays monotonically, but starts to contain an exponentially damped oscillatory component. This oscillation

reflects the tendency of the copolymer to order the A monomers of the system.

- The Lifshitz line (LL) is the locus of points at which the peak in the structure function begins to move away from the zero wave vector. It therefore indicates the point at which oscillatory components begin to dominate the particular structure function, in contrast to the disorder line which indicates the point at which oscillatory components appear in all correlation functions. In Ref. [15] it is shown that the Lifshitz line of the structure function of all A monomers is quite close to the disorder line.

In the phase diagram in Fig. 2.1 two Lifshitz lines are shown: the total LL and the homopolymer LL. The homopolymer-homopolymer Lifshitz line shows the positions, where the maximum of the homopolymer-homopolymer structure factor begins to move from zero position, i.e., where the homopolymers start to order. The “total” Lifshitz line is defined in a case of a symmetric matched system, i.e. when one homopolymer and one block of diblock copolymers are matched.

The Lifshitz line and the disorder line meet at a Lifshitz critical point (LCP). The behavior near the Lifshitz point in mean field approximation is characterized by a Q^4 dependence of the inverse scattering intensity.

The critical exponents predicted for MF-behavior near LCP are listed in Table 2.2. When fluctuations are relevant, the renormalization group theory is not yet able to calculate the values of critical exponents near LCP in the conventional ϵ -expansion. ϵ is depicted as

$$\epsilon = d_U - d, \quad (2.8)$$

where $d=3$ is the dimension of the system, and d_U the upper critical dimension. Below the upper critical dimension, fluctuation effects are important near the critical point and the exponents differ from their classical values. The upper critical dimension is given by $4L$, where L is defined by the scaling behavior of the structure factor near the critical point according to [38,39]

$$S(Q) \sim (Q^2)^L. \quad (2.9)$$

In case of the isotropic Lifshitz critical point $L=2$, and therefore the upper critical dimension is equal to $d_U = 8$. Due to this high upper critical dimension ϵ is not a small expansion parameter with the result that the corresponding critical exponents cannot be calculated with sufficient accuracy. In order to get reliable exponents one has to take into account an infinite number of terms in the ϵ -expansion.

Near liquid-liquid critical points the ϵ -expansion works well, because $d_U = 4$.

The critical exponents near the isotropic Lifshitz critical point are not yet known from theoretical evaluations, so that a measurement of any of them would

be of considerable interest. In this respect ternary homopolymer/copolymer systems are an ideal reference object. Three critical exponents are bonded by scaling relations which near the Ising and Lifshitz critical point are given by

$$\eta = 2L - \frac{\gamma}{\nu}, \quad (2.10)$$

$$\alpha = 2 - d \cdot \nu, \quad (2.11)$$

$$\beta = \frac{1}{2} (2 - \alpha - \gamma), \quad (2.12)$$

$$\delta = \left(\frac{d}{2L - \eta} + 1 \right) / \left(\frac{d}{2L - \eta} - 1 \right). \quad (2.13)$$

Table 2.2: *Theoretical critical exponents near the Lifshitz critical point*

<i>Exponent</i>	Mean field	Mean field(LCP)	RG-Ising	RG-LCP
ν	1/2	1/4	0.63	?
γ	1	1	1.24	?
η	0	0	0.03	?
β	1/2	1/4	0.326	?

Bates et al. [16] studied the critical behavior in a system of rather large polymer mass of Polyethylene(PE)/Polyethylenepropylene(PEP)/PE-PEP ($N_{A,B} \approx 400$, $\alpha = 0.205$). In this system mean field critical exponents as predicted for the Lifshitz critical point were observed. Fluctuations are suppressed in system of large polymer weights because the Ginzburg number follows the scaling law $N^{-2/3}$ near LCP. Another related study on a mixture of significantly reduced polymer mass gave a sharp transition with increasing diblock content from 3D-Ising ($\gamma = 1.24$, $\nu = 0.63$) to the isotropic Lifshitz critical exponents of $\gamma = 1.62$ and $\nu = 0.9$ [17, 18].

2.3 Polymer Blends: A/B

2.3.1 Thermodynamics of Polymer Blends: Critical Behavior – Flory-Huggins Theory

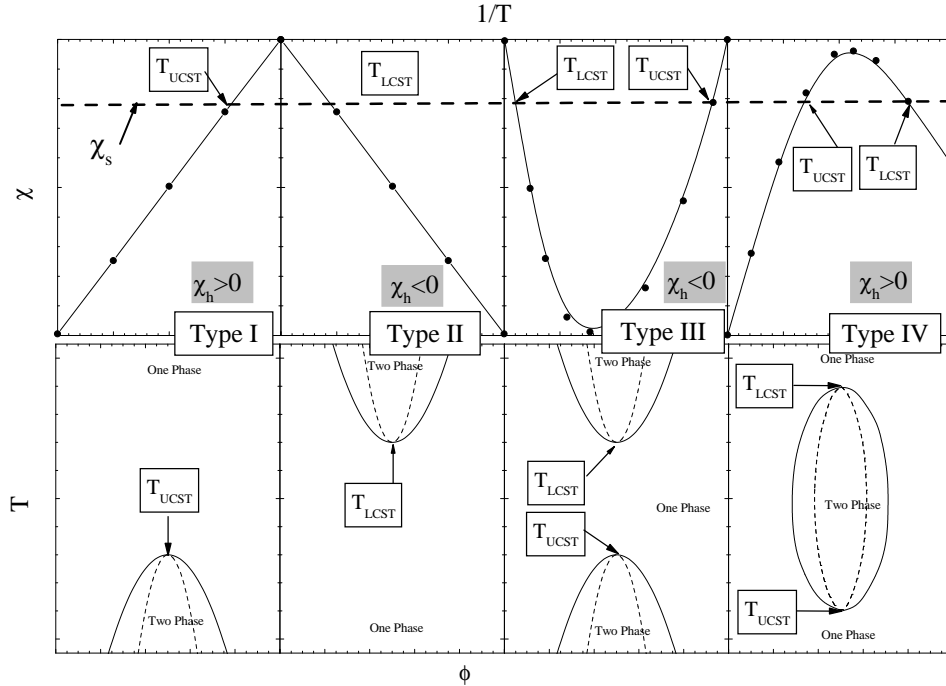


Figure 2.2: *Polymer blends: Classification of phase diagrams. The different temperature behavior of the Flory-Huggins parameter χ induces different types of critical behavior: (I) upper critical point T_{UCST} ; (II) lower critical point T_{LCST} ; (III) reentrance two-phase coexistence $T_{UCST} < T_{LCST}$; (IV) closed-loop phase diagram $T_{UCST} > T_{LCST}$.*

In this part of the theoretical introduction we give the thermodynamic definition of the critical point of binary blends, because ternary systems of two homopolymers with a small amount of a third component is represented as a quasi binary system which is analyzed as a binary one.

Usually, blends are described by two theoretical concepts: (i) the random phase approximation of binary polymer blends as a limiting case of ternary system is discussed in Sec. 2.5.1; (ii) the development of an expression for the free energy of mixing in polymer systems by Huggins and Flory [40, 41].

The Flory-Huggins theory was extended to polymer-solvent systems and other multicomponent systems by R.L. Scott [42]. In this theory, the thermodynamics of mixing is controlled by the Flory-Huggins parameter χ . Within the

mean field approximation the Gibbs free energy of mixing for polymer blend in Flory-Huggins representation is given as [1, 4, 43]

$$\frac{\Delta G}{RT} = \Phi \ln \frac{\Phi}{V_A} + (1 - \Phi) \ln \frac{1 - \Phi}{V_B} - \Phi(1 - \Phi) \left[\chi_\sigma - \frac{\chi_h}{T} \right], \quad (2.14)$$

where χ_h and χ_σ are enthalpic and entropic contributions of the Flory-Huggins parameter χ , V_i the molar volume of the components and Φ the volume fraction of the A-polymer.

By SANS the structure factor $S(Q)$ describing thermal composition fluctuations, is measured directly. The structure factor at the momentum transfer $Q = 0$ determines the susceptibility, $S(0)$, of the binary blend. The fluctuation-dissipation theorem gives the relation of the susceptibility and the Gibbs free energy according to [4, 20, 43, 44]

$$S^{-1}(0) = \frac{\delta^2}{\delta\Phi^2}(\Delta G/RT). \quad (2.15)$$

The combination of the fluctuation-dissipation theorem with the Flory-Huggins theory gives the expression for the susceptibility as

$$S^{-1}(0) = 2(\Gamma_s - \Gamma), \quad (2.16)$$

where Γ is the effective Flory-Huggins parameter

$$\Gamma = \Gamma_h/T - \Gamma_\sigma \quad (2.17)$$

with Γ_h and Γ_σ are enthalpic and entropic contributions, respectively, Γ_s is the FH-parameter at the spinodal. From the translatorial entropy of mixing the FH-parameter at the spinodal is derived

$$\Gamma_s = \frac{1}{2} \left(\frac{1}{\Phi V_A} + \frac{1}{(1 - \Phi)V_B} \right). \quad (2.18)$$

In case of a symmetric polymer blend with identical molar volumes of the components $V_A = V_B = V$ the critical FH-parameter transforms to

$$\Gamma_s = \frac{2}{V}. \quad (2.19)$$

A number of different phase behavior have been observed in polymer blends [45, 46]. The type of critical point depends on the character of the FH-parameter behavior. In a blend with a monotonically increase or decrease of the the χ -parameter with inverse temperature there exist an upper (T_{UCST}) or a lower (T_{LCST}) critical solution points. In Fig. 2.2 the first two types reflect this situation. In case of non-monotonic temperature dependence of χ a reentrance one-phase or two-phase region would appear. The two last types of Fig. 2.2 demonstrate reentrance phase diagrams.

The binary polymer blend of the two homopolymers Polybutadiene and Polystyrene is miscible at high temperatures and immiscible at low temperatures. This polymer blend therefore belongs to type I of the classification scheme in Fig. 2.2.

2.3.2 Effect of thermal fluctuations in polymer blends

Binary polymer blends represents liquid-like mixtures, and therefore obey to the same critical universality class as simple liquids which is the 3D-Ising model.

Far from the critical point ($\tau \gg 1$) when the correlation length of thermal concentration fluctuations is comparable with the polymer size (smaller than the polymer radius of gyration) the mean field approximation offers a suitable description. In this case the so-called Gaussian approximation usually plays the role of the mean field one, as thermal fluctuations can be handled as individual fluctuation modes.

Near the critical point ($\tau \ll 1$) the correlation length is the dominating length parameter and therefore the critical behavior should be universal, i.e. system independent. A liquid-liquid phase transition belongs to universality class of the 3D-Ising model.

The intermediate temperature regime ($\tau \sim 1$) is described by a crossover function connecting the different universal behaviors at low and high temperatures. So, a more complex description of the critical behavior of thermal fluctuations as measured by the susceptibility $S(0)$ is discussed in terms of universality classes and the crossover between them. Theoretical predictions for the critical exponents of different properties are tabulated in Table 2.3.

Table 2.3: *Theoretical predictions for the critical exponents: Ising [47] and mean field [20]*

Property	Symbol	Critical Exponent	Scaling Law	Ising	Mean Field
Susceptibility	$S(0)$	γ	$\tau^{-\gamma}$	1.240	1
Correlation Length	ξ	ν	$\tau^{-\nu}$	0.630	1/2
Critical Isotherm	$S(Q) _{T=T_c}$	η	$Q^{2-\eta}$	0.033	0
Heat Capacity	C_{px}	α	$\tau^{-\alpha}$	0.109	0
Order Parameter	φ	β	τ^{β}	0.326	1/2
Scaling correction		Δ		0.54	

Equations (2.10)-(2.13) are valid for critical exponents.

The mean field to 3D-Ising transition in polymer blends is characterized by continuous crossover as described by the Kiselev-Belyakov crossover model. This model could be successfully fitted to the temperature dependence of the susceptibility as shown in several references [48, 49, 50].

2.3.3 Belyakov-Kiselev Crossover Model

Belyakov and Kiselev derived an expression for the susceptibility $S(0)$ of polymer blend of critical composition connecting the mean field and 3D-Ising asymptotic regimes [6, 44]. This expression is given by

$$\hat{\tau} = (1 + 2.333\hat{S}(0)^{\Delta/\gamma})^{(\gamma-1)/\Delta}[\hat{S}^{-1}(0) + (1 + 1.2333\hat{S}(0)^{\Delta/\gamma})^{-\gamma/\Delta}]. \quad (2.20)$$

The exponents $\gamma = 1.24$ and $\Delta = 0.54$ are the critical exponents of the 3D-Ising model. The rescaled reduced temperature $\hat{\tau} = \tau/Gi$ is formulated as a function of the rescaled susceptibility $\hat{S}(0) = S(0)Gi/C_{MF}$. Gi , C_{MF} , and T_C are the experimental parameters characterizing the system. Gi is the Ginzburg number and C_{MF} the mean field critical amplitude of $S(0)$. Far from the critical point, in the asymptotic limit $t \gg 1$, the susceptibility in Eq. 2.20 follows the well-known scaling law

$$S(0) = C_{MF}\tau^{-1} \quad (2.21)$$

with the mean field critical exponent $\gamma = 1$ and the critical amplitude of the scaling law C_{MF} . Near the critical point, in the another asymptotic limit $\tau \ll 1$, the critical behavior of system does not depend on the internal structure of the system and the susceptibility follows the 3d-Ising model scaling law

$$S(0) = C_+\tau^{-\gamma} \quad (2.22)$$

where $\gamma = 1.24$ being the theoretically predicted exponent of this model, and C_+ the critical amplitude of the scaling law. Experimentally, $S(0)$ is obtained from the Ornstein Zernike approximation Eq. 2.61. The Ginzburg number is related to the ratio between the critical amplitudes of the 3D-Ising and the mean field susceptibilities according to Refs. [6, 51, 52]

$$Gi = 0.069(C_+/C_{MF})^{1/(\gamma-1)}. \quad (2.23)$$

In the FH-model the susceptibility is given as

$$S^{-1}(0)/2 = \Gamma_c - \Gamma \quad (2.24)$$

with the Flory-Huggins parameter $\Gamma = \Gamma_h/T - \Gamma_\sigma$ and the respective enthalpic and entropic contributions Γ_h and Γ_σ [1, 4]. The mean field critical amplitude is thus related to the FH-parameters according to

$$C_{MF} = 1/2|\Gamma_s + \Gamma_\sigma| = T_C^{MF}/(2\Gamma_h) \quad (2.25)$$

In order to evaluate the enthalpic term one needs the ‘‘mean field’’ critical temperature T_C^{MF} which is approximately related to the real critical temperature T_C by [44]

$$T_C^{MF} = T_C/(1 - Gi). \quad (2.26)$$

Thermal composition fluctuations stabilize the disordered phase of the system, and thereby lowers T_C .

2.4 Diblock Copolymer Melts

A-B diblock copolymer additions strongly influence the thermodynamics of A/B homopolymer blends, e.g. consisting of the same components. Therefore, it seems to be useful to shortly summarize the most important aspects governing the thermodynamic behavior of diblock copolymers [3,11,53]. Additionally, in this section the structure factor of the diblock copolymer melt are viewed within mean field approximation [11] and considering the effect of thermal fluctuations [12].

2.4.1 Thermodynamics of Block Copolymers

Chemically connected homopolymers of type A and B constitute a new class of materials called block copolymers. Within this class different molecular architectures are possible, like A-B diblock copolymers, A-B-A triblock copolymers, or even more complex structures as statistical or star copolymers.

The phase behavior of diblock copolymer melts depends on three parameters. (i) The volume fraction of one component f ; the parameter f crucially influences the morphology of the ordered state. (ii) The segment-segment interaction parameter χ and (iii) the total degree of polymerization N are important parameters for the location of the order-disorder microphase separation temperature.

2.4.2 RPA: A-B Melts

The random phase approximation describes the structure factor of the diblock copolymer as

$$S^{-1}(Q) = \frac{2}{V} \left[\frac{F(x, f)}{2} - \Gamma V \right] \quad (2.27)$$

with the effective Flory-Huggins (FH) parameter Γ . The inverse structure factor $F(Q)$ is expressed as

$$F(x, f) = g(1, x) / \{g(f, x)g(1 - f, x) - \frac{1}{4}[g(1, x) - g(f, x) - g(1 - f, x)]^2\}, \quad (2.28)$$

with the Debye function $g(f, x)$

$$g(f, x) = 2[fx + \exp(-fx) - 1]/x^2. \quad (2.29)$$

The FH parameter at the order-disorder critical point is a function of the molecular volume V , and given as

$$\Gamma_S V = \frac{F(x^*, f)}{2} = 10.495. \quad (2.30)$$

In RPA the susceptibility $S(Q^*)$ diverges at T_{ODT} . The FH parameter is found from the susceptibility $S(Q^*)$

$$S^{-1}(Q^*) = 2[\Gamma_S - \Gamma]. \quad (2.31)$$

2.4.3 Effect of Thermal Fluctuations in Diblock Copolymers Melts

Composition fluctuations in disordered diblock copolymers can only be relevant on the length scale of polymer chains. This is the reason why $S(Q)$ shows an interference peak at a finite value of Q^* . Fluctuation effects are considered by a renormalized Flory-Huggins parameter which for diblock copolymers can be approached according to

$$\Gamma_{ren}V = \Gamma V - \tilde{G}i\sqrt{S(Q^*)/V} + G_d/\sqrt{S(Q^*)/V} \quad (2.32)$$

with the Ginzburg number $\tilde{G}i$ defined in Eq. 2.50 [31]. The corresponding expression for Γ_{ren} was derived for pure diblock copolymers by Fredrickson Helfand [12], accordingly to

$$\Gamma_{ren}V = \Gamma V - \tilde{G}i\sqrt{S(Q^*)/V} \quad (2.33)$$

and is the same as Eq. 2.46 with the third term equal to zero.

2.5 Homopolymers-Diblock Copolymer Ternary Blend: A/B/A-B

2.5.1 The Structure Factor of a three Component Polymer Blend-Diblock Copolymer Mixture in Mean field Approximation

The structure factor of the three component mixture of a polymer blend and the corresponding diblock copolymer is described within the random phase approximation according to [11, 12, 19]

$$S^{-1}(Q) = F(Q)/V - 2\Gamma, \quad (2.34)$$

with the effective Flory-Huggins (FH) parameter $\Gamma = \Gamma_h/T - \Gamma_\sigma$. $F(Q)$ is the inverse form factor, which can be calculated in terms of the partial structure factors S_{AA} , S_{BB} and S_{AB} describing the correlation between the monomers of type A and B [31]

$$F(Q)/V = \frac{S_{AA}(Q) + S_{BB}(Q) + 2S_{AB}(Q)}{S_{AA}(Q)S_{BB}(Q) - S_{AB}^2(Q)} \quad (2.35)$$

For a ternary system composed of a critical mixture of A and B homopolymers of equal molar volume ($V_A = V_B$), conformation ($S_{AA}(Q) = S_{BB}(Q)$ and $\Phi_A = \Phi_B$) and an AB diblock with molar volume V , $F(Q)$ can be reduced to

$$F(Q)/V = 2 / (S_{AA}(Q) - S_{AB}(Q)). \quad (2.36)$$

Assuming that the polymers in the mixture remain as unperturbed Gaussian chains, $F(Q)$ can be written in terms of the Debye-function,

$$g_D(f, x) = \frac{2[f x + \exp(-f x) - 1]}{x^2} \quad (2.37)$$

as

$$F(x) = 4 / ((1 - \Phi)\alpha g_D(1, x\alpha) - \Phi g_D(1, x) + 4\Phi g_D(0.5, x)), \quad (2.38)$$

where $x = R_g^2 Q^2$, R_g is the radius of gyration of the diblock copolymer; and α the ratio of the molar volumes of the homopolymers relative to the diblock copolymer

$$\alpha = \frac{\sqrt{V_A V_B}}{V}. \quad (2.39)$$

Figure 2.3 depicts the inverse form factor $F(x)$ given by Eq. 2.38, as calculated with parameters equal to those of the experimentally investigated samples discussed in Sec. 3.1.1. From the minimum of $F(x)$ one gets both the Flory Huggins parameter Γ_S at the spinodal and critical point, and the corresponding characteristic $Q = Q^*$ value.

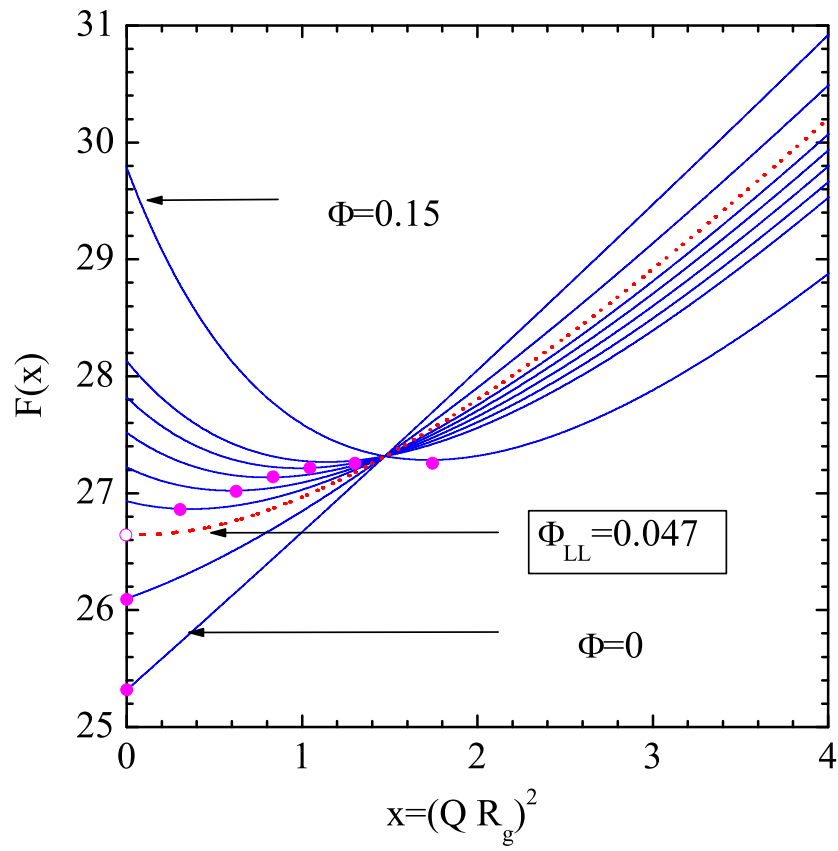


Figure 2.3: The inverse form factor $F(x)$ for different diblock concentrations ($\Phi = 0 - 0.15$) calculated based on Eq. 2.38. The circles shows the maximum value of the form factor. The open circle indicates the Lifshitz line concentration

Position of the Lifshitz line does not depend on the concentration of copolymer in RPA, the position ϕ_{LL} is function of α and given as

$$\Phi_{LL} = \frac{2\alpha^2}{1 + 2\alpha^2} \quad (2.40)$$

For concentrations, Φ , smaller than the Lifshitz critical value Φ_{LL} (according to Eq. 2.40) Φ_{LL} the critical point occurs for $Q = 0$, corresponding to macrophase separation [31]. For Φ larger than Φ_{LL} the maximum occurs at Q^* value, corresponding to microphase separation. These critical values of (Q^* and Γ_s) are represented by the circles in Fig. 2.3, and plotted vs. diblock concentration Φ in Fig. 2.4(a)-(b).

According to Eq. 2.3 with the coefficients given in terms of the parameters of the Hamiltonian in Eq. 2.1 the structure factor in Eq. 2.34 and 2.36 can be expanded into powers of Q^2 . The first term is represented by the inverse susceptibility $S^{-1}(0) = r$, as discussed above, and for concentrations less than the Lifshitz value equal to

$$S^{-1}(0) = 2(\Gamma_s - \Gamma). \quad (2.41)$$

The coefficients L_2 and L_4 are proportional to c_2 and c_4 in the Hamiltonian in Eq. 2.1, respectively, and can be determined in terms of the polymer parameters and the concentration Φ [54].

$$c_2 \sim L_2 = \frac{R_g^2}{V} \frac{4\alpha^2(1 - \Phi) - 2\Phi}{3\alpha^2(1 - \Phi^2)} \quad (2.42)$$

$$c_4 \sim L_4 = \frac{R_g^4}{V} \frac{(1 - \Phi)^2(4\alpha^4 + 16\alpha^2 - 9\alpha + 4)}{36\alpha^3(1 - \Phi)^3}. \quad (2.43)$$

At the Lifshitz line $L_2 = 0$ and the characteristic mean field behavior, $S^{-1}(Q) \sim Q^4$, clearly appears from this equation.

2.5.2 Effect of thermal fluctuations in blend/copolymer mixtures

Near the Lifshitz line thermal composition fluctuations are expected to become strong as its upper critical dimension, $d_U = 8$, is twice as large as that of binary polymer blends. This large value of d_U is related to the reduction of the surface energy described through the c_2 -term in the Hamiltonian, Eq. 2.1, and which acts as a threshold force for thermal composition fluctuations.

The structure factor of blend/diblock mixtures was recently derived beyond the mean field approximation by Kielhorn and Muthukumar [54]. They used the Hartree approximation in the Brazovskii formalism, equivalent to the procedure developed by Fredrickson and Helfand for pure diblock copolymer melts [12].

The structure factor, Eq. 2.34, was approximated and parameterized into a more simple form according to [18]

$$S^{-1}(Q^*) = \frac{a}{b + Q^2} + c + dQ^2 \quad (2.44)$$

with the parameters, $a \equiv A/(\sigma V)$, $b \equiv B/(\sigma^2)$, $c \equiv C/V$, and $d \equiv D\sigma^2/V$, where σ is the statistical segment length of the copolymer and is related to the radius of gyration according to

$$R_g^2 = \sigma^2 V / 6\Omega = \sigma^2 N / 6$$

V and N being the monomer molar volume and the degree of polymerization respectively. The effects of thermal fluctuations are considered by the renormalized parameters A , B , C , and D . These parameters were calculated assuming that the general shape of $S(Q)$ is unaltered in comparison with the mean field results. The expressions are given in full detail in Eqs.(3.9)-(3.12) of [54]. The susceptibility $S(Q^*)$ is given by

$$S^{-1}(Q^*) = 2[\Gamma_s - \Gamma_{ren}], \quad (2.45)$$

with a renormalized Flory Huggins parameter Γ_{ren} that includes the effect of thermal fluctuations. The detailed form of Γ_{ren} is given separately for the two cases, for the ‘‘diblockcopolymer’’-like one ($\Phi > \Phi_{LL}$) and the ‘‘blend’’-like one ($\Phi < \Phi_{LL}$) in correspondence with the susceptibility represented by $S(Q^*)$ at finite Q^* and $S(0)$ at $Q^* = 0$, respectively. In the block copolymer like case Γ_{ren} is given as

$$\Gamma_{ren}V = \Gamma V - G \sqrt{6x^*d_+} \frac{b/Q^{*2} - \sqrt{1 + b/(dQ^{*4}S(Q^*))} + 2 - 1/(dQ^{*2}S(Q^*))}{\sqrt{1/(dQ^{*2}S(Q^*)) - 2 + 2\sqrt{1 + b/(dQ^{*4}S(Q^*))}}}. \quad (2.46)$$

The parameter G is determined by the degree of polymerization N , the monomer molar volume, V , and the relative volume fractions of the polymer components Φ_A , Φ_B , and Φ according to

$$G = \frac{N\Gamma_4(0,0)}{16\pi\sqrt{d_+^3}} \frac{1}{N} \quad (2.47)$$

and with the parameters d and d_+ given by the equation:

$$d \equiv d_+\sigma^2/\Omega \quad (2.48)$$

$$d_+ = 1/(12(\Phi_A + f\Phi)(\Phi_B + (1-f)\Phi)) \quad (2.49)$$

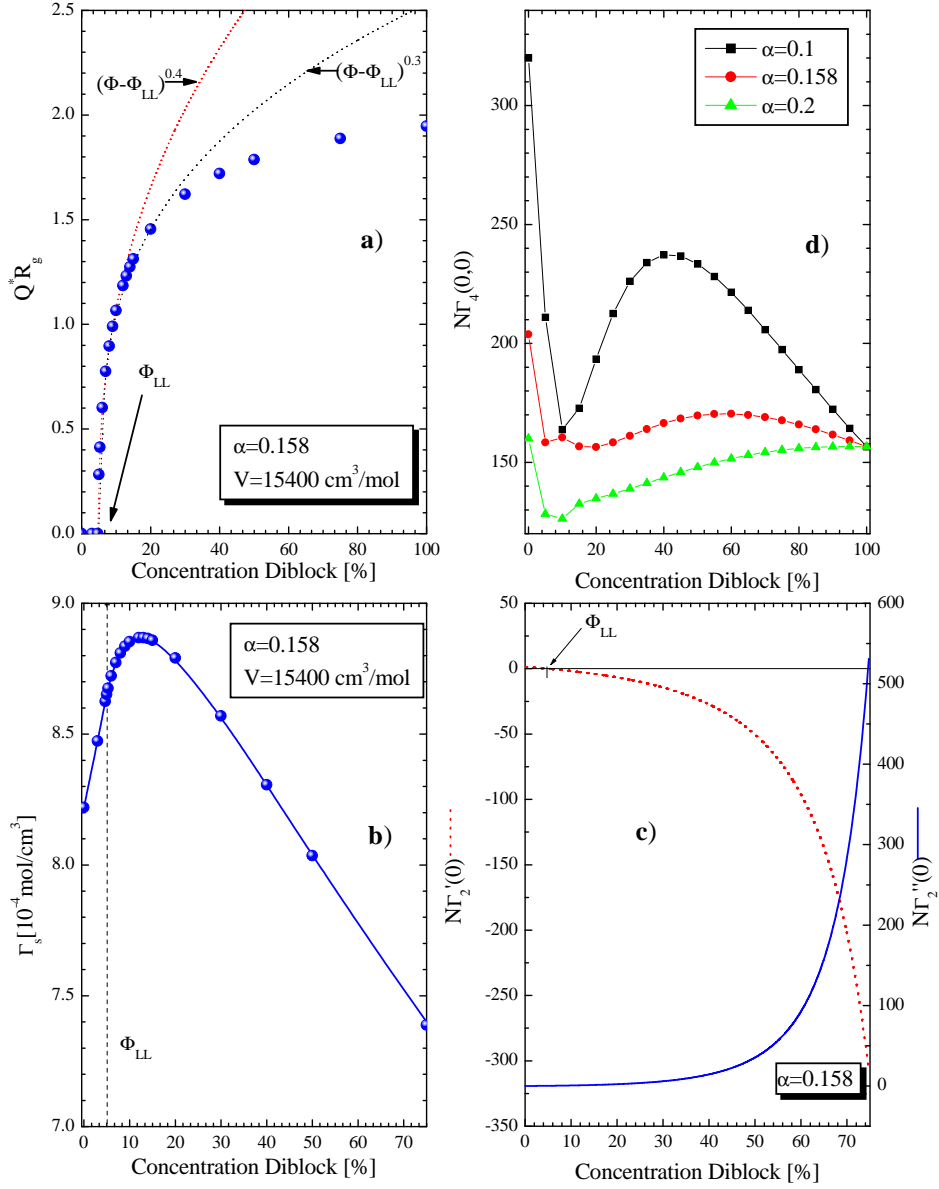


Figure 2.4: (a): The value of $Q = Q^*$ representing the maximum of the susceptibility $S(Q^*)$ evaluated from $F(x)$ in Fig. 2.3. Below the Lifshitz line $Q = Q^*$ and in the vicinity of LL Q^* follows a scaling behavior with exponent between 0.3 and 0.4. (b): Theoretical Flory-Huggins parameter at the spinodal and critical point evaluated from minimum of $F(x)$ in Fig. 2.3. (c): First and second order vertex function. (d): Concentration dependences of fourth order vertex function for $\alpha = 0.1, 0.158, 0.2$.

The parameter $\Gamma_4(0,0)$ is the fourth order vertex function, which was evaluated by the same procedure as used by Leibler [11] but is a function of f , Φ_A , Φ_B , and α [54]. In Fig. 2.4(d) for the studied samples the numbers of $N\Gamma_4(0,0)$ have been given for various diblock concentrations Φ and α . The parameter

$$\sqrt{\bar{N}} = \frac{R_0^3}{V}$$

is the average number of chains in the volume R_0^3 . R_0 is the end-to-end distance of the polymer ($R_0 = \sqrt{6}R_g$ for Gaussian chains). The reciprocal value of $\sqrt{\bar{N}}$ is a measure of the effect of thermal fluctuations [4] and proportional to the Ginzburg number

$$\tilde{Gi} = 6x^*d_+G(1 + b/Q^{*2}) \quad (2.50)$$

In the “blendlike” case of $\Phi < \Phi_{LL}$, where the susceptibility is represented by $S(0)$, the renormalized FH-parameter is given according to [54]

$$\Gamma_{ren}V = \Gamma V - G \frac{b_0 - V/S(0) - \sqrt{b_0V/S(0)}}{\sqrt{V/S(0) + b_0c_0 + 2\sqrt{b_0V/S(0)}}} \quad (2.51)$$

with the parameters

$$b_0 = 12d_+(6d_+ - N\Gamma'_2(0))/(N\Gamma''_2(0)) \quad (2.52)$$

and

$$c_0 = N\Gamma'_s(0)/(6d_+) \quad (2.53)$$

where $N\Gamma'_2(x)$ is the second order vertex function [11] which within mean field approximation is equal to the inverse structure factor according to $N\Gamma_2(x) = V/S(Q)$ [54]. Its derivatives with respect to x are obtained from Eq. 2.3 according to $N\Gamma'_2(0) = L_2V/R_g^2$ and $N\Gamma''_2(0) = 0.5L_4V/R_g^4$; both derivatives of $\Gamma_2(0)$ have been plotted in Fig. 2.4(c).

2.5.3 Scaling Behavior

Below the Lifshitz line the decrease of the surface energy with increasing copolymer content leads to a structure factor near the critical temperature that can be given as Eq. 2.3 [15]. The structure function is rewritten in the following form

$$S^{-1}(Q) = S^{-1}(0)[1 + (\xi Q)^2 + Kp^{-2}(\xi Q)^4]. \quad (2.54)$$

According to the scaling laws near the critical point the susceptibility $S^{-1}(0)$ follows the relation,

$$S^{-1}(0) = C_+^{-1}\tau^\gamma \quad (2.55)$$

with the reduced temperature

$$\tau = |T - T_c|/T, \quad (2.56)$$

the critical amplitude C_+^{MF} , and the critical exponent of the susceptibility γ . The parameter ξ represents the correlation length of concentration fluctuations and is given by

$$\xi \hat{=} \xi_{Q^2} = \sqrt{S(0)L_2}, \quad (2.57)$$

and the prefactor Kp^{-2} is given as

$$Kp^{-2} = L_4/[L_2^2 S(0)]. \quad (2.58)$$

The parameter p is amplitude of a scaling field, which is given by the square gradient term of the Hamiltonian Eq. 2.1 as

$$p = c_2/\sqrt{2c_4r}. \quad (2.59)$$

and is thus a measure of the deviation from the Lifshitz point [15]. The scaling field amplitude is proportional to the amphiphilicity factor f_a . At the Lifshitz line $L_2 = 0$. Therefore the correlation length ξ_{Q_2} loses its meaning. ξ has then to be redefined from the then dominating Q_4 term

$$\xi \hat{=} \xi_{Q^4} = \sqrt[4]{S(0)L_4}. \quad (2.60)$$

In Eq. 2.3 the corresponding scaling field p is constant.

At smaller copolymer content, the Q_4 term in the structure factor Eq. 2.3 becomes negligible, and the structure factors follows the Ornstein-Zernike equation

$$S^{-1}(Q) = S^{-1}(0)[1 + (\xi Q)^2], \quad (2.61)$$

as predicted for binary systems, and therefore ξ follows the usual scaling law

$$\xi = \xi_0 \tau^{-\nu}, \quad (2.62)$$

with the critical exponent of the correlation length ν . The parameters p and l_2 follow from the correlation length accordingly to the scaling laws [48]

$$p^2 \propto \xi^{2+\nu}/l_4, \quad l_2 \propto \xi^\eta$$

with the Fisher critical exponent $\eta = 2 - \gamma/\nu$ obtained from the critical exponents γ and ν of the susceptibility and correlation length, respectively. ξ and p both become infinite at the critical temperature.

2.6 Polymeric Microemulsion

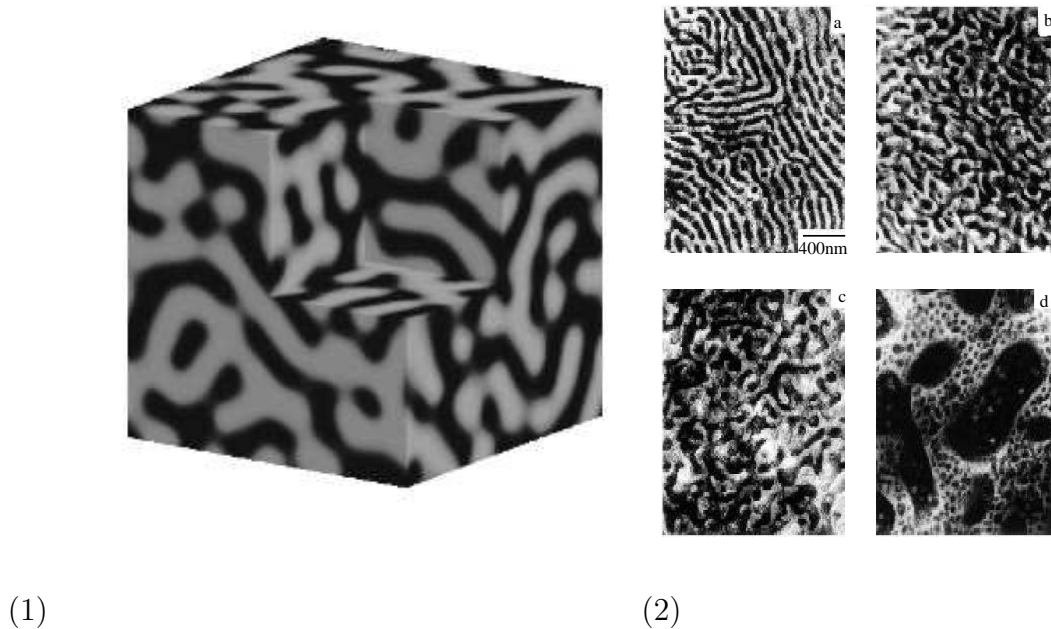


Figure 2.5: (1): 3D-numerical calculations of final configuration of bicontinuous microemulsion at $\alpha = 0.1$ [55]. (2): Transmission electron microscopy from the symmetric PE/PEP/PE-PEP blend: (a) lamellar, (b) and (c) bicontinuous microemulsion, (d) a two-phase state [19].

The addition of an A-B diblock copolymer to an A/B binary homopolymer blend increases the compatibility between A and B homopolymers. Therefore, those polymer blends are similar to water/oil/surfactant system. A surfactant in oil-water microemulsion stabilizes the interface as the surfactant significantly reduces the interfacial tension between the oil and water domains. Under some conditions oil, water and surfactant forms a thermodynamically stable structure, known as the microemulsion phase. Microemulsion phases could have the morphologies of oil-in-water, water-in-oil, and bicontinuous phases. Oil-in-water and water-in-oil microemulsion consists of droplets of the minor phase spreaded in the second one. This type of microemulsion is called droplet microemulsion. Bicontinuous microemulsions are found in systems with approximately equal oil and water composition. The morphology of bicontinuous microemulsions is a spongelike structure.

Depending on the amount of the surfactant Oil-water/surfactant systems of the 50/50 water and oil mixture show a two-phase, lamellar-phase, or bicontinu-

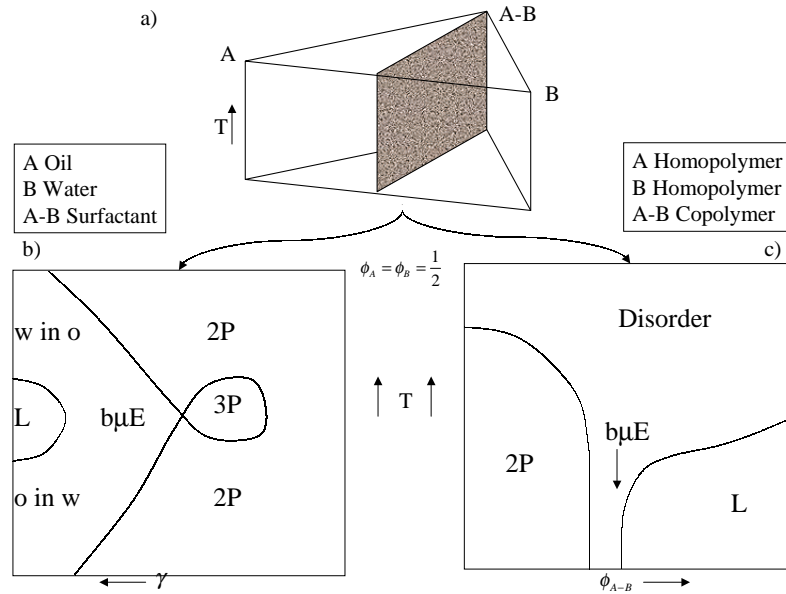


Figure 2.6: (a): Phase prism for a three-component system. (b): “Fish-cut” isopleth for water-oil microemulsion. (c): “Fish”-cut isopleth for an A/B/A-B polymer blend

ous microemulsion phase. The transition from lamellar to the two-phase regime occurs typically between 10% and 30% of the surfactant content.

The complex thermodynamics of symmetric oil/water/surfactant mixtures can be represented by a phase diagram with temperature and concentration of the surfactant as parameters. The schematic phase diagram of oil/water surfactant mixture and homopolymer/homopolymer/diblock copolymer blend are shown in Fig. 2.6(b)-(c).

Recently, in ternary polymer blends A/B/A-B of two homopolymers and diblock copolymers a channel of bicontinuous microemulsion phase was located [18, 19, 56, 57, 57, 58, 59, 60, 61].

Chapter 3

Experimental

3.1 Sample

3.1.1 Polymer Synthesis and Characterization

All polymers in this study were prepared by anionic polymerization. The techniques used were similar to those described by [62, 63]. The homopolymers polystyrene (PS), deuterated polystyrene (dPS) and deuterated polybutadiene (dPB) were prepared from styrene, deuterated styrene and deuterated butadiene monomers with *s*-butyllithium as initiator and benzene as polymerization solvent. The diblock copolymer dPB-PS and triblock copolymer dPB-PB-dPS were synthesized by sequential addition of corresponding monomers. The molecular weights and their distributions were determined by size exclusion chromatography in THF relative to PS-standards. Transformation to the dPB molecular weights was performed by $M_{PB} = 0.581M_{PS}^{0.997}$ derived from the PS and dPB Mark-Houwink-Sekurata relations in THF [64]. The higher molecular weight due to deuteration was considered during the calculations for the deuterated polybutadiene and polystyrene. The molar volume of the homopolymers were relatively small and approximately equal: $V_{dPB} = 2720\text{cm}^3/\text{mol}$, $V_{PS} = 2000\text{cm}^3/\text{mol}$ and $V_{dPS} = 2065\text{cm}^3/\text{mol}$ as shown in Tables 3.1 and 3.2. The molar volume of the symmetric diblock copolymer was chosen approximately six times larger ($V_{dPB-PS} = 15400\text{cm}^3/\text{mol}$), in order to match the ordering temperatures of the homopolymer blend and diblock copolymer. The ratio of the molar volumes of the homopolymers and copolymer in different contrasts is approximately to be equal $\alpha = 0.15$ (only in “film” contrast a little bit less $\alpha = 0.14$). The ratio of the two homopolymers was kept constant with the critical value ($\phi_{PB} = 0.42$).

Table 3.1: *Sample characteristics: Bulk contrast*

Sample	Polymer Blend		Diblock copolymer	
	Polybutadiene 93% (1,4)	Polystyrene	Polybutadiene 93% (1,4)	Polystyrene
Chem. Structure	C_4D_6	C_8H_8	C_4D_6	C_8H_8
	dPB	PS	dPB-PS	
$\Omega [\frac{cm^3}{mol}]$	60.6	99.1	60.6	99.1
Density [$\frac{g}{cm^3}$]	0.99	1.05	1.02	
	1.025			
$\sum \frac{Nab_i}{\Omega_i} [10^{10} cm^{-2}]$	6.62	1.41	6.62	1.41
$V_w [\frac{cm^3}{mol}] (\frac{V_w}{V_n})$	2720 (1.05)	2000 (1.06)	15400 (1.05)	
N	45	22	137.7	71.5
\bar{N}	33.6		209.2	
PB-composition	$\phi = 0.42$		f=0.54	
$\alpha = \frac{\sqrt{V_{PB}V_{PS}}}{V_{PB-PS}}$	0.158			

Table 3.2: *Sample characteristics: Film contrast*

Sample	Polymer Blend		Triblock copolymer		
	Polybutadiene 93% (1,4)	Polystyrene	Polybutadiene 93% (1,4)	Polybutadiene 93% (1,4)	Polystyrene
Chem. Structure	C_4D_6	C_8D_8	C_4D_6	C_4H_6	C_8D_8
	dPB	dPS	dPB-PB-dPS		
$\Omega [\frac{cm^3}{mol}]$	60.6	100.1	60.6	60.1	100.1
Density [$\frac{g}{cm^3}$]	0.99	1.12	1.05		
	1.07				
$\sum \frac{Nab_i}{\Omega_i} [10^{10} cm^{-2}]$	6.62	6.41	6.62	0.41	6.41
$V_w [\frac{cm^3}{mol}] (\frac{V_w}{V_n})$	2720 (1.05)	2065 (1.06)	17200 (1.05)		
N	45	22	135	16	81
\bar{N}	33.6		232		
PB-composition	$\phi = 0.42$		0.47	0.06	0.47
$\alpha = \frac{\sqrt{V_{PB}V_{PS}}}{V_{PB-PS}}$	0.140				

Table 3.3: *Investigated samples*

"Bulk"		"Film"		"Block"		Characteristic
Alias	Volume Fraction	Alias	Volume Fraction	Alias	Volume Fraction	
B00	0.000	F00	0.000	F00	0.000	Disorder- Two-Phase Transition
B03	0.030	F03	0.030	C03	0.030	
B04	0.040	-	-	-	-	
B05	0.050	F05	0.050	-	-	
B06	0.060	F06	0.060	-	-	
B066	0.066	-	-	C065	0.065	Disorder- Two-Phase- Microemulsion Transition
B07	0.070	F07	0.070	-	-	
B071	0.071	-	-	-	-	
B072	0.072	-	-	-	-	
B073	0.073	-	-	C074	0.074	Disorder- Microemulsion Transition
B075	0.075	-	-	-	-	
B08	0.080	F08	0.080	C08	0.079	
B09	0.090	-	-	-	-	
B10	0.100	F10	0.100	C10	0.100	
B13	0.131	-	-	-	-	Disorder- Lamellar Transition
B15	0.150	F15	0.150	-	-	
B20	0.200	-	-	-	-	
B30	0.300	-	-	C30	0.302	
B40	0.400	-	-	-	-	
B50	0.500	-	-	-	-	
B100	1.000	F100	1.000	B100	1.000	

3.1.2 Sample Preparation

A preparation of a blend consisting of two immiscible homopolymers at room temperature differs from mixing of simple liquids. Due to the high viscosity and the temperature range of experiment (20-160°C) there was not possible to use conventional quartz cells. The cells are shown in Fig. 3.1.

The preparation of polymer blends for SANS was done by the freeze-dried method. First, the two polymer blends of dPB/PS and dPB/dPS with identical volume fraction of deuterated Polybutadiene $\phi = 0.42$ were prepared. The volume fraction of the final sample was determined by recalculating the weight of the components considering the density of the homopolymers depicted in Tables 3.1 and 3.2. At room temperature the PB/PS blend is immiscible. In order to get a macroscopically homogeneous blend the follows procedure was exploited.

The homopolymers were dissolved in benzene followed by two hours of shaking and quickly frozen to a temperature of approximately $-10... -5^{\circ}\text{C}$. At this temperature benzene is in solid state. The frozen mixture was then set up to a vacuum line. In order to avoid a distribution of the material inside of vacuum line the sublimation of benzene was done step by step by opening and closing the valve of the vacuum line. During the first few minutes more than 95% of the solvent was sublimated. The samples were dried under vacuum conditions during 24 hours at least. Ternary polymer blends in bulk, film and block contrast conditions were prepared by the above mentioned method by mixing the homopolymer blend and the diblock (triblock) copolymers. The parameters of the explored samples are listed in Table 3.3. After preparation the blends were closed in an argon atmosphere and kept in the refrigerator.



Figure 3.1: *Cell for SANS*

The next step of the sample preparation was to transfer the sample to the SANS cell. The cells were filled in a glove box under argon atmosphere at a temperature slightly above of the melting temperature.

3.1.3 Thermostat

Near the critical point a small change of temperature induces a large and non-linear change of the degree of thermal fluctuations. Therefore, investigations of critical phenomena require a precise and stabile temperature. An oven with a

two-level temperature control was used [65]. The “real” temperature of sample was corrected to temperatures of inner T_{inside} and tube T_{tube} parts of the oven as

$$T_{sample}[^{\circ}C] = T_{inside} - 0.060 (T_{inside} - T_{tube})^2 - 5.45 \cdot 10^{-4} (T_{inside} - T_{tube}) \quad (3.1)$$

in order to take into account temperature gradient effects inside the thermostat. The temperatures were measured by a 10 Ohm platinum resistance element. Two level temperature heating devices in conjunction with the vacuum chamber allowed to keep the temperature of a sample as long as it is necessary with a temperature stability better than 0.02 K.

3.2 Small Angle Neutron Scattering

The scattering measurements were performed at the KWS1 and KWS2 diffractometers at the FRJ-2 research reactor of the Forschungszentrum Jülich (FZJ) [66]. The characteristics of both diffractometers and the experimental conditions are shown in Table 3.4.

Table 3.4: *Instruments details*

Characteristic	KWS1	KWS2
Monochromator	Velocity selector [DORNIER]	Velocity selector
$\Delta\lambda/\lambda$	0.2	0.1
Wavelength, λ	7Å	7Å
Sample aperture, d_s	0.7 cm	0.9 cm
Collimation aperture,	3×3 cm	3×3 cm
Collimation length	2 - 20 m	2-20 m
Detector length	1.25 - 20 m	1.4-20 m
Detector:		
Active area	60×60 cm ²	50×50 cm ²
Scintillator	⁶ Li - Glas	³ He
Space resolution	8 mm	8 mm
Max.pulse rate	12.5 kHz	7 kHz
Dead time, τ_d	8.8 μ s	15 μ s
Q-range	$2 \cdot 10^{-3} - 0.2$ Å	$2 \cdot 10^{-3} - 0.2$ Å
Neutron flux at sample	$2 \cdot 10^5 - 2 \cdot 10^7$ n/cm ² s	$10^5 - 6 \cdot 10^6$ n/cm ² s

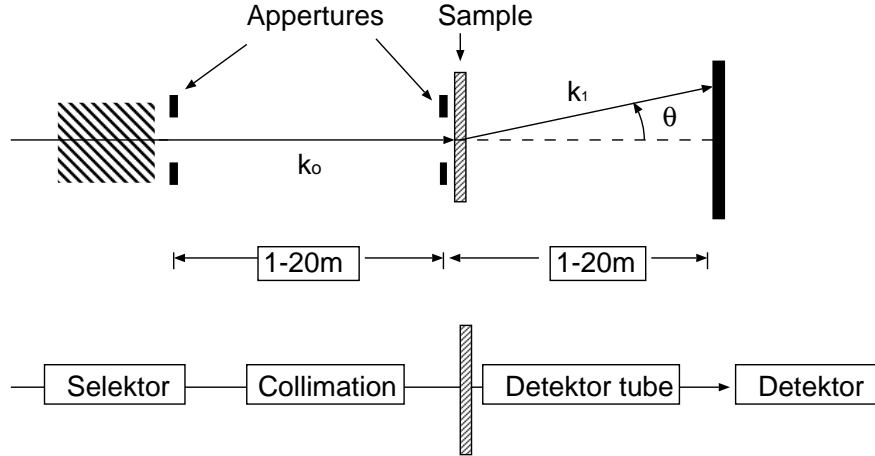
3.2.1 Basics of Small Angle Neutron Scattering

The experimental setup and the geometry of a scattering experiment of the small angle scattering instrument is schematically depicted in Fig. 6.2. An important advantage of the neutrons is their deep penetration into samples due to their weak interaction with atomic nuclei.

The scattering vector is defined as the difference between the propagation vectors of the scattered and incident beam (Fig. 6.2)

$$\vec{Q} = \vec{k} - \vec{k}_0 \quad (3.2)$$

In case of elastic small-angle scattering the energy transfer is neglected ($|\vec{k}| = |\vec{k}_0|$) and the scattering intensity is discussed in terms of momentum transfer Q given

Figure 3.2: *General layout of a scattering experiment*

as

$$Q = \frac{4\pi}{\lambda} \sin \frac{\Theta}{2}, \quad (3.3)$$

where λ is the wavelength of neutrons adjusted by the frequency of the velocity selector. The macroscopic cross-section $d\Sigma/d\Omega(Q)$ is connected with the scattering intensity $\Delta I(Q)$ in solid space angle $\Delta\Omega$ and given by the equation

$$\frac{d\Sigma}{d\Omega}(Q) = \frac{1}{\epsilon V_p T I_0} \frac{\Delta I(Q)}{\Delta\Omega}, \quad (3.4)$$

with the scattering sample volume V_p , the transmission T , the incoming neutron intensity I_0 , and the efficiency of the detector channels ϵ . In polymer blends the scattering cross-section can be expressed in terms of the structure factor $S(Q)$ as

$$\frac{d\Sigma}{d\Omega}(Q) = K \cdot S(Q), \quad (3.5)$$

with the contrast factor K given by

$$K = \frac{(\Delta\rho)^2}{N_A}, \quad (3.6)$$

with scattering contrast $(\Delta\rho)^2$ and the Avogadro number N_A . The scattering contrast of i and j polymers is calculated as the function of the molar monomer volume Ω_i and the coherent scattering length b_i

$$(\Delta\rho)^2 = N_A^2 \left(\frac{\sum_i b_i}{\Omega_i} - \frac{\sum_j b_j}{\Omega_j} \right)^2. \quad (3.7)$$

The coherent lengths of a few isotopes are listed at Table 3.5. The huge difference between 1H and 2D in the coherent scattering length is the basis of contrast

variation and the matching technique. An isotopical substitution does not change the physical and chemical properties of the mixture in most cases, but crucially changes the scattering properties of the system. In Table 3.6 the scattering contrast $(\Delta\rho)^2$ and the contrast factor K are shown for the investigated polymers.

Before the data interpretation the incoherent scattering has to be subtracted:

$$\left. \frac{d\Sigma}{d\Omega} \right|_{coherent} = \left. \frac{d\Sigma}{d\Omega} \right|_{measured} - \left. \frac{d\Sigma}{d\Omega} \right|_{incoherent}. \quad (3.8)$$

The incoherent scattering of polymer given by

$$\left. \frac{d\Sigma}{d\Omega} \right|_{incoherent} = \frac{1}{4\pi} \cdot \frac{\sum_i \sigma_i^{inc}}{\Omega_i}. \quad (3.9)$$

The incoherent scattering lengths σ_i^{inc} are listed at Table 3.5. The strongest incoherent scattering comes from hydrogen. Table 3.7 contents the incoherent structure factor for several systems.

3.2.2 Raw Data Reduction

The scattering patterns were corrected in a standard way by detector sensitivity, background, and is given in absolute units after being calibrated by a Lupolen secondary standard.

The scattering intensity is related to cross section by

$$\Delta I(Q) = I_0 \epsilon \Delta\Omega A d T \frac{d\Sigma}{d\Omega}(Q)$$

where A is illuminated area, d the sample thickness. By using Lupolen as a secondary standard with the scattering intensity $I_{Lupolen}$ the intensity of the sample I_{Sample} could be rewritten in terms of the scattering cross-section

$$\frac{I_{Sample}}{I_{Lupolen}} = \frac{\Delta\Omega_{Sample}}{\Delta\Omega_{Lupolen}} \cdot \frac{d_{Sample}}{d_{Lupolen}} \cdot \frac{T_{Sample}}{T_{Lupolen}} \cdot \frac{d\Sigma/d\Omega|_{Sample}}{d\Sigma/d\Omega|_{Lupolen}}. \quad (3.10)$$

Reorganizing of Eq. 3.10 using the definition of solid space angle $\Delta\Omega \sim 1/L^2$ with the sample-detector distance L , the scattering cross-section of sample follows next equation

$$\frac{d\Sigma}{d\Omega}(Q) = cal \cdot I_{Sample} \quad (3.11)$$

where constant cal is given by

$$cal = \frac{L_{Sample}^2}{L_{Lupolen}^2} \cdot \frac{d_{Lupolen}}{d_{Sample}} \cdot \frac{T_{Lupolen}}{T_{Sample}} \cdot \frac{d\Sigma/d\Omega|_{Lupolen}}{\langle I_{Lupolen} \rangle}. \quad (3.12)$$

Addition measurements of scattering from empty cell I_{cell} , blocked beam I_{BG} was carried out. The final scattering cross-section becomes

$$\frac{d\Sigma}{d\Omega}(Q) = \frac{I_{Sample} - I_{BG} - T_{Sample}/T_{Empty}(I_{Empty} - I_{BG})}{I_{Lupolen} - I_{BG} - T_{Lupolen}/T_{Empty}(I_{Empty} - I_{BG})} \cdot cal. \quad (3.13)$$

Table 3.5: *The coherent and incoherent scattering lengths of some isotopes*

<i>Isotope</i>	1H	2D	<i>C</i>
$b [10^{-12}cm]$	-0.3740	+0.6674	+0.6648
$\sigma_{inc} [10^{-24}cm^2]$	80.2	2.05	< 0.018

Table 3.6: *Contrast factor*

<i>System</i>	$(\Delta\rho)^2 [10^{-20}cm^{-4}]$	$K = N_A/(\Delta\rho)^2 [cm^4/mol]$
<i>dPB/dPS</i>	0.043	$1.41 \cdot 10^5$
<i>dPB/PS</i>	27.0	222.2
<i>dPB/PB</i>	38.5	156.6
<i>PB/dPS</i>	36.0	167.4

Table 3.7: *Incoherent background*

<i>System</i>	$\left. \frac{d\Sigma}{d\Omega} \right _{inc} [cm^{-1}]$	$S_{inc} [cm^3/mol]$
<i>dPB/PS</i>	0.184	40.97
<i>dPB - PS</i>	0.148	32.90
<i>dPB/dPS</i>	0.0087	1220
<i>dPB - PB - PS</i>	0.0276	4.47

3.2.3 Dead Time Effect

Local sensitive detectors of SANS instruments have a characteristic time for detection a single event. This finite time of detector can lead to dead-time effects with a characteristic time τ_d . This time gives a characteristic restriction, which has to be taken into account specially at high counting rates. Within the dead-time counts are lost. The reasons for this restriction are the electronic devise limitations and data acquisition electronics. The scattering profile could be corrected with respect to dead-time effects as given by

$$\left. \frac{d\Sigma}{d\Omega}(Q_0) \right|_{corrected} = \frac{\frac{d\Sigma}{d\Omega}(Q_0)}{1 - \tau_d N_{tot}}. \quad (3.14)$$

Dead-times of KWS1 and KWS2 diffractometers are $8.8\mu s$ and $15\mu s$, respectively. The dead-time correction was applied for samples that scatter strongly in high-Q range.

3.2.4 Resolution Function

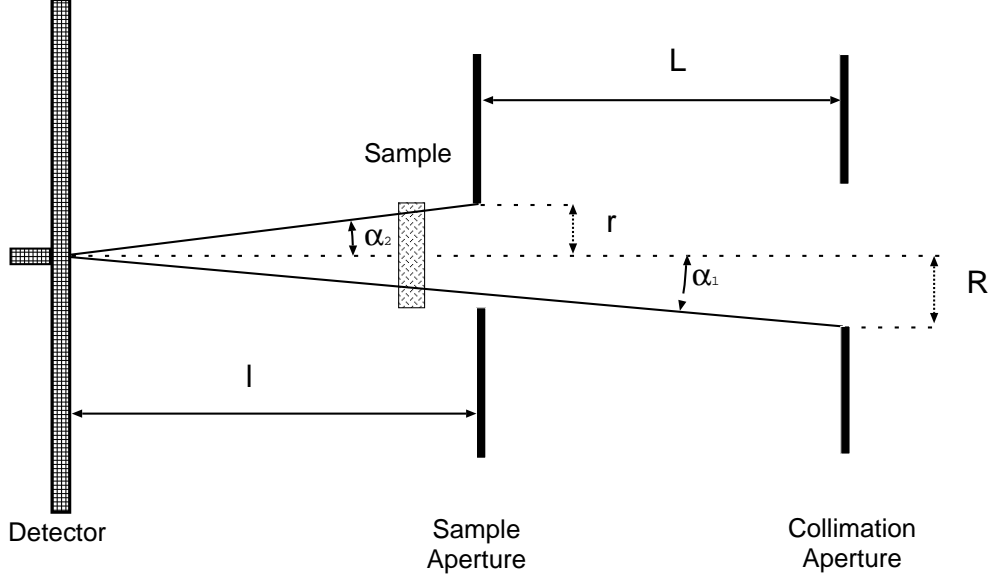


Figure 3.3: *Aperture configuration*

The observed scattering intensity is smeared by the distribution of the wavelength, a finite beam divergence, and the finite channel size of a detector.

The experimentally measured intensity $I(Q)$ and the scattering cross section $d\Sigma/d\Omega(Q_0)$ as a function of the average scattering vector Q_0 are connected as [67, 68, 69]

$$I(Q) = \int_0^{\infty} R(Q, Q_0) \frac{d\Sigma}{d\Omega}(Q_0) dQ_0 \quad (3.15)$$

where $R(Q, Q_0)$ is the resolution function. Pedersen et al. [67, 68, 69] approximated the resolution function by Gaussian functions given as

$$R(Q, Q_0) = \frac{1}{\sigma_Q \sqrt{2\pi}} \exp\left(-\frac{(Q - Q_0)^2}{2\sigma_Q^2}\right) \quad (3.16)$$

with the dispersion coefficient σ_Q . The smearing effects are mainly caused by wavelength spread $\Delta\lambda$ (the velocity selector), collimation effects (the finite beam divergence), and detector resolution (the discreteness of the detector). These three effects are included in the dispersion coefficient as

$$\sigma_Q^2 = \frac{1}{8 \ln 2} \left[Q_0^2 \left(\frac{\Delta\lambda}{\lambda} \right)^2 + k_0^2 (\Delta\Theta)^2 + k_0^2 \left(\frac{D}{l} \right)^2 \right], \quad (3.17)$$

with $k_0 = 2\pi/\lambda$, and $\Delta\lambda$ being the full-width at half-maximum of wavelength spread, D the size of the detector channel, l the detector-to-sample distance. The second term in Eq. 3.17 takes the collimation effect into account. The configuration of the apertures is shown at Fig. 3.3. The $\Delta\Theta$ vs. the geometrical parameters of the experiment L (the sample aperture - detector distance), r (the radius of the sample aperture), R (the radius of the collimation apertures) are expressed as [68, 69]

$$\Delta\Theta = \begin{cases} \frac{2R}{L} - \frac{r^2}{2R} \frac{(l+L)^2}{l^2L}, & \alpha_1 \leq \alpha_2 \\ 2r \left(\frac{1}{l} + \frac{1}{L} \right) - \frac{r^2}{2R} \frac{l}{L(l+L)}, & \alpha_1 > \alpha_2 \end{cases}. \quad (3.18)$$

The experimental data were fitted by a model considering the resolution function.

Chapter 4

Experimental results

4.1 Phase Diagram

The temperature-diblock concentration plane of the phase diagram of the ternary dPB/PS/dPB-PS mixture with fixed critical concentration of the dPB/PS blend has been depicted in the range from 0 to 20% in Fig.4.1. This phase diagram represents the principle results of this work and is therefore a reference for the presentation of the experimental data. The depicted boundaries will be discussed in the following.

The phase diagram in Fig.4.1 is globally divided by the Lifshitz line into two characteristically different parts with respect to the behavior of the system. On the left from the LL in the disordered phase at higher temperature the ternary system demonstrates a so-called “blend”-like behavior of the structure factor with the maximum intensity at $Q = 0$. On the right side from the Lifshitz line the maximum of the intensity is observed at a finite Q^* value and the behavior of the mixture is called “diblock copolymer”-like one. At high temperature randomly distributed diblock copolymers modulate the homopolymers.

4.1.1 Lifshitz Line

The mean field theory predicts the Lifshitz line at a constant concentration determined from the ratio of the molar volumes $\alpha = 0.158$ and is accordingly estimated with 4.7% Eq. 2.40 for the present system.

The Lifshitz line in Fig. 4.1, however, shows characteristic deviations. At high and low temperatures it is observed at the larger diblock concentration of 7%, in comparison with the mean field prediction of 4.7%, and it bends to even larger concentrations at intermediate temperatures near the two-phase regime. Such bending is caused by thermal composition fluctuations as has been shown from recent renormalization group theory calculations [32].

The Lifshitz line was detected by an isothermic and isopleth approach. In Fig. 4.2 the concentration dependence of Q^* is shown for three temperatures.

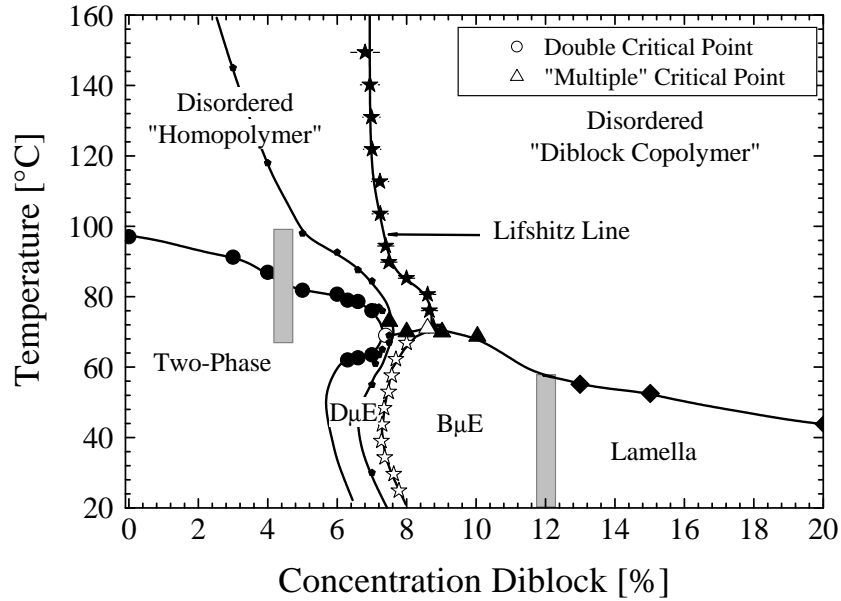


Figure 4.1: *Experimental phase diagram of the dPB/PS/dPB-PS blend. The filled circles (●) represent the upper and lower critical temperatures of the 3D-Ising and isotropic Lifshitz case separated by grey box, the open circle (○) the double critical point, the filled stars (★) the disordered Lifshitz line, the open stars (✱) the microemulsion Lifshitz line, the filled triangle (▲) the disorder-microemulsion boundary, the diamonds (◆) the disorder-order (lamellar) transition, (◊) the disorder line. The dashed area separates the lamellar phase and bicontinuous microemulsion*

Already at 50°C and the other temperatures a visual distinction can be made for the scaling behavior of Q^* . From an analysis of a concentration scaling behavior $Q^* \sim |\Phi - \Phi_{LL}|^{\beta_Q}$ two parameters were determined for each temperature, namely the LL position Φ_{LL} and the exponent β_Q . This analysis was performed in a temperature range from 25 to 160°C . There is a clear difference in the behavior of the exponent β_Q below and above 71°C as depicted in Fig. 4.3. Two exponents of $\beta_Q = 0.3$ and $\beta_Q = 0.42$ were observed above and below 71°C , respectively. These two exponents are due to the different nature of the LL in the disordered and ordered regimes of the phase diagram. In the sections of 5.3 and 4.1.3 the evidence of a disorder-microemulsion boundary is represented. This boundary is shown by the filled triangles in Fig. 4.1. The LL crosses the microemulsion boundary exactly at 71°C where we detected the abrupt change of the scaling behavior of the Q^* position. We call the LL at high temperatures the “disordered” Lifshitz line (dLL), at low temperatures in an ordered part of phase diagram the

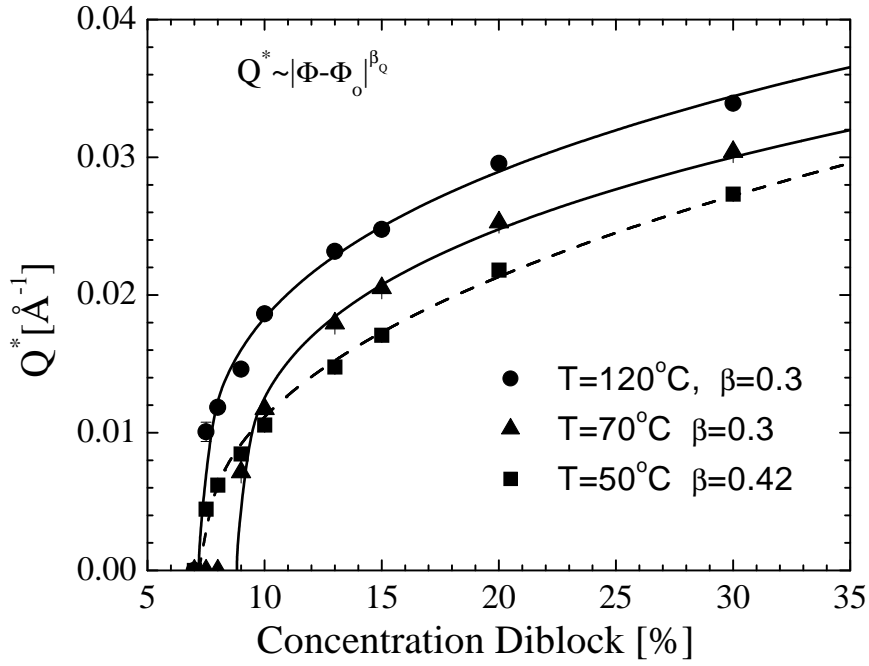


Figure 4.2: Concentration scaling of the peak position $Q^* \sim |Q - Q_{LL}|^{\beta_Q}$ near the disordered Lifshitz line at 120°C (●), near the microemulsion Lifshitz line at 50°C (▲), and near “intersection” of dLL and μ LL at 70°C (■)

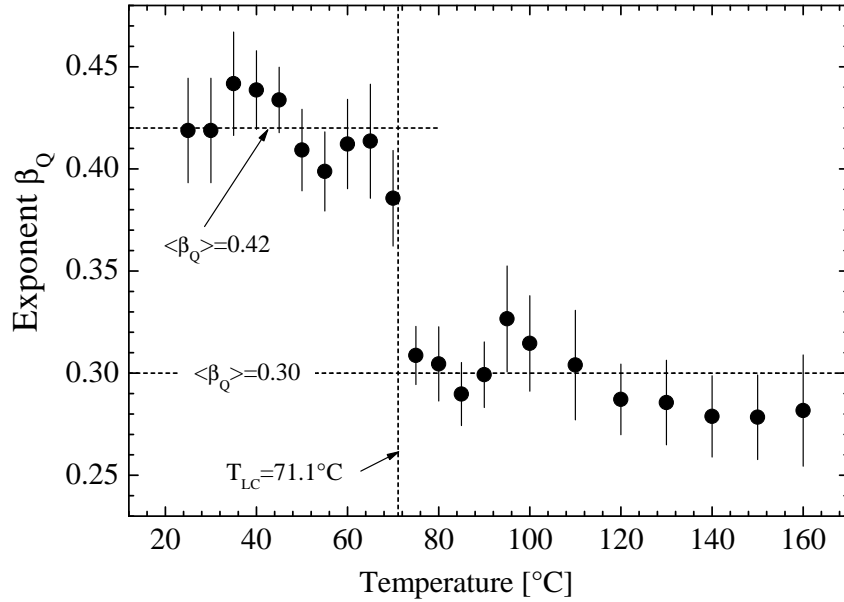


Figure 4.3: The concentration dependence of the β_Q exponent.

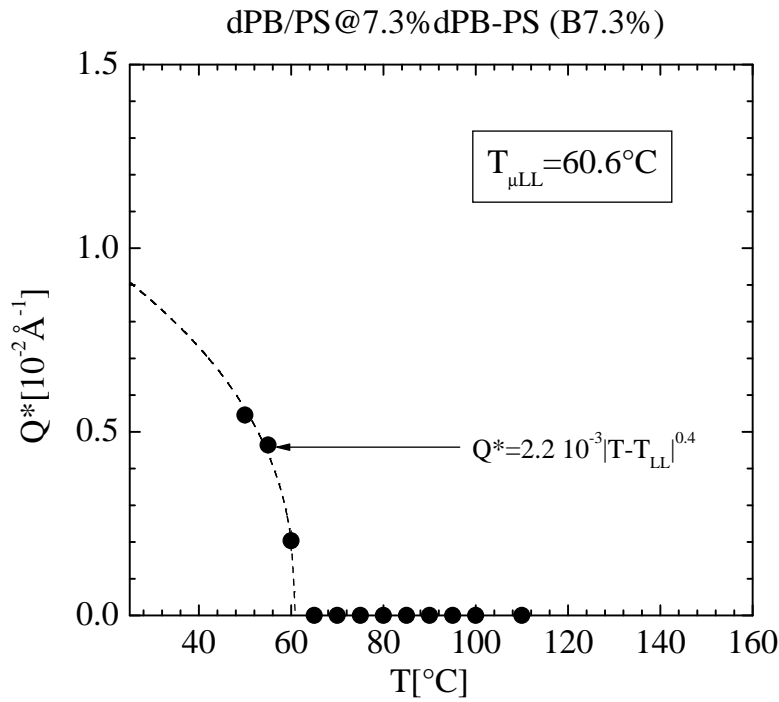


Figure 4.4: *The temperature dependence of Q^* -value near the LL: the 7.3% sample*

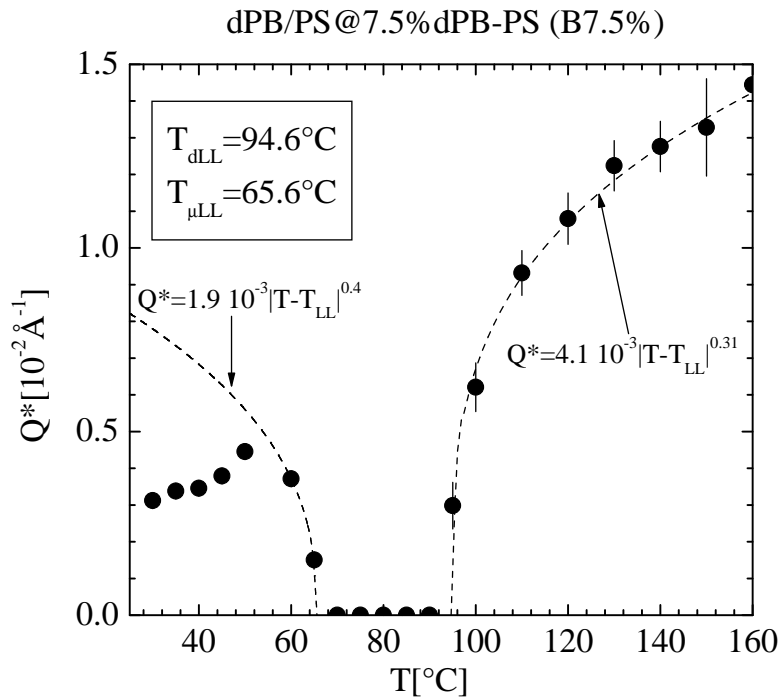


Figure 4.5: *The temperature dependence of Q^* -value near the LL: the 7.5% sample*

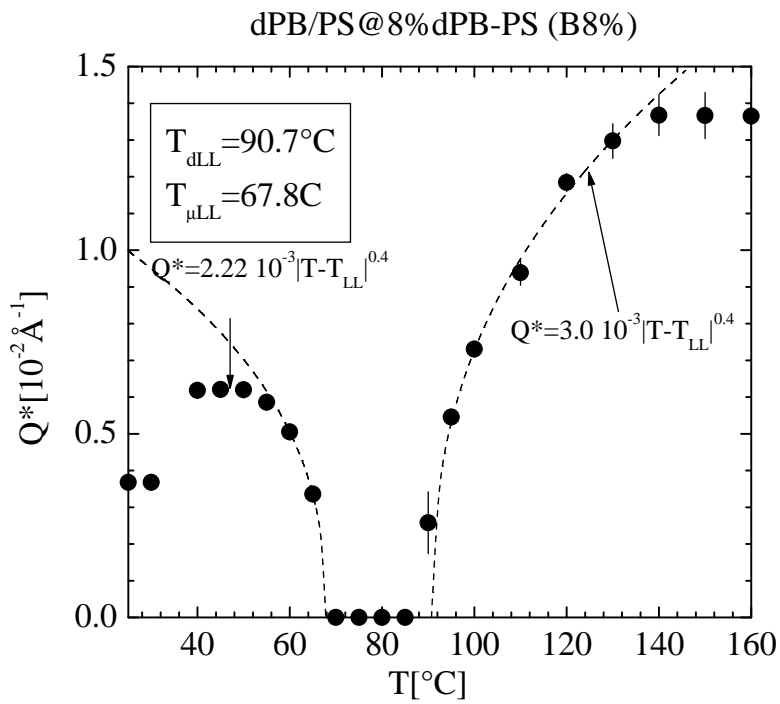


Figure 4.6: The temperature dependence of Q^* -value near the LL: the 8% sample

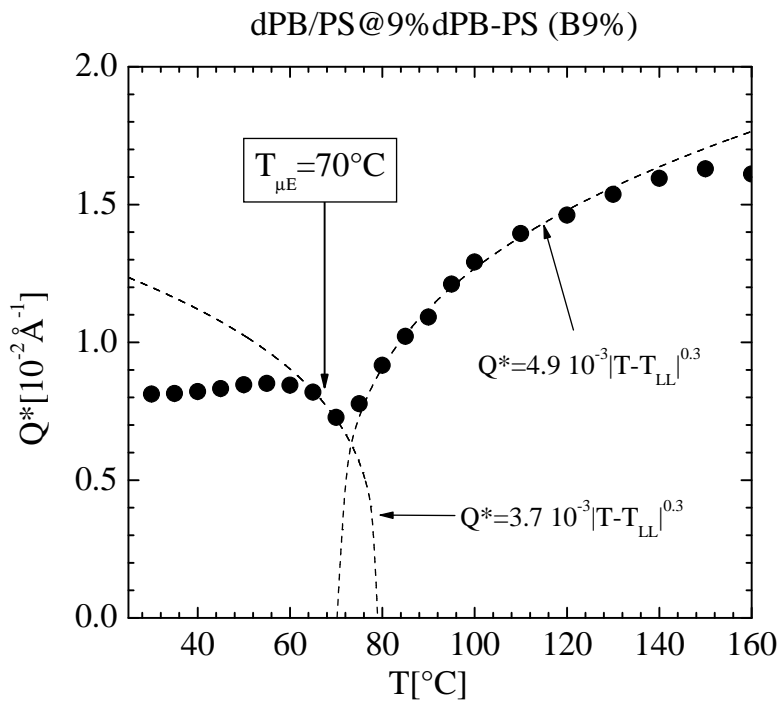


Figure 4.7: The temperature dependence of Q^* -value near the LL: the 9% sample

“microemulsion” Lifshitz line accordingly to (μLL) , while the total line according to LL.

In the disordered phase the appearance of the peak above the dLL is mainly caused by the diblock-diblock structure factor. On the other hand the μLL is the result of cooperative phenomena and represents a transition from a droplet to a bicontinuous microemulsion phase. So, the μLL is caused by the disappearance of the correlation between the microemulsion particles. We already mentioned here that the depicted line does not separate correlated droplets ($d\mu E$) but a bicontinuous microemulsion phase. This will be discussed later in more detail and could only be concluded from measuring samples with different scattering contrasts.

In Fig. 4.9(b) the temperature dependence of the peak position is plotted vs. temperature in block and film contrasts. In both contrasts the Lifshitz lines are located at the same temperatures. The point of intersection of the two Lifshitz lines is a special point of the phase diagram, where two disordered and two microemulsion phases coexist.

According to Brasovskii [70] the transition from a disordered to the lamellar phase is predicted to be first order therefore it is a discontinuous one.

The temperature dependence of the Q^* -values near the LL samples 7.3%, 7.5%, 8% and 9% is shown in Figures 4.4-4.7. At the Lifshitz temperature Q^* becomes 0. The behavior of Q^* near the Lifshitz line can approximately be described by a scaling law $Q^* \sim |T - T_{LL}|^{\beta_T}$ with an exponent β_T being 0.4 and 0.3 when approaching T_{LL} from microemulsion and disordered phases, respectively. The MF approximation predicts a scaling behavior of the peak position vs. temperature in the vicinity of the Lifshitz line with an exponent of 0.4 [18]. The change of Q^* with Φ has been plotted in Fig. 2.4(b), it does not follow simple scaling law over the whole diblock concentration regime. Only near the Lifshitz line a power law behavior with an exponent between 0.3 and 0.4 is predicted depending on the chosen fitting range of the scaling law.

4.1.2 Disorder Line

As mentioned in Chapter 2 the correlation function shows damping oscillations on the right side of the disorder line. From an experimental point of view this line can be detected by SANS. Approaching to DL from the “diblock”-like part of the phase diagram the periodicity length in the system increases, which thus leads to decrease of the maximum position of the scattering profile. The mean field definition of the disorder line is expressed by the structure factor parameters $S^{-1}(0)$, L_2 and L_4 ; exactly at the disorder line the parameter λ_{TS} becomes infinite. The DL was determined from the temperature and concentration dependence of λ_{TS} . In Fig. 4.8 the temperature dependence of λ_{TS} is shown for the 6.6% sample.

A more clear physical meaning of the disorder line can be obtained from the correlations length ξ_{L_2} and ξ_{L_4} . At the disorder line both correlation length

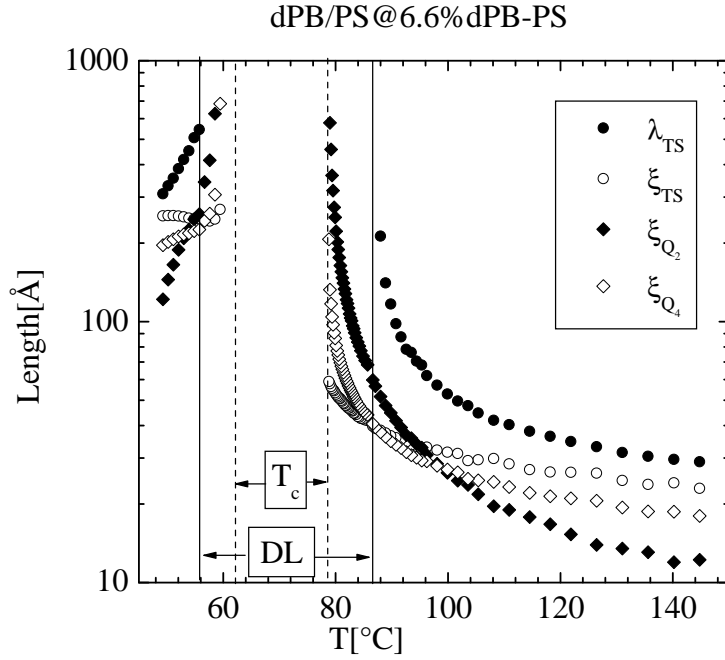


Figure 4.8: The temperature dependence of the different length scale parameters λ_{TS} , ξ_{TS} , ξ_{L_2} and ξ_{L_4} of the sample with $\phi = 6.6\%$ diblock content. Dashed lines limit the two-phase range. Lines are the disorder lines of this sample

becomes equal. In Fig. 4.8 the correlation lengths ξ_{L_2} and ξ_{L_4} are plotted together with other relevant length scales λ_{TS} and ξ_{TS} .

Due to the vanishing of the Q^2 -term of the inverse structure factor $S^{-1}(Q)$ at LL, two correlation lengths, namely ξ_{Q^2} and ξ_{Q^4} , have to be considered. Below 5% the ξ_{Q^2} correlation length dominates in the whole temperature range, $\xi_{Q^2} \gg \xi_{Q^4}$, and the structure factor follows the Ornstein-Zernike approximation. Above 5% diblock content at high temperatures, ξ_{Q^4} , dominates. In decreasing temperature the system crosses the disorder line, where the oscillations of the correlation function vanish. At the DL the two correlation lengths become equal, and below the DL thermal fluctuations are ordered by the diblock copolymer. Below DL thermal fluctuations rearrange the diblock copolymers by accumulating them at their interface.

4.1.3 Microemulsion Phases

A microemulsion channel was detected between the two-phase and lamellar ordered phase in the dPB/PS/dPB-PS system between $\Phi = 6\%$ and 13%. The

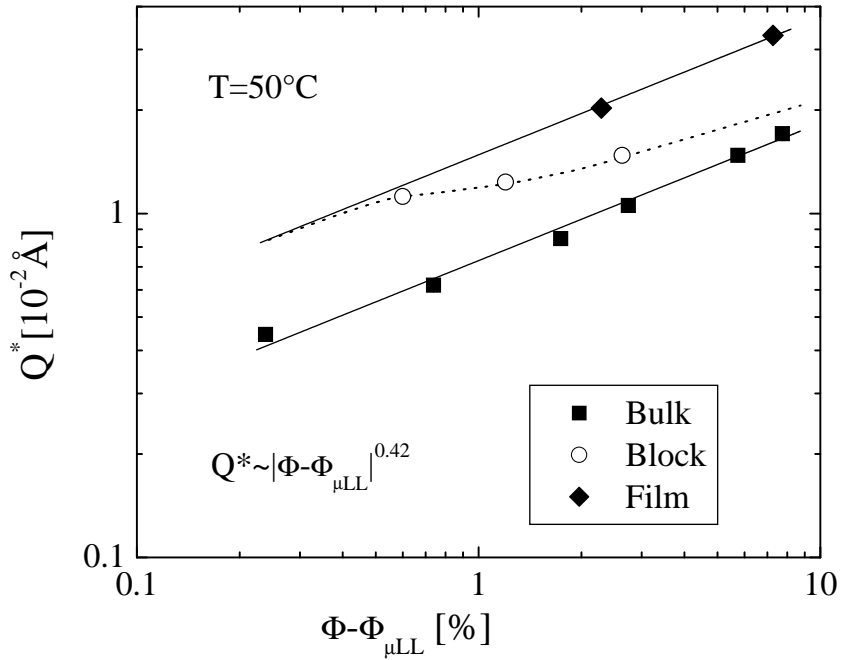


Figure 4.9: Q^* -scaling vs. the reduced copolymer concentration: film, block and bulk contrasts

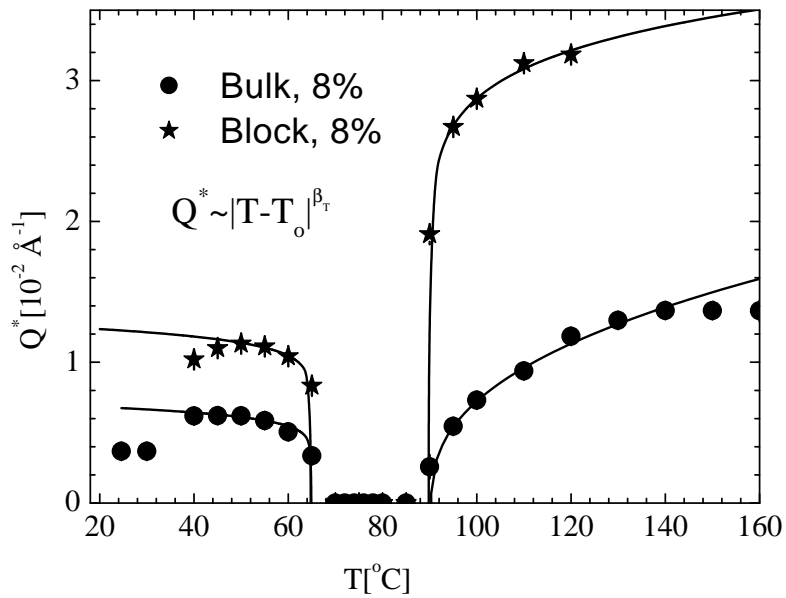


Figure 4.10: The temperature dependence of Q^* for the 8% sample in the bulk and block contrast

polymeric microemulsion phase represents a transparent, slightly Raleigh scattering colored melt. The word “channel” has in mind the continuous transition from the disordered “diblock” phase to the bicontinuous microemulsion phase [19]. In the present study three boundaries are present as shown in the phase diagram of Fig. 4.1. The microemulsion channel should be mapped on the phase diagram by the borderline with

- disordered phase
- lamellar ordered phase
- two-phase.

The transition from the bicontinuous microemulsion to the two phase region is more complex. Between these phases a droplet microemulsion phase could be identified. The droplet-bicontinuous boundary was already discussed in context with the Lifshitz and disorder lines.

Contrast variation technique allows to identify the phase on the right side of the microemulsion Lifshitz line of bicontinuous type. In Fig. 4.9 the peak positions Q^* vs. diblock concentration distance to the Lifshitz line ($\Phi - \Phi_{\mu LL}$) at $50^\circ C$ are plotted as measured in bulk, block and film contrasts in double logarithmic scale. On the right side of the Lifshitz line the peak positions of the film and bulk contrast samples in their ordered states (lamellar and microemulsion) scales with exponent 0.42 in consistence with the results in Fig. 4.3. A indication of a bicontinuous microemulsion phase is the two times difference in the amplitude of the scaling laws. That means at the same distance from the Lifshitz line the peak position of the samples with film contrast was twice as large as from the bulk contrast ones. This is because the periodicity in film and bulk contrasts has factor of two difference.

The block contrast sample represents an intermediate case between film and bulk contrasts. Above $\Phi = 20\%$ of diblock content bulk and block contrasts have the same peak position because the periodicity of blends is comparable with the end-to-end distance of the copolymer; the homopolymers are just swelling the lamellar phase. Another situation appears in the bicontinuous microemulsion. The microemulsion phase is characterized by a characteristic size much larger than the radius of gyration of the matched blocks of the copolymer. At this conditions the peak position in the block contrast approaches to film contrast conditions.

4.1.4 Temperature Induced Disorder–Microemulsion Transition

In the phase diagram Fig. 4.1 two temperature induced transitions from disorder to microemulsion phase are shown: right and left from LL.

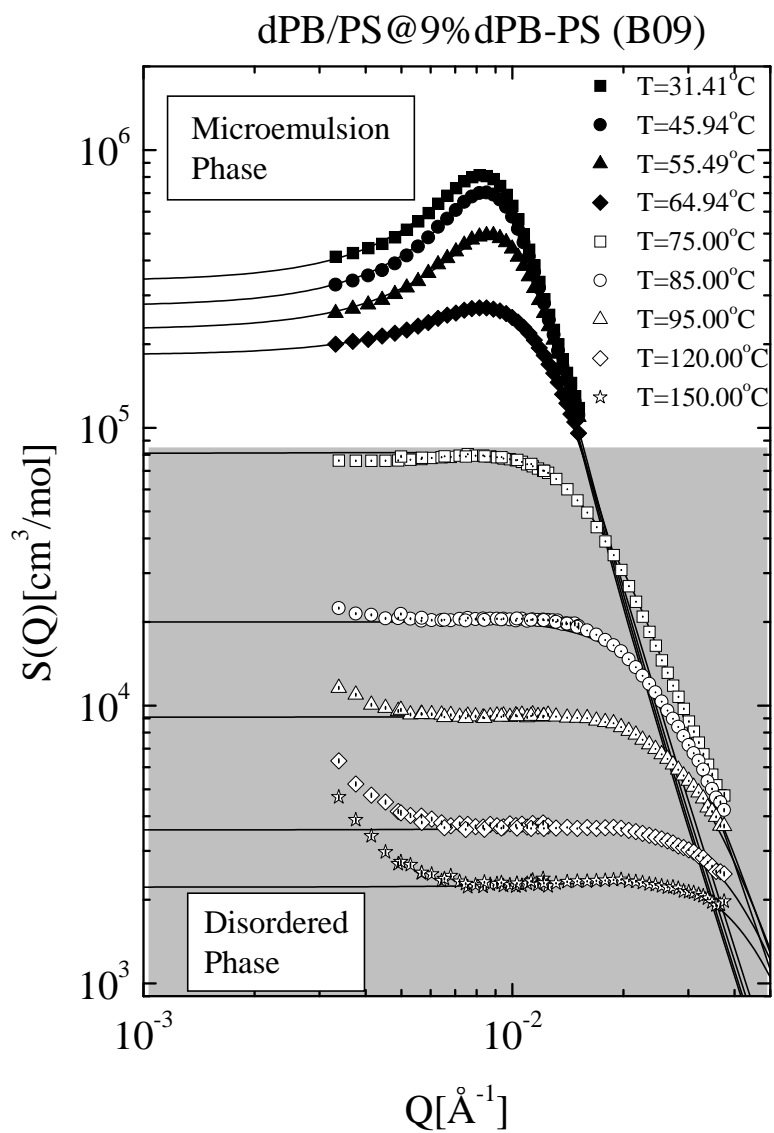


Figure 4.11: *B09%*: Temperature induced bicontinuous microemulsion formation. The lines represent fits accordingly to Eq. 2.3

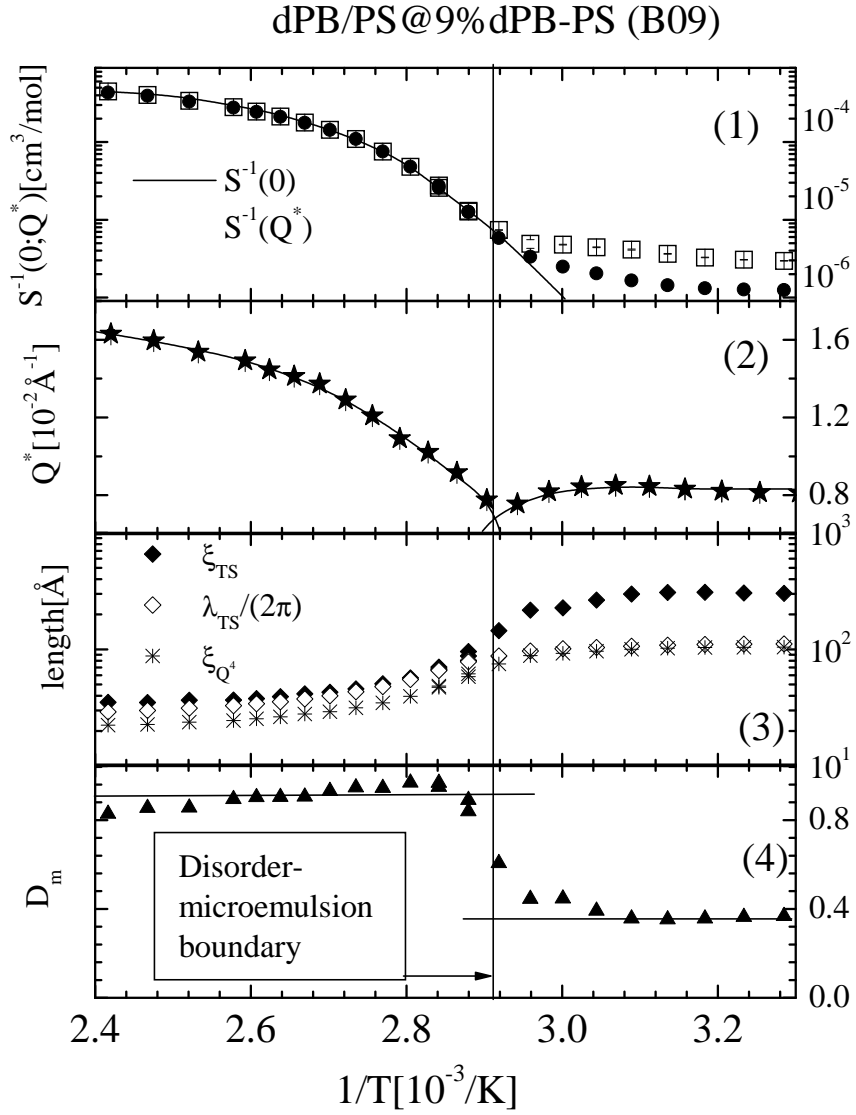


Figure 4.12: B09%: Temperature induced bicontinuous microemulsion formation. The temperature dependence of the parameters: (1):the susceptibilities $S^{-1}(0)$ and $S^{-1}(Q^*)$, (2): the peak position Q^* ; (3) the TS-periodicity λ_{TS} , the TS-correlation length ξ_{TS} , the Q^4 -correlation length ξ_{Q^4} ; (4) the disorder parameter D_m

On the left side from the Lifshitz line a transition from the disordered state to the droplet microemulsion phase is shown by the filled triangles. The structure factors measured above and below this borderline have their maximum at $Q = 0$. This line is plotted at temperatures, where the susceptibility has a maximum value as shown in Section 5.3.

On the right side of the LL, in the diblock-like part of the phase diagram the disorder-bicontinuous microemulsion boundary is plotted at a position where the structure factor changes its behavior. In Fig. 4.11 the structure factors of the ternary blend with 9% diblock content are shown for several temperatures. The structure factors were fitted by Eq. 2.3 taking into account resolution effects as described above in theory section. Parameters of the fit, namely the susceptibility ($S(0)$ and $S(Q^*)$), the peak position (Q^*), the length scales (ξ_{Q^4} , ξ_{TS} , λ_{TS}) and the disorder parameter D_m , are depicted at the Fig. 4.12(1-4). Plotted properties shows a different behavior in disordered and bicontinuous microemulsion phases separated by the line in Fig. 4.12.

The susceptibility $S(Q^*)$ continuously changes from disordered to microemulsion phase in contrast to $S(0)$. Above and below $T = 69^\circ C$ the “0-susceptibility” shows a distinguished temperature behavior.

The peak position has a different nature above and below the microemulsion borderline. Above the disorder-microemulsion boundary the existence of a peak in the structure factor is caused by the diblock-diblock structure factor. Below the microemulsion boundary diblock copolymers are distributed on the homopolymer-homopolymer interface. In microemulsion phase the peak of the scattering curve is caused by an alternative distribution of PB- and PS-homopolymer.

The correlation function ξ_{Q^4} demonstrates two different behavior at high and low temperature. The Teubner-Strey and “ Q^4 ”-correlation length have the same temperature behavior, as one can see in Fig. 4.12(3). In disordered phase the decreasing of the temperature increases the correlation length. Bicontinuous microemulsion phase is characterized by an approximately temperature-independent correlation length.

4.1.5 Lamellar - Bicontinuous Microemulsion Transition

Between $\Phi = 10\%$ and 13% we identified the boundary between the lamellar ordered phase and the bicontinuous microemulsion phase. This transition has a first order nature. From the SANS measurements the susceptibility $S^{-1}(Q^*)$ and the peak position Q^* change continuously from lamellar phase to bicontinuous microemulsion phase. The peak positions Q^* in different contrasts at $50^\circ C$ are shown in Fig. 4.9 and no indication of the transition is visible. The distinction of the ordered lamellar phase is the appearance of a second order peak and a jump of the susceptibility indicating a first order disorder-order boundary. Clearly, one can see in the Fig. 4.13 the second order peak at $Q^* = 2Q^*$ for 13% of the diblock

content and no second order peak for 10%.

4.1.6 Order-Disorder Transition of the Diblock Copolymer melt

The order-disorder transition of the symmetric copolymer dPB-PS melt was also studied in “bulk” and “block” contrast. The characteristics of the diblock copolymers are listed in Table 3.1. The diblock copolymer melt dPB-PS with a molecular volume $15400\text{cm}^3/\text{mol}$ has already been under investigation in early studies [71, 72]. There the temperature dependence of the scattering profile was measured at different pressure field and solvent [73]. In Fig. 4.15 the temperature dependence of the structure factor, the susceptibility and peak position of this diblock copolymer are shown. The copolymer melt has a disorder-order transition at 69.4°C . As the diblock copolymers is symmetrical the ordered phase has a lamellar structure.

A melt with triblock copolymers dPB-PB-dPB was also measured and was used for film contrast measurements. The protonated PB-part of the triblock copolymers occupies roughly 6% of the copolymer volume. The structure factor of triblock copolymers is discussed in Sec. 4.3 and their peak positions vs. temperature are displayed in Fig. 4.15 together with the peak position of the diblock copolymer dPB-PS. With temperature an overall increase of Q^* is observed indicating a chain stretching with decreasing temperature.

A clear disorder-order transition is visible from a sudden change of Q^* for the sample under film contrast. At the T_{ODT} the copolymer appears slightly relaxed by the ordering process. This decrease of length could also be a result of the ordering and not from the chain itself, this effect is not visible in the “bulk” melt.

The periodicity of the ordering to the lamellar phase appears in two respects different in bulk and film contrast. The peak position Q^* of the structure function of the triblock copolymer melt dPB-PB-dPS should be twice as large as in the dPB-PS case of equal molecular volumes. In Fig. 4.15 by stars are depicted twice as larger Q^* of diblock copolymer melt dPB-PS corrected to difference of molecular volumes between diblock and triblock copolymers.

In the ordered phase a factor of two difference for the peak positions for bulk and film contrast is evident.

4.1.7 Ordering Transition in A/B/A-B Blend

The analysis of the structure factor $S(Q)$ measuring thermal composition fluctuations in the disordered state of the three component polymer mixture was mainly performed on the basis of the formalism developed by Kielhorn and Muthukumar [74]. This theory takes the effects of thermal fluctuations into consideration,

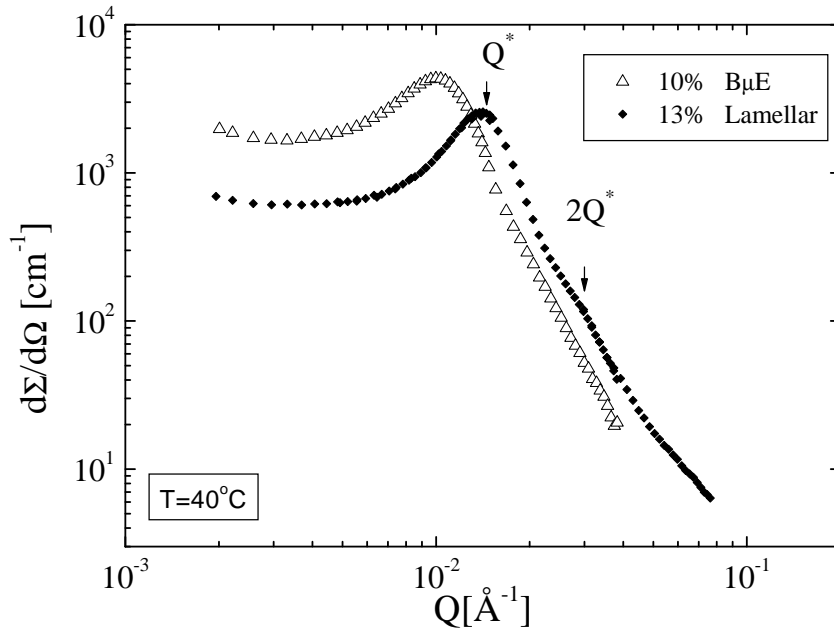


Figure 4.13: *The scattering profile of the 10% and 13% samples, in the bicontinuous and lamellar phase, respectively, at $T = 40^\circ\text{C}$*

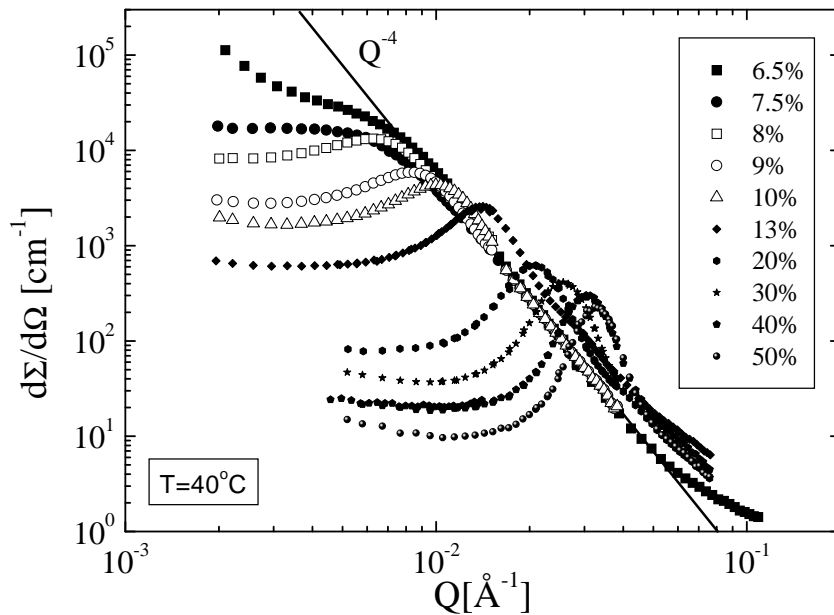


Figure 4.14: *The scattering profiles at $T = 40^\circ\text{C}$: two-phase, droplet, bicontinuous, lamellar phases*

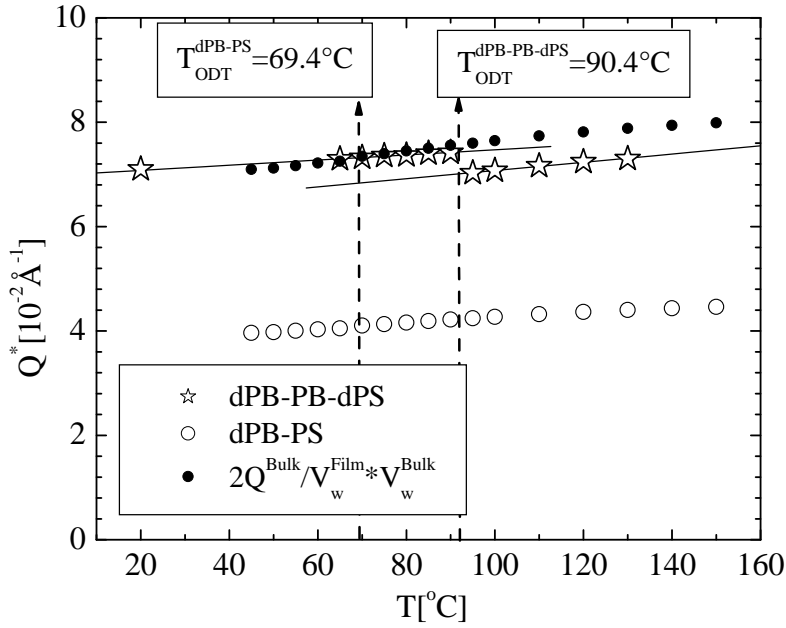


Figure 4.15: *The position of the maximum intensity Q^* vs. temperature: dPB-PS(\circ) and dPB-PB-dPS (\star), the filled circles (\bullet) being the twice large position of maximum of diblock copolymer (\circ) corrected to the different volume of diblock and triblock copolymers.*

as was reviewed in the theoretical part. For samples with diblock concentrations larger than the Lifshitz line with the maximum of $S(Q)$ occurring at a finite Q , the most general application started with the analysis of $S(Q)$ by Eq. 2.44 (see solid lines in Fig. 4.16), which for each equilibrium state delivers four parameters, namely, a , b , c , d . Based on these four values and their expressions, the FH-parameter, the Ginzburg parameter, and the statistical segment length were calculated for each temperature. The obtained FH-parameter has been listed in Table 5.2.

4.1.8 Phase Diagram in Different Contrasts

In order to better understand the role of diblock copolymers in a binary melt of homopolymers the contrast variation method was used. Most of the investigations of the ternary blend PB/PS/PB-PS were carried out in “bulk”-contrast using the dPB/PS/dPB-PS blend, when the fluctuations of only one polymer component were made visible to SANS.

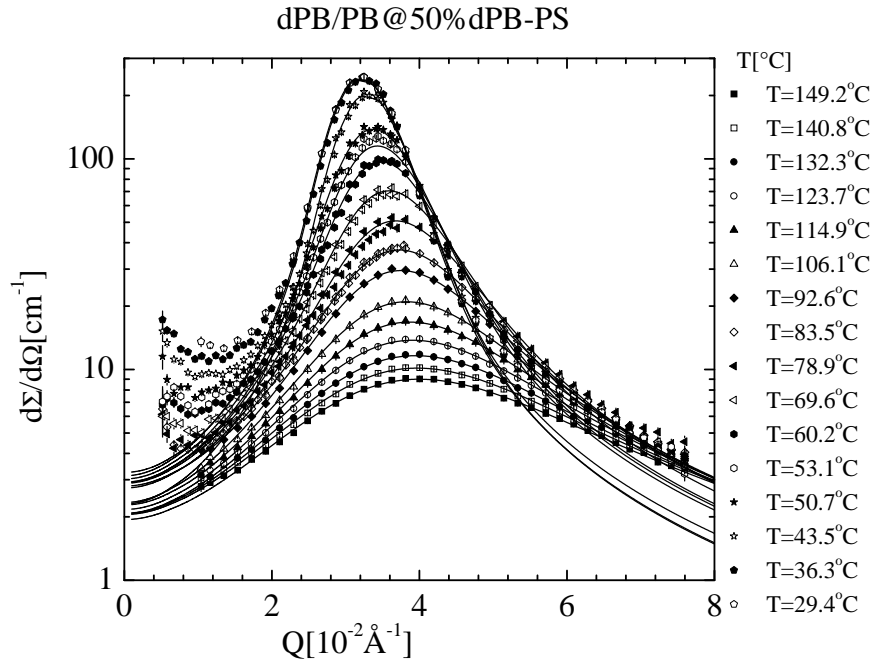


Figure 4.16: The scattering profile of the 50% sample at different temperatures. The solid lines represents a fit of the structure factor by Eq. 2.44

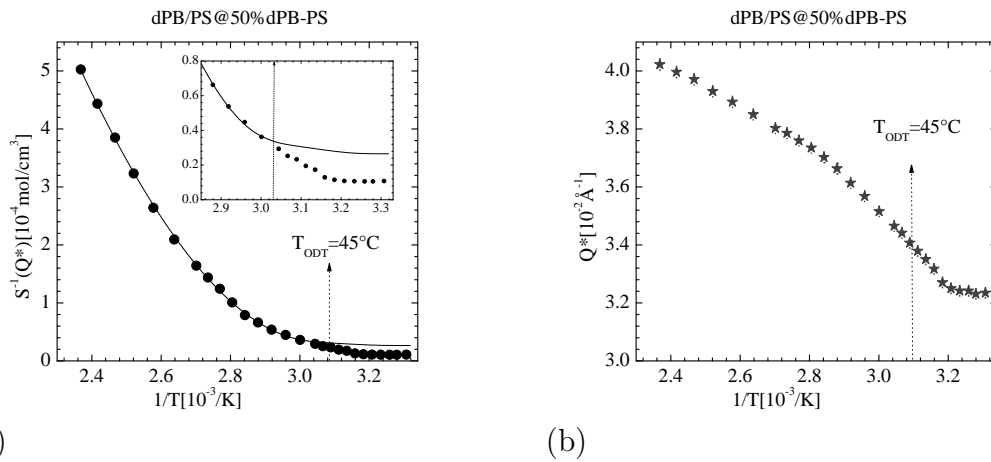


Figure 4.17: The susceptibility $S^{-1}(Q^*)$ and the peak position Q^* vs. inverse temperature $1/T$

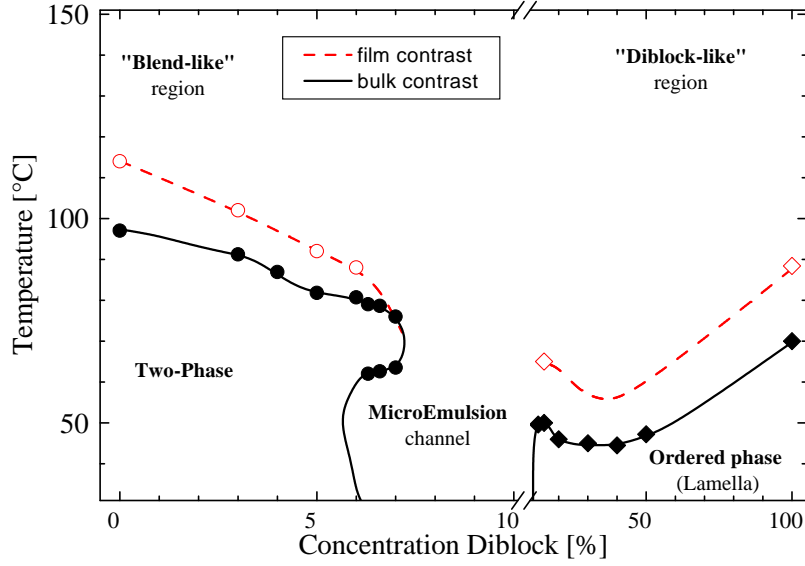


Figure 4.18: *Phase diagram: the bulk (solid lines) and film contrast (dashed lines)*

The scattering length density of investigated polymers are listed in Tables 3.1 and 3.2. Deuterated polybutadiene and deuterated polystyrene have approximately the same scattering length density, thus in the ternary system of dPB/dPS/dPB-PS only the polystyrene block of the diblock copolymers is visible. Isotopical exchange has some influence on the Flory-Huggins parameter and leads to a shift of the phase transition as well as critical temperature. A similar situation is met for isotopical exchange of diblock copolymers.

In addition a slightly different chain length can also have some influence on the phase transition line. In Fig. 4.18 for comparison the phase boundaries of the PB/PS/PB-PS blends in “bulk” and “film” contrasts are depicted. The “film” contrast samples always shows a phase transition lines between 10 and 20K above “bulk”. In the limiting cases of $\Phi = 0$ and $\Phi = 1$ the exchange of the homopolymer and diblock copolymers is the responsible one, respectively.

Due to the vanishing scattering contrast between dPB and dPS we were not able to measure the critical solution point by SANS. Instead the cloud points below the Lifshitz line were determined by turbidity measurements. This method of determination of the critical temperature is not so precise as SANS, but allows a sufficient precise estimation of T_c . In both blends the components dPS and PS have an approximately identical molecular volume. Therefore, the shifting of the critical temperature is mainly caused by a variation of the FH parameter due to

the exchange of deuteration.

With the increase of diblock copolymer content the differences between the critical temperatures of bulk and film contrast samples are reducing and the microemulsion channel seems not to be affected from reasons we presently do not understand.

The phase boundaries of the “block” contrast sample is not plotted in this graph. But for obvious reasons, their line of critical points follows the same one as the “film” contrast one, as the homopolymer blend is identical, while the order-disorder borderline follows the bulk contrast sample, since the diblock copolymer was not changed.

4.2 Critical Exponents and Crossover

In this section the behavior of thermal composition fluctuations in the disordered regime below the Lifshitz line is discussed in terms of critical exponents of the susceptibility and the corresponding correlation length as obtained from asymptotic scaling laws.

4.2.1 Ising Critical Behavior

Below $\Phi = 5\%$ the critical behavior of the investigated ternary blend behaves similarly to binary homopolymer blends. The structure factor of thermal fluctuations follows to the Ornstein-Zernike approximation. In Fig. 4.19(a-c) the structure factor of three samples with diblock content less 5% are plotted for several temperatures in the Zimm representation $S^{-1}(Q)$ vs. Q^2 . In the range of small Q the inverse structure factor $S^{-1}(Q)$ is fitted by a line in Zimm representation. Below $\Phi = 5\%$, the 0%, 3% and 4% samples were fitted by the OZ-equation with the susceptibility $S^{-1}(0)$ and the correlation length ξ_{Q^2} as adjustable parameters.

At the binodal temperature the susceptibility $S(0)$ has a maximum. The spinodal temperature can be determined by the approximation of the inverse susceptibility by a scaling law to an infinite value. At the critical point (critical concentration) the binodal and spinodal temperatures are equal.

One can see from Fig. 4.22(a) the binary blend dPB/PS with concentration of PB $\phi = 0.42$ is not the “critical” blend, i.e. the concentration is a little bit off-critical. For the blend B0% the distance between binodal and spinodal is 1.4K. The diblock copolymer additive decreases the critical concentration, and above 3% of diblock content the phase separation goes with spinodal decomposition, as shown in Fig. 4.22(b) for the 3% sample.

The crossover behavior from mean field to 3D-Ising of three samples is fitted by the Belyakov-Kiselev and Anisimov crossover models with a single crossover length parameter. The fits are shown in Fig. 4.20 and Fig. 4.22. An advantage of the Anisimov model is the possible simultaneously fit of the correlation length and susceptibility with the same parameters of the crossover function. But, as one can see from Fig. 4.20 the correlation length is fitted by the simple scaling law $\xi_0 t^{-0.63}$ in whole temperature range. The results of the fits and the evaluated parameters are listed in Table 4.1.

The critical temperatures (spinodal temperature for the blend) of the samples were plotted by filled circles in the phase diagram (Fig. 4.1).

So, small diblock additions ($\Phi < 5\%$) do not change the universality class but lead to an improved compatibility and to a sharp increase of the Ginzburg number. This is shown in Fig. 6.4 where the increase of the Ginzburg number with diblock concentration is demonstrated. The Ginzburg number was extracted from analyzing the susceptibility with the Belyakov-Kiselev crossover function.

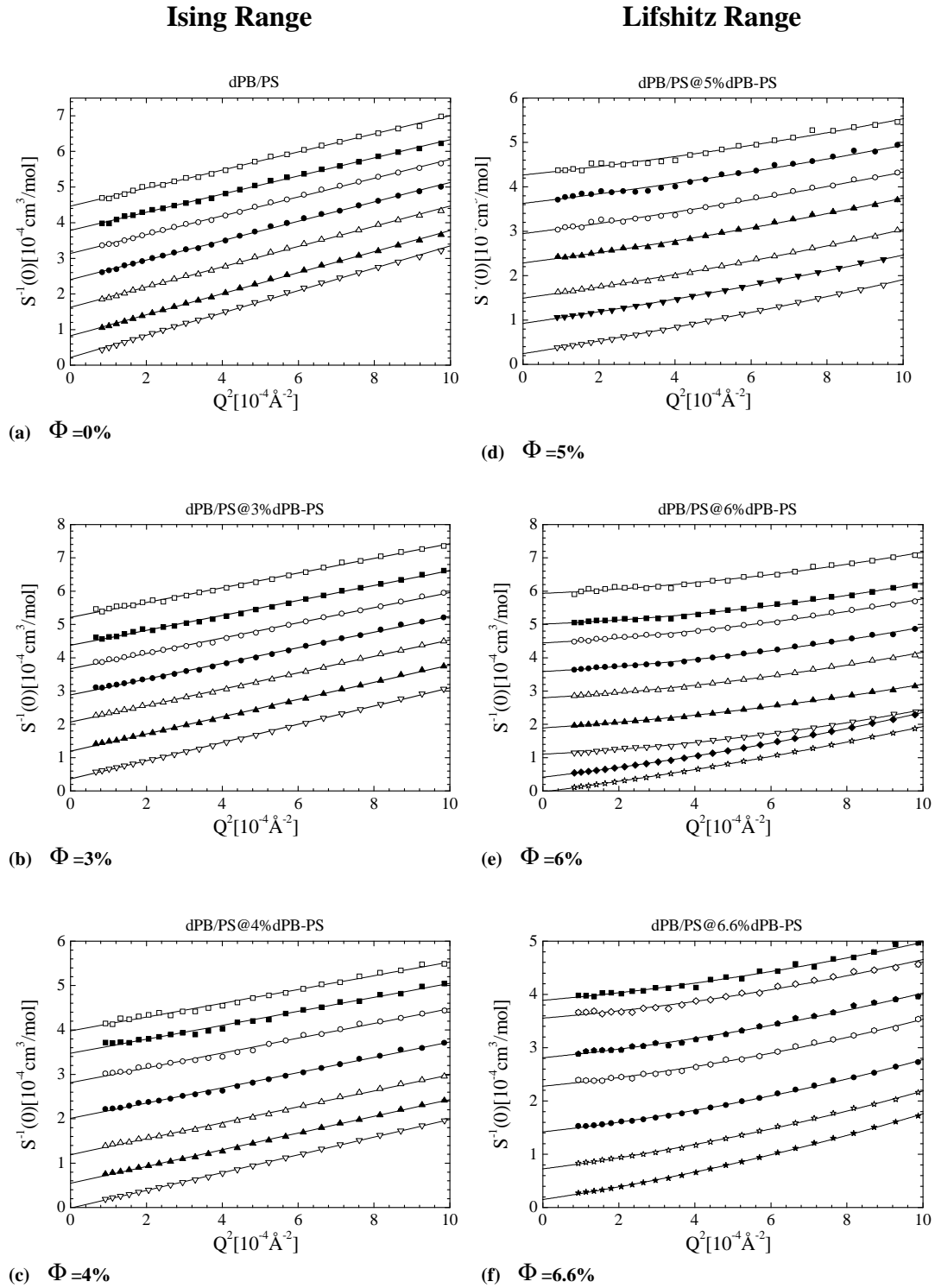


Figure 4.19: Structure factor in Zimm representation below LL . Below 5% (a,b,c) $S(Q)$ follows the Ornstein-Zernike law, but above 5% (d,e,f) contributions from the Q^4 term becomes visible

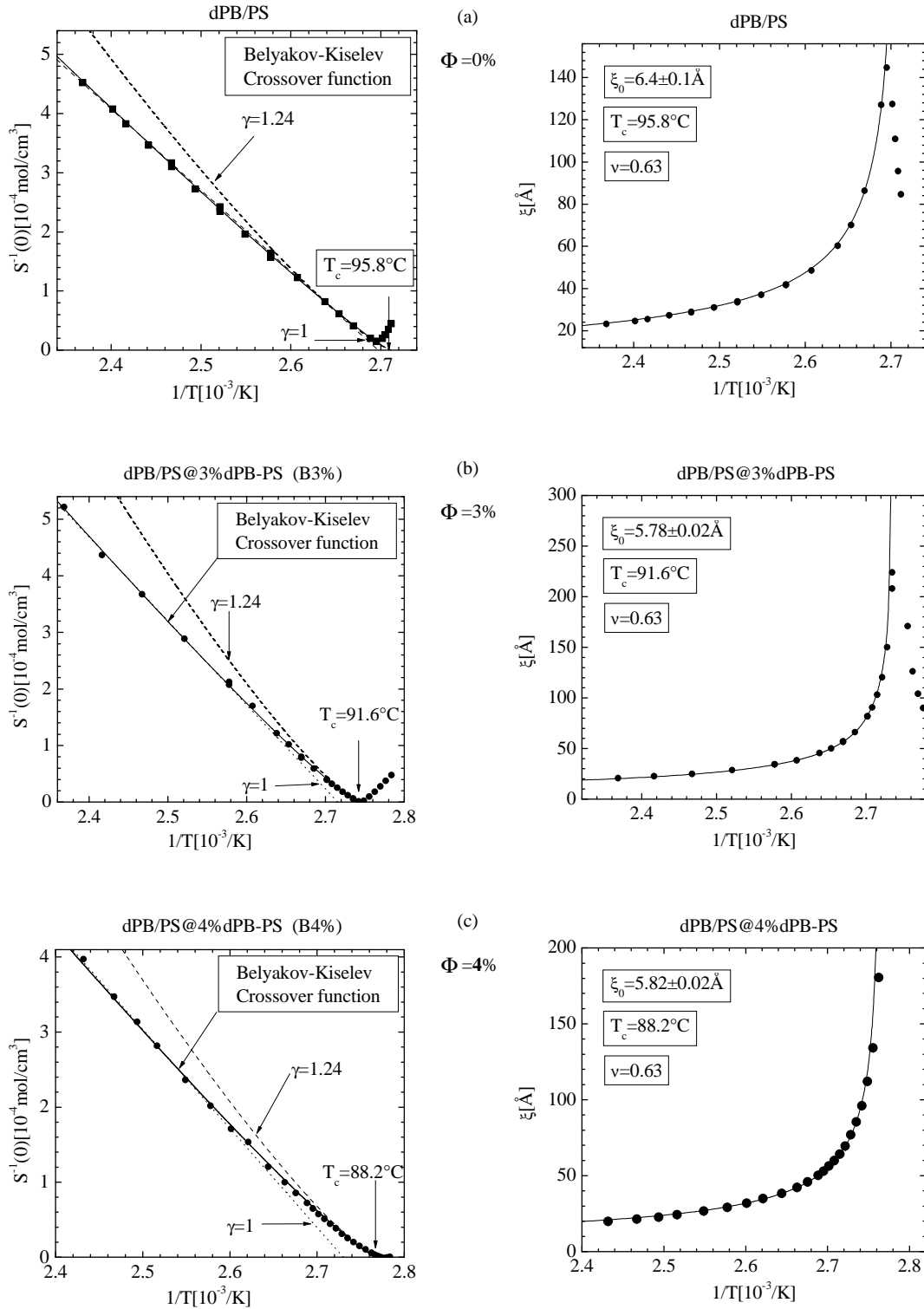


Figure 4.20: *The inverse susceptibility $S^{-1}(0)$ and the correlation length ξ_{Q^2} vs. inverse temperature $1/T$ in Ising regime of the critical behavior. (a): B0% (homopolymer blend); (b): B3%; (c): 4%. Lines are fits of $S^{-1}(0)$ and ξ_{Q^2} by Belyakov-Kiselev crossover model and simple scaling law $t^{-\nu}$, respectively*

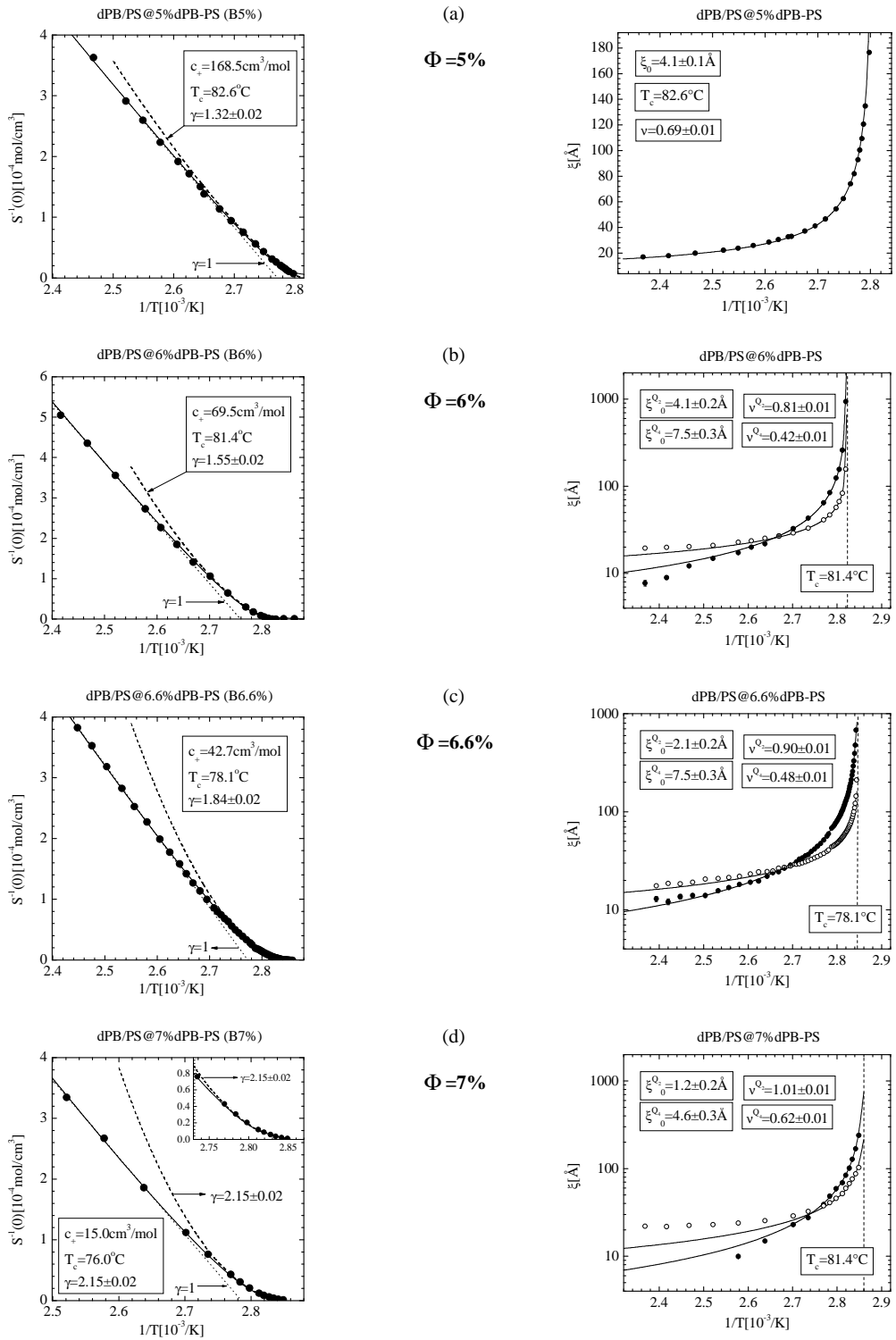


Figure 4.21: The inverse susceptibility $S^{-1}(0)$, the correlation lengths ξ_{Q^2} and ξ_{Q^4} vs. inverse temperature $1/T$. (a): 5% ; (b): 6% ; (c): 6.6% ; (d) 7%.

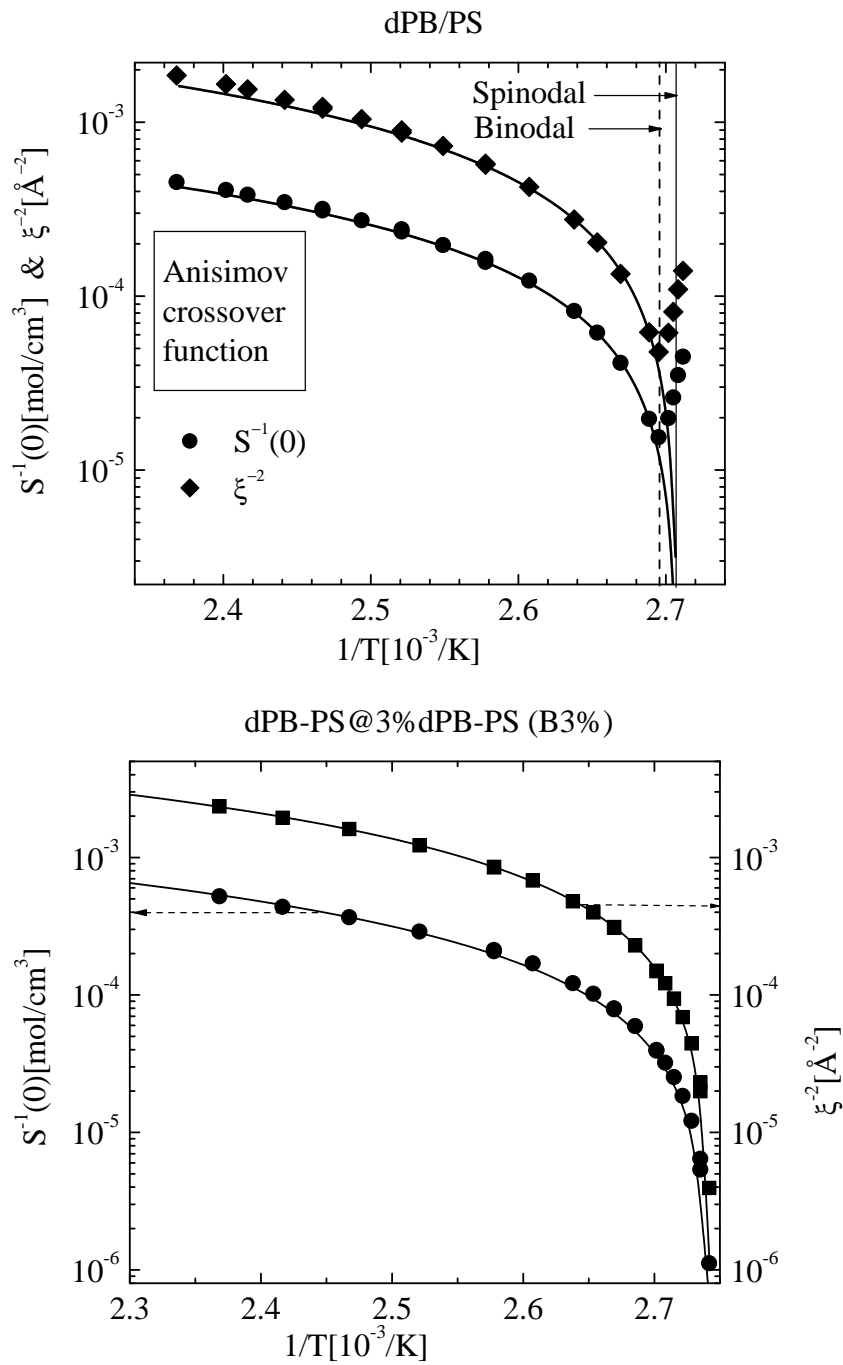


Figure 4.22: The inverse susceptibility $S^{-1}(0)$ and the correlation length ξ vs. temperature T . (a): B0% (binary blend); (b): B3%. Lines are simultaneous fits of ξ and $S^{-1}(0)$ by Anisimov crossover model

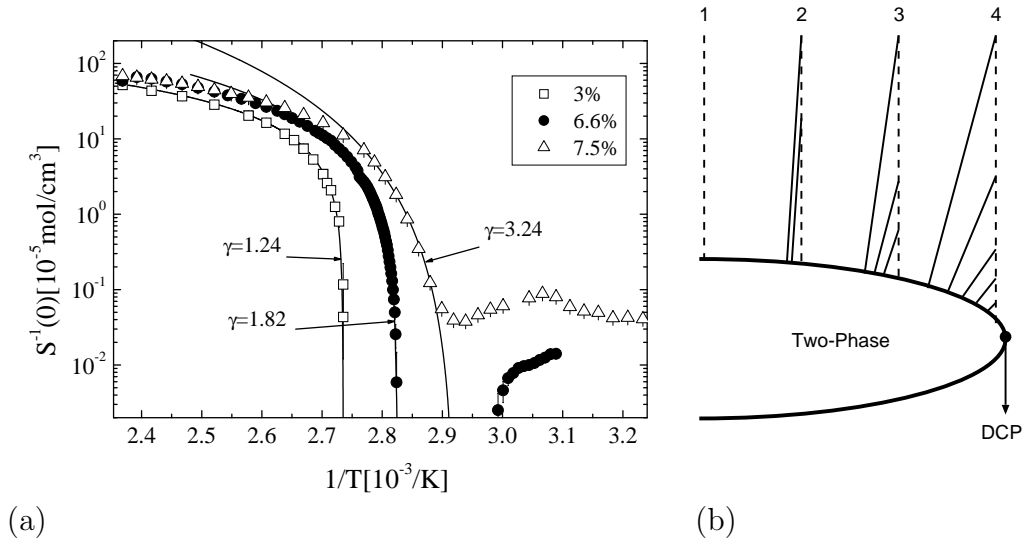


Figure 4.23: (a): The temperature dependence of the susceptibility: 3%, 6.6% and 7.5% diblock copolymer content. (b): A schematic explanation of the tangential approach to the double critical point

4.2.2 Lifshitz Critical Behavior

Above 5% of diblock content (in the phase diagram separated by the grey box) the critical behavior of the samples differs from the homopolymer blend.

(i) The structure factor of the thermal fluctuations cannot be fitted by OZ-approximation. In Zimm presentation the structure factor has some curvature. The structure factor above 5% was fitted by Eq. 2.3, as shown in Fig. 4.19(d)-(e) for 6%, 6.6% and 7%. From the fit the susceptibility $S(0)$, the correlation lengths ξ_{Q^2} and ξ_{Q^4} are extracted.

(ii) The critical exponents differ from the 3D-Ising, as the critical exponents of the susceptibility and correlation length increase. The critical exponents of the susceptibility γ and correlation length ν_{Q^2} (ν_{Q^4}) are plotted in Fig. 4.24. The susceptibility and correlation length were fitted by the scaling laws $C_0^+ \tau^\gamma$ and $\xi_0^+ \tau^\nu$ with the reduced temperature $\tau = \tau_U = |T_{UCST} - T|/T$. The circles represent these exponents. As one can see, above 5% the exponents grow continuously with diblock content. The critical exponent of the susceptibility increases from 3D-Ising value at 4% to 3.24 at 7.2%; simultaneously, the critical exponent of the correlation length from 0.63 to 1.82.

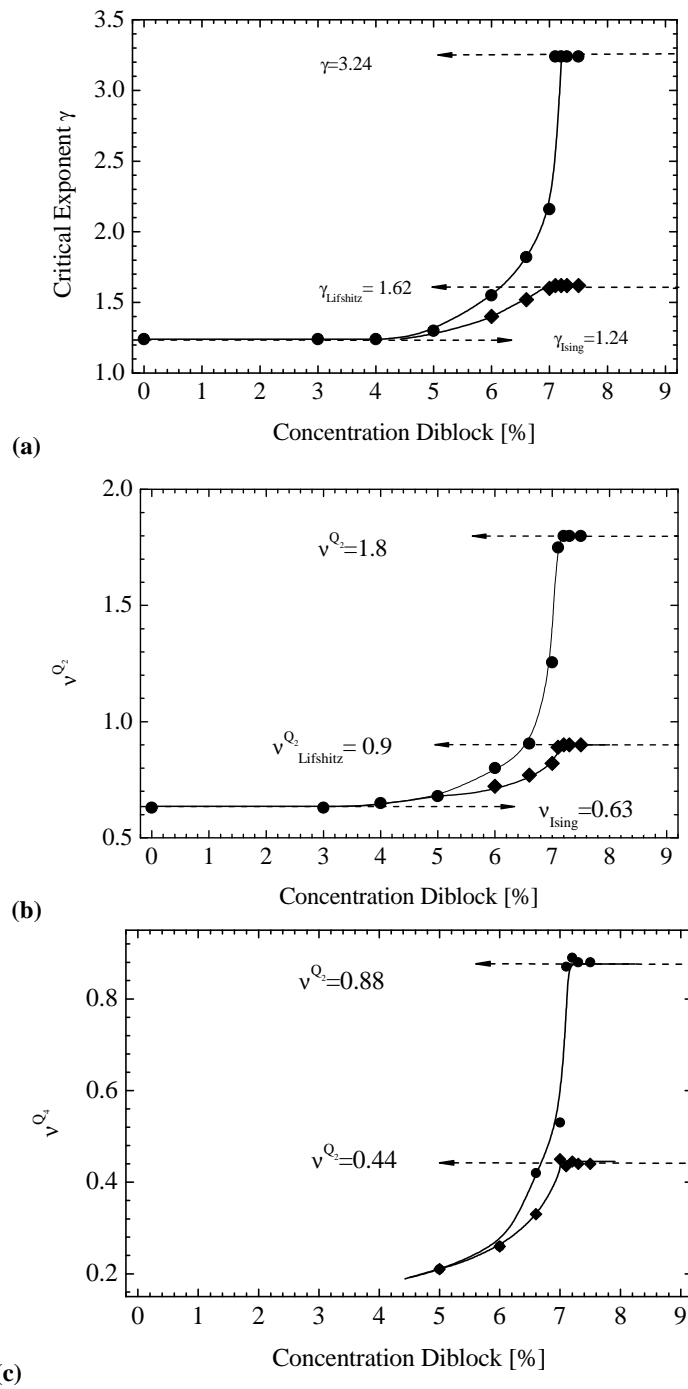


Figure 4.24: The critical exponents of the susceptibility γ (a) and correlation length ν_{Q^2} (b) and ν_{Q^4} (c)

4.2.3 Reentrance Behavior and Double Critical Point

A surprising observation is the reentrance coexistence phase near the Lifshitz line between 6% and 7.2% of diblock content. In this range the two-phase region is limited by the upper and lower critical solution temperatures T_{UCST} and T_{LCST} , respectively. In Fig. 4.23(a) at T_{UCST} and T_{LCST} the inverse susceptibility of the 6.6% sample is zero. The temperature gap of the immiscibility $\Delta = |T_{UCST} - T_{LCST}|$ decreases from 15K at $\phi = 6.6\%$ to zero degree at the double critical point (DCP). At the double critical point at $\phi_{DCP} = 7.2\%$ and $T_{DCP} = 71^\circ\text{C}$ the two-phase region shrinks to a point. As we know this is the first observation of a double critical point in polymeric systems within the Lifshitz universality class.

At a double critical point theories generally predict twice as large critical exponents in comparison with the corresponding ordinary values [75, 76]. The doubling of the critical exponents can be understood from the tangential approach (constant diblock concentration) to the critical point and the quadratic nature of the critical line [77] as schematically shown in Fig. 4.23(b). In ternary systems an isopleth is not a critical path because of a temperature dependent critical line (Scott line). The critical path is perpendicular to the Scott line. Therefore, at the double critical point the critical path is the critical isotherm.

Thus, above 5% the critical behavior near the upper critical point is different from 3D-Ising systems due to the approach to a Lifshitz line and a double critical point.

In the mixture 3-Methylpyridine/Water/Heavy Water Prafulla et al. [76] analyzed a double critical point within the 3D-Ising universality class with a newly defined reduced temperature considering both critical temperatures according to

$$\tau_{UL} = \frac{|(T - T_{UCST})(T - T_{LCST})|}{T^2} \quad (4.1)$$

from which they derived the effective exponent $\gamma = 1.24$ in accordance with the 3D-Ising model. So, we reexamined the temperature dependence of the susceptibilities and correlation length by the scaling law with the newly defined reduced temperature $t = \tau_{UL}$.

The filled diamonds in Fig. 4.24 correspond to the critical exponents approaching the double critical point corrected to the “not-perpendicular” approach to the critical line. We found a continuous increase of the critical susceptibility (correlation length) exponent from the Ising γ_{Ising} (ν_{Ising}) to so-called isotropic Lifshitz critical exponent $\gamma_{Lifshitz} = 1.62$ ($\nu_{Lifshitz} = 0.92$). Both open symbols in Fig. 4.24 correspond to the critical exponents at the DCP. The obtained $\gamma_{Lifshitz} = 1.62$ and $\nu_{Ising} = 0.92$ are consistent with the corresponding number derived in an earlier study [18].

The parameters of scaling laws are listed in Table 4.2 for the samples between $\Phi = 5\%$ and 7% .

Table 4.1: *Fitting results of the temperature dependence of the susceptibility and correlation length in quasi-binary system (“blend-like” range of phase diagram) by Belyakov-Kiselev and Anisimov crossover function*

Parameter		B0%		B3%		B4%	
		An	BK	An	BK	An	BK
T_c	[$^{\circ}C$]	96.2	95.8	91.9	91.6		88.2
T_c^{MF}	[$^{\circ}C$]	97.5	97.5	95.2	95.2		93.5
Gi	[10^{-2}]	0.34	0.44	0.5	0.98		1.451
c_+^{MF}	[cm^3/mol]	287	221	249	195.6		218
c_+	[cm^3/mol]	139	115	152	122.7		150
ξ_+^{MF}	[\AA]	7.8		6			
ξ_+	[\AA]	5.27		6.51			
Γ_s	[$10^{-4}mol/cm^3$]	8.30	8.30	8.47	8.47	8.65	8.65
Γ_h	[$molK/cm^3$]	0.645	0.834	0.740	0.939		0.840
Γ_σ	[$10^{-4}mol/cm^3$]	9.11	14.2	11.6	17.0		14.3

Table 4.2: *Critical parameters of the isotropic Lifshitz critical range. Exponents are listed corrected to DCP*

Φ [%]	T_C	c_+ [cm^3/mol]	γ	$\xi_0^{Q^2}$	ν_{Q^2}	$\xi_0^{Q^4}$	ν_{Q^4}	η_{Q^4}
5	82.6	165	1.32	4.1	0.68	8.2	0.34	0.21
6	81.4	69.5	1.55	2.6	0.81	7.5	0.42	0.21
6.6	78.1	42.7	1.84	2.1	0.90	6.7	0.48	0.42
7	76.0	15	2.15	1.2	1.01	4.6	0.62	0.53

4.3 Role of the Diblock Copolymer in the Disordered and Ordered Regime

The ternary polymer blend PB/PS/PB-PS demonstrates a rich phase behavior. Two tunable parameters, namely temperature and diblock copolymer concentration, were employed to reach the different phases. In this work the polymer blend PB/PS/PB-PS is mainly characterized in terms of different phase transitions, phases, phase boundaries, and critical universality classes.

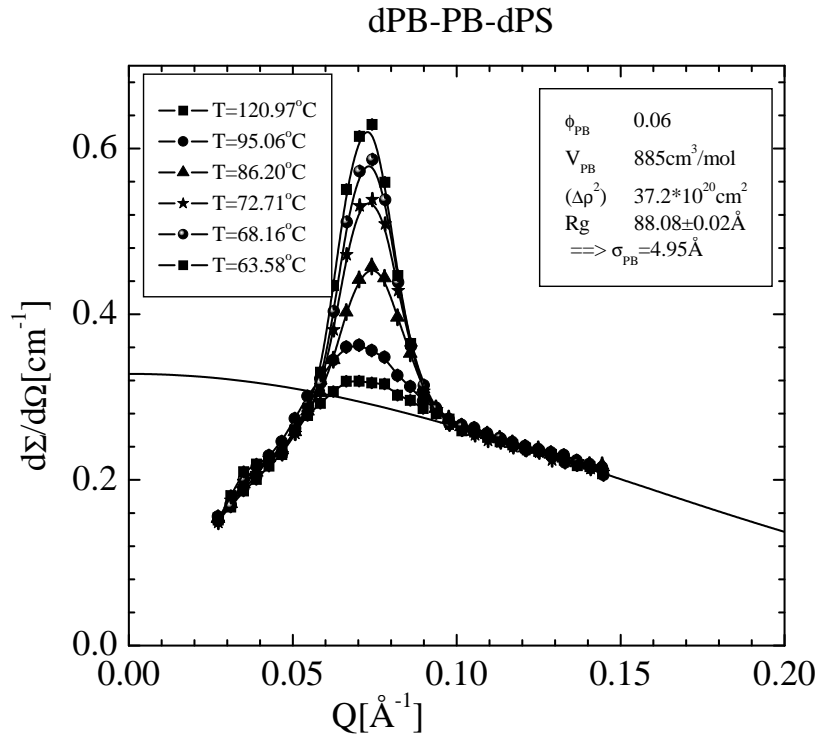


Figure 4.25: *The scattering profile of the dPB-PB-dPS melt*

In the film contrast only the middle part of the diblock copolymers is visible by SANS. In Fig. 4.25 there is shown the scattering profile of the dPB-PB-dPS melt at different temperatures. The scattering intensity above $Q = 0.1 \text{\AA}^{-1}$ is independent from temperature. The line is a fit of the data from above $Q = 0.1 \text{\AA}^{-1}$ by an equation given by

$$\frac{d\Sigma}{d\Omega}(Q) = \phi_{PB} V_{PB} (\Delta\rho)^2 \exp - \frac{(R_g Q)^2}{3} \quad (4.2)$$

with R_g and V_{PB} as adjustable parameters (Guinier approximation). Assuming a Gaussian morphology the segmental length of polybutadiene was found

$\sigma_{PB} = 4.9\text{\AA}$ ($R_G^2 = \frac{1}{6}\sigma^2 N$). Molecular volume of the triblock copolymer middle part determined by SANS ($V_{PB} = 885\text{cm}^3/\text{mol}$) is in the agreement with GPC obtained $V_{PB} = 1000\text{cm}^3/\text{mol}$. Therefore, in the melt the segmental length of the PB-chain is not a function of temperature, it is the same in the disordered and lamellar phases.

The scattering profiles of the ternary blends dPB/dPS/dPB-PB-dPS with the 3%, 7% and 10% copolymer content are shown in Figures 4.26-4.28 at different temperatures. Systematically, it can be seen that the peak position (in limit of the experimental resolution) does not depend on temperature. With the decreasing temperature the peak intensity $I(Q^*)$ decreases, but the general shape of $S(Q)$ remains unchanged. The peak position is found at a high-Q range, suggesting that the peak of the copolymer form factor is observed. With decreasing temperature the number of free (not bonded in large-scale structure formation) decreases. Assuming a Gaussian shape of the ‘‘individual’’ form factor the scattering profiles at different temperatures were fitted by the Gaussian function simultaneously. Only the prefactor of the Gaussian exponent was found to be temperature dependent. The temperature dependence of the prefactor I_0 is depicted in the inset in Figures 4.26-4.28.

The Q-range profiles demonstrates a rearrangement of the copolymers from randomly distributed chains at high temperatures to self-assembled large-scale objects. The scattering profile of the F07% sample is shown over the whole Q-range in Fig. 4.29. Assuming the parameter I_0 is proportional to the number of ‘‘free’’-copolymers, one can calculate the relative number of chains in the ordered phases. I_0 shows a continuous decrease and no feature at the disorder-order interface.

The peak position versus of the diblock PB-block volume fraction is plotted in Fig. 4.30. Surprisingly, the peak position moves to large value with the dilution of the sample. This fact we describe as shrinking of diblock copolymers at the dilution.

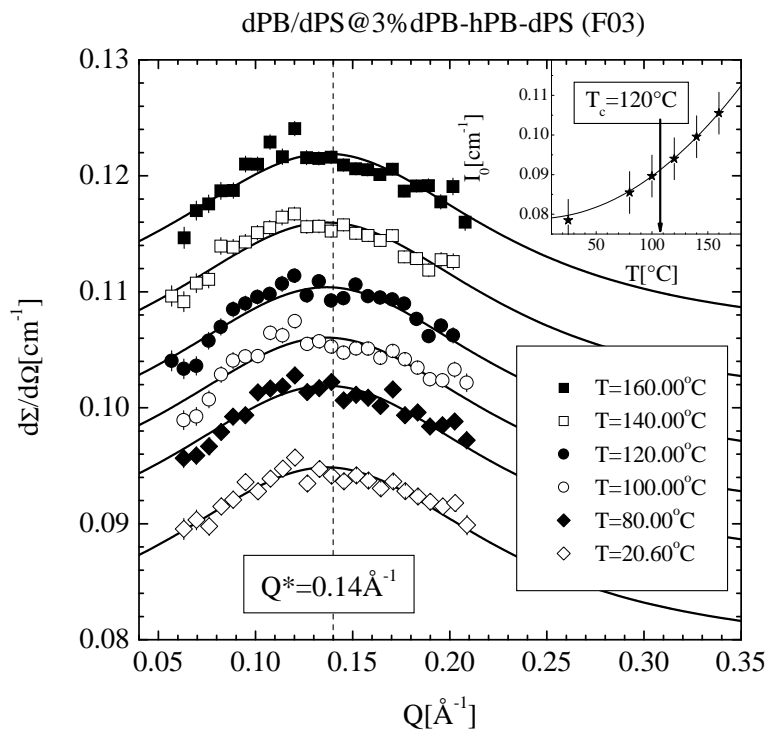


Figure 4.26: The temperature dependence of the scattering profile for 3% of the triblock copolymers dPB-PB-dPS (film contrast)

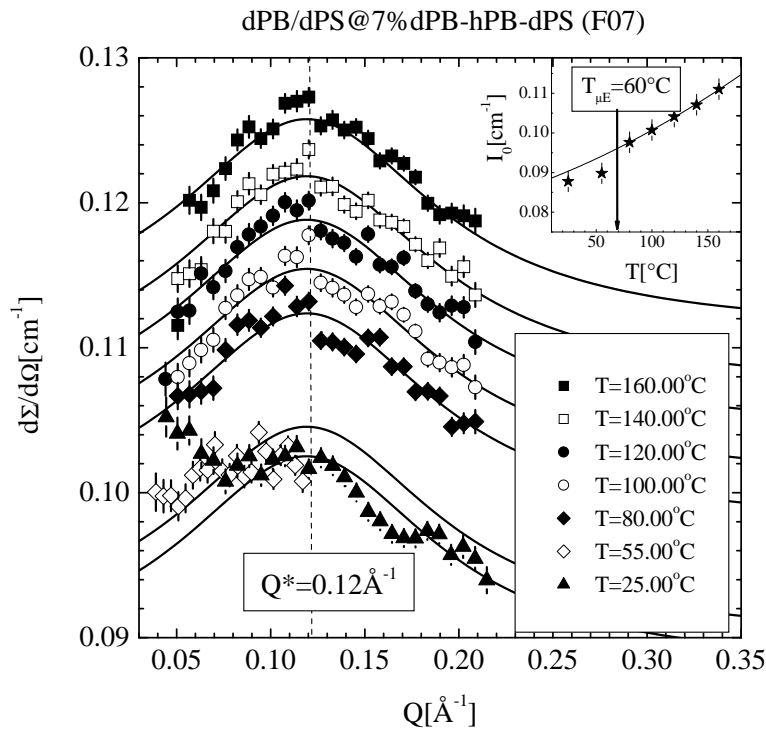


Figure 4.27: The temperature dependence of the scattering profile for 7% of the triblock copolymers dPB-PB-dPS (film contrast)

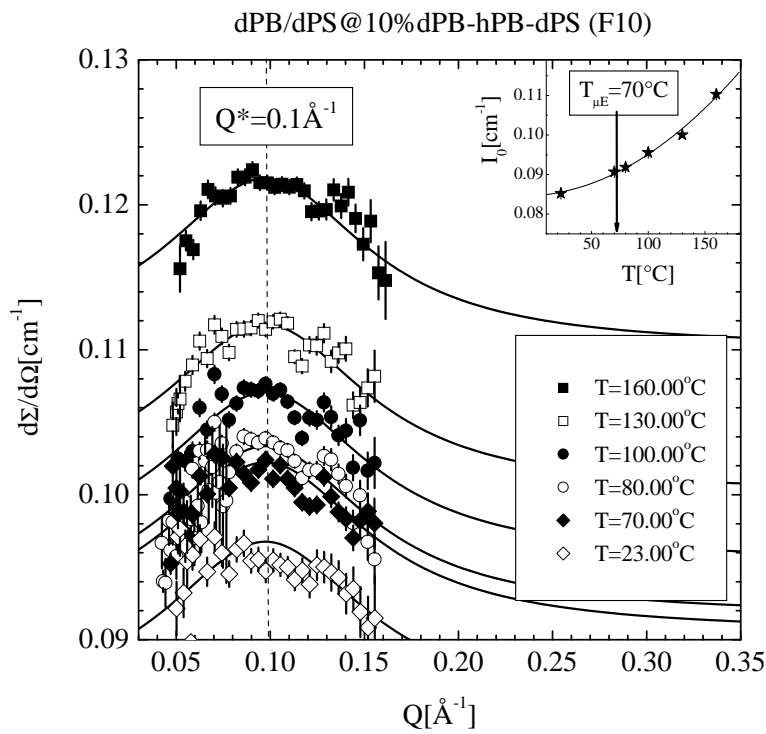


Figure 4.28: The temperature dependence of the scattering profile for 3% of the triblock copolymers dPB-PB-dPS (film contrast)

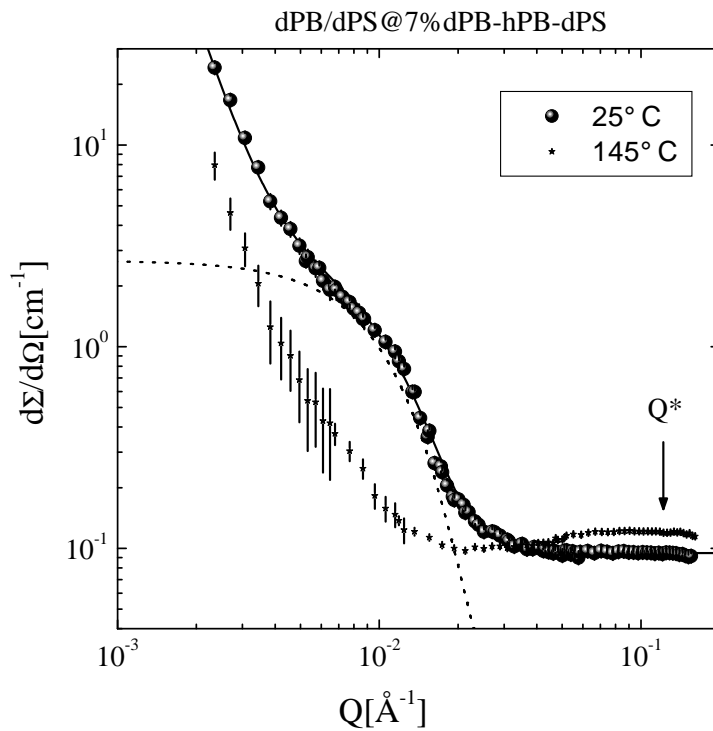


Figure 4.29: Scattering profile of the 7% sample at disordered (145°C) and droplet microemulsion (25°C) phases

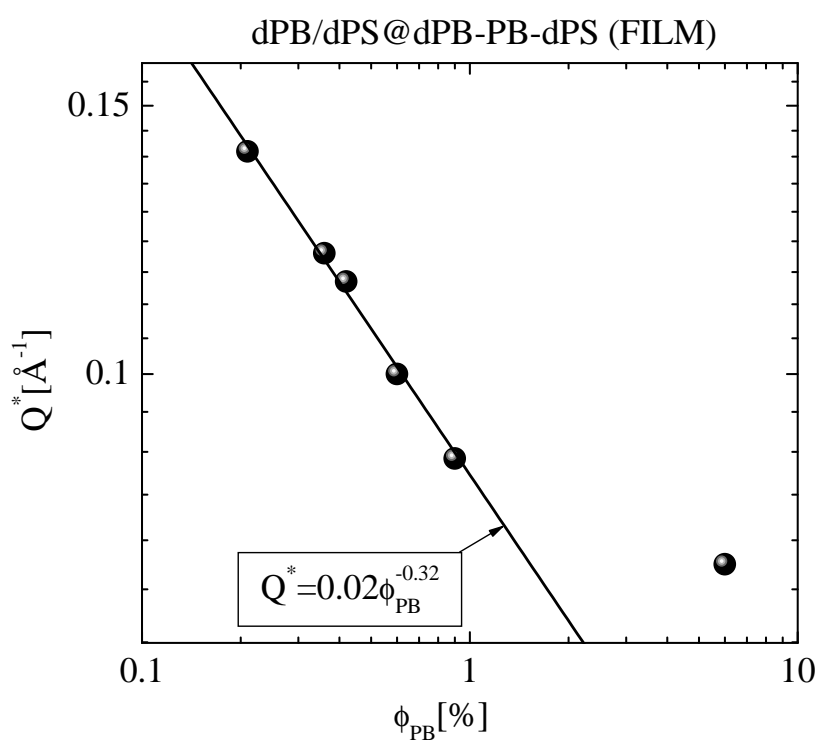


Figure 4.30: *Scaling of the peak position with PB-block volume fraction*

Chapter 5

Interpretation of the Data

The ternary polymer blend PB/PS/PB-PS demonstrates a complicated phase behavior due to the different nature of the components. The location and evidences of the phase boundaries were given in Chapter 4.

Temperature induced transitions from a disordered phase to (a) two-phase, (b) microemulsion phase, (c) lamellar phase are influenced by the Ginzburg number. The Ginzburg number characterizes the crossover temperature from mean-field to: 3D-Ising ($0\% < \Phi < 5\%$), isotropic Lifshitz ($5\% \leq \Phi < 13\%$), and Brasovskii ($13\% \leq \Phi < 100\%$) universality classes.

The measured temperature dependence of the susceptibility [$S(0)$ or $S(Q^*)$] is described by theories depending from the type of phase transition (universality class). Generally, the experimental data are fitted by a crossover function determined by three parameters, namely, the Ginzburg number Gi , the enthalpic and entropic contributions of the Flory-Huggins parameter Γ_h and Γ_σ , respectively. In next sections the analysis of the temperature dependence of the susceptibility within the different universality classes will be presented.

5.1 Structure Factor and Susceptibility below the Lifshitz Line ($\Phi < \Phi_{LL}$)

In Fig. 4.19 the structure factor $S(Q)$ of samples with copolymer content below the Lifshitz line has been plotted for various temperatures vs. the momentum transfer Q in a Zimm representation, i.e., $S^{-1}(Q)$ vs. Q^2 . The solid lines represent fits of Eq. 2.3 from which three parameters, namely the susceptibility $S(0)$ and the coefficients L_2 and L_4 were obtained. Below $\Phi = 5\%$, namely, at 0%, 3% and 4% of the diblock content $S(Q)$ is sufficiently well described by the Ornstein Zernike approximation with $L_4 = 0$ similar to blends. For larger Φ the Q_4 term in $S(Q)$ becomes visible as demonstrated for the $\Phi = 5\%$, 6.6% and 7% samples which is due to the reduction of the interfacial energy caused by the diblock component.

In Figures 4.20 and 4.21 the inverse susceptibility $S^{-1}(0)$ has been plotted vs. the inverse temperature $1/T$ for the six investigated samples with Φ lower than the Lifshitz line. The critical temperatures determined from $S^{-1}(0) = 0$ decreases with increasing Φ . These points are shown in the phase diagram of Fig. 4.1 (solid points). The $\Phi = 3\%$ and $\Phi = 4\%$ samples behave similar to pure blends. $S^{-1}(0)$ shows mean field characteristics at high temperature, and near the critical point 3D-Ising critical behavior with a crossover regime determined by the Ginzburg number in Eq. 2.23. This is demonstrated by the corresponding fitted solid line obtained from the crossover function by Belyakov et al. in Eq. 2.20 [6,44]. This crossover function has successfully been used for the interpretation of critical scattering in polymer blends [48,49]. The dashed and dotted lines in the figure represent the asymptotic 3D-Ising scaling and mean field laws with the critical exponent $\gamma = 1.24$ and $\gamma = 1$, respectively, as calculated from the parameters of the crossover function.

The temperature behavior of the susceptibility of the other four samples, plotted in Fig. 4.21 with $\Phi > 4\%$ could be analyzed with the expressions of the susceptibility $S(0)$ derived from Eq. 2.45 with $Q^* = 0$ and the corresponding renormalized the FH-parameter of Eq. 2.51. The fits are depicted by solid lines; they describe the stronger curvature of the experimental data near the critical point rather well.

The temperature dependence of the susceptibility is a function of the FH-parameter, G , b_0 and c_0 . Due to the large number of parameters, some of them should be fixed in order to obtain stable fits. The parameter G was calculated as predicted by Eq. 2.47. The value of \bar{N} was estimated to be 1070 assuming a mean statistical segment length of $\sigma = 6.5\text{\AA}$. The temperature dependence of the segmental length σ at $\Phi = 13\%$ is shown in Fig. 5.1. The fourth order vertex function for $\alpha = 0.158$ and different diblock concentrations is plotted in Fig. 2.4(d).

Another fixed parameter was c_0 . It is not possible to calculate c_0 according to Eq. 2.53, due to the shifting of the Lifshitz line in real systems in comparison with the theoretically predicted ($c_0 = 0$ at LL). The c_0 parameter was calculated according to

$$c_0 = \frac{N\Gamma_2(0)}{6d_+} = \frac{L_2V}{6R_g^2d_+} = \frac{L_2V}{N\sigma^2d_+}, \quad (5.1)$$

where L_2 parameter was defined experimentally from the structure factors (Eq. 2.3) and averaged with temperature.

The numerical values are collected in Table 5.1. The Ginzburg number was calculated according to Eq. 2.50 in terms of the parameters listed in Table 5.1.

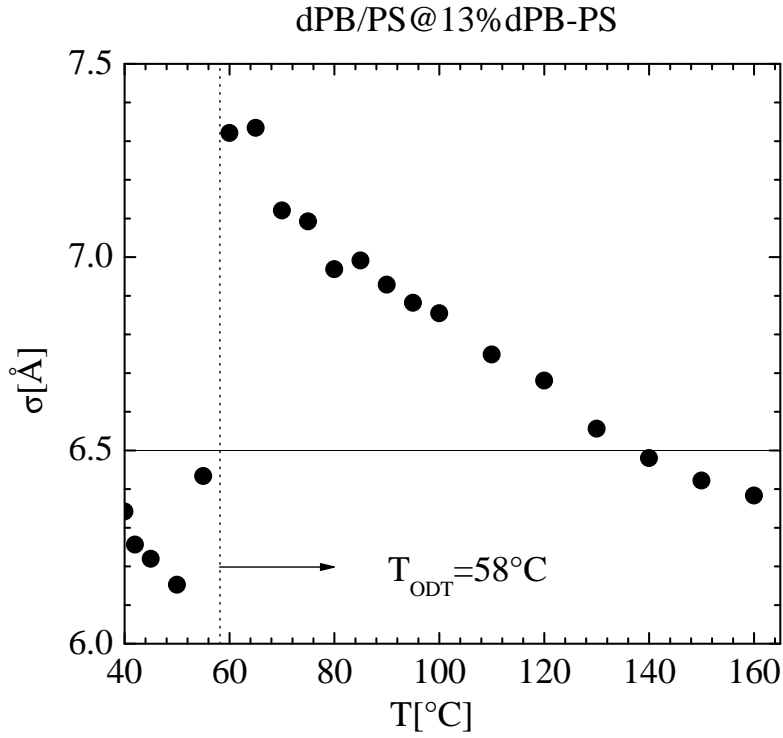


Figure 5.1: *Temperature dependence of the segmental length at $\Phi = 13\%$*

Table 5.1: *Parameters of the samples with diblock content less than the Lifshitz line, but above “blend-like” regime, evaluated from the susceptibility $S(0)$ using Eq. 2.51 and the BK-crossover function. The 0%, 3% and 4% samples could not be appropriately described by Eq. 2.51. $\bar{N} = 1070$ was evaluated assuming $\sigma = 6.5\text{\AA}$.*

$\Phi(\%)$	T_C	Γ_S	Γ_h	Γ_σ	b_0	c_0	G
	C	$10^{-3} \frac{mol}{cm^3}$	$\frac{molK}{cm^3}$	$10^{-3} \frac{mol}{cm^3}$			
5	82.6	0.865	0.627 ± 0.007	0.86 ± 0.01	16 ± 2	0.040	0.507
6	81.4	0.872	0.906 ± 0.010	1.66 ± 0.02	0.38 ± 0.01	0.035	0.507
6.6	78.1	0.880	0.732 ± 0.003	1.18 ± 0.01	0.36 ± 0.02	0.029	0.507
7	76.0	0.877	0.816 ± 0.006	1.42 ± 0.01	0.52 ± 0.06	0.020	0.505

5.2 Structure Factor and Susceptibility beyond the Lifshitz Line ($\Phi > \Phi_{LL}$)

The order-disorder transition beyond 13% diblock copolymer content have been studied for six samples. In a disordered phase the structure factors were fitted by the Kielhorn and Muthukumar theory (Eq. 2.44) [54]. The scattering profile of the 50% sample is plotted in Fig. 4.16. For all temperatures between 20 and 143°C the structure factor $S(Q)$ has a maximum at finite Q^* -values. The susceptibility $S(Q^*)$ of these samples is plotted in Fig. 5.2. The solid lines in Fig. 5.2 represent the best fits of the renormalized susceptibility as given by Eq. 2.45, and the corresponding Flory-Huggins parameter of Eq. 2.33. The parameters of the fits are listed in Table 5.2. In the insets of Fig. 5.2 the temperature range of the ordering transition has been amplified. Below T_{ODT} the susceptibility shows deviations from its theoretical prediction and, additionally, a second order peak appears in the structure factor.

From the analysis of the susceptibilities the FH-parameters and Ginzburg number \tilde{Gi} were extracted. Within the mean field theory the order-disorder transition has a second order nature, and therefore the susceptibility should be zero at T_{ODT} . Thermal fluctuations change the type of the ordering transition to a weakly first order one. An important characteristic of any phase transition is the question of the validity of the mean field theory. The Ginzburg number gives a qualitative information about the crossover from the mean field to the fluctuation dominated regime.

As one can see from Fig. 5.2 the increase of the diblock content leads to an increase of the curvature of the susceptibility near the ordering transition. This indicates an increasing role of the fluctuations and to larger value of Gi , as depicted in Fig. 6.4.

Table 5.2: *Parameters of approximation of the susceptibility of samples above LL*

$\Phi[\%]$	Γ_s $10^{-4}mol/cm^3$	Γ_σ $10^{-4}mol/cm^3$	Γ_h $molK/cm^3$	\tilde{Gi}
13	8.869	8.8 ± 0.2	0.63 ± 0.01	0.65 ± 0.01
15	8.859	9.3 ± 0.1	0.65 ± 0.01	0.91 ± 0.03
20	8.790	7.9 ± 0.3	0.58 ± 0.01	0.98 ± 0.05
30	8.569	8.7 ± 0.2	0.62 ± 0.01	1.61 ± 0.06
40	8.306	9.0 ± 0.2	0.64 ± 0.01	2.46 ± 0.08
50	8.035	10.3 ± 0.4	0.70 ± 0.02	4.02 ± 0.20

In the Fig. 5.3 the temperature dependence of the peak position is plotted

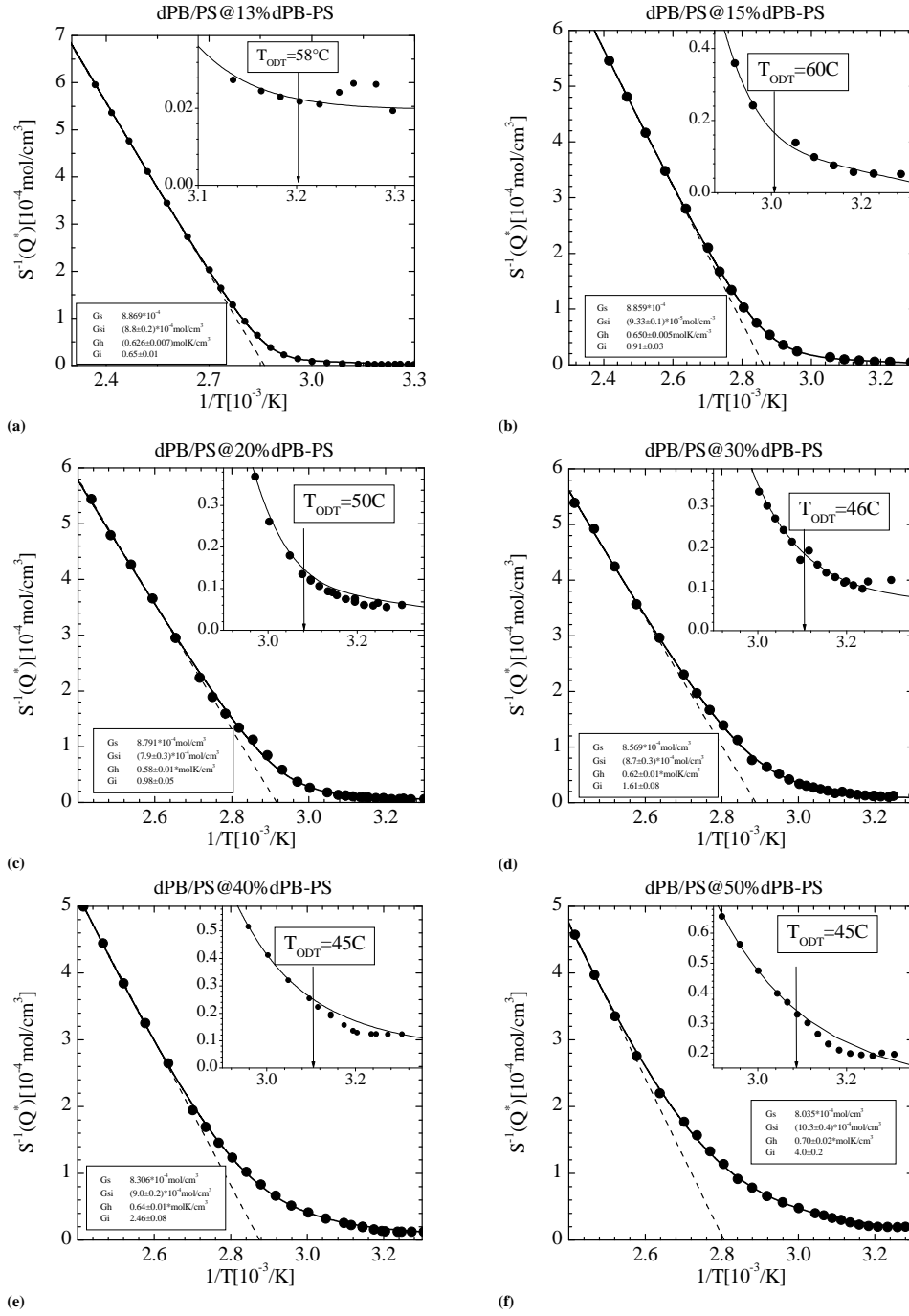


Figure 5.2: The inverse susceptibility $S(Q^*)$ vs. the inverse temperature $1/T$: the disorder-lamellar part of the phase diagram, above LL

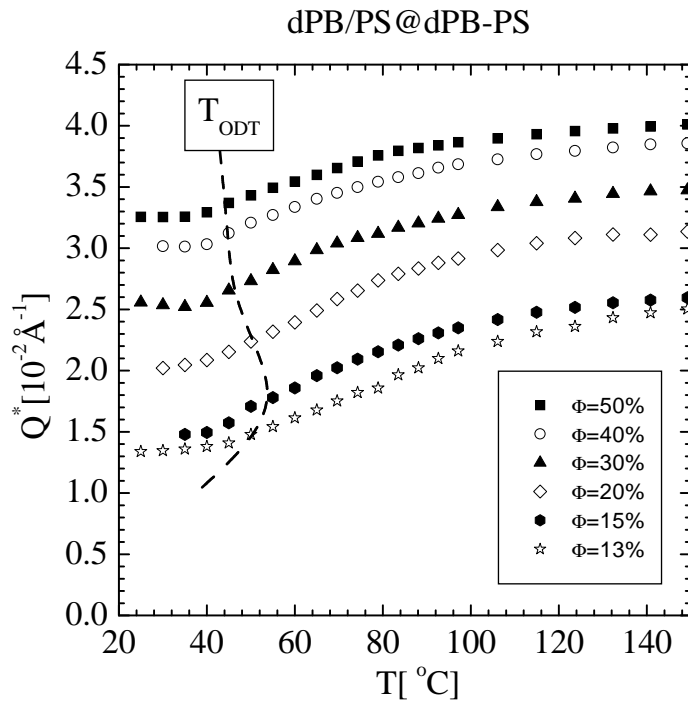


Figure 5.3: Q^* vs. T : 50%, 40%, 30%, 20%, 15% and 13% samples

for the samples between 13%-50% diblock content. A small discontinuity of Q^* below T_{ODT} is observed as reflected by the dashed line.

5.3 Structure Factor and Susceptibility near the Lifshitz Line

The SANS data of the samples between 7% and 9% diblock content show a reentrance “diblock” behavior at high and low temperatures. The structure factor $S(Q)$ has non-zero maximum ($Q^* \neq 0$) at high and low temperatures, but at intermediate temperature regime $S(Q)$ shows a “blend-like shape” with maximum at $Q=0$. The curvature of the Lifshitz line in Fig. 4.1 reflects this reentrant behavior. The temperature dependence of the peak position in this concentration range are shown in Figures 4.4-4.7.

The susceptibility $S^{-1}(0)$ between 7% and 8% always shows a minimum at some temperature. This minimum is interpreted as a disorder-microemulsion boundary. A decrease of the temperature in the disordered regime leads to an increase of the thermal fluctuations, and therefore to a larger susceptibility $S(0)$. But at the disorder-microemulsion boundary the thermal fluctuations strongly correlate, and the structure factor decreases by forming micro-particles, usually referred as a droplet microemulsion.

At $\Phi = 7.2\%$ a double critical point is located. On the right side of Φ_{DCP} the change of temperature along the isopleth leads to a tangential approach to the DCP as shown in Fig. 5.4(f). In a ternary system near a double critical point the dashed lines depicted in Fig. 5.4(f) are the critical paths instead of the isopleth (line). Approaching the critical line along an isopleth increases the value of the critical exponents by a factor two as described in Sec. 4.2.

The boundary between disordered and droplet microemulsion starts at the double critical point ($\Phi = 7.2\%$ and $T = 71^\circ C$) and terminates at the Lifshitz “meeting” point ($\Phi = 8.8\%$ and $T = 69^\circ C$). The inverse susceptibility along the droplet microemulsion - disorder borderline is plotted in Fig. 6.3. The susceptibility increases when the double critical point is approached, and diverges at DCP.

The structure factor has been fitted in terms of Ginzburg-Landau-Wilson Hamiltonian (Eq. 2.3) and a Hartree approximation in the Brasovskii formalism (Eq. 2.44).

The corresponding susceptibilities $S(0)$ and $S(Q^*)$ of 7.1%, 7.2%, 7.3%, 7.5% and 8% are plotted in Fig. 5.4 vs the inverse temperature. The temperature dependence of the susceptibility was fitted in terms of the renormalized Flory-Huggins parameter. Eq. 2.46 represents the limit of a diblock copolymer as indicated by the solid line. The resulting numerical values are collected in Table 5.3.

The general characteristics of the structure factor and related parameters, are similar for the samples in the microemulsion channel. The temperature dependence above microemulsion boundary is described sufficiently good by Muthukumar theory. Below the microemulsion temperature the inverse susceptibility

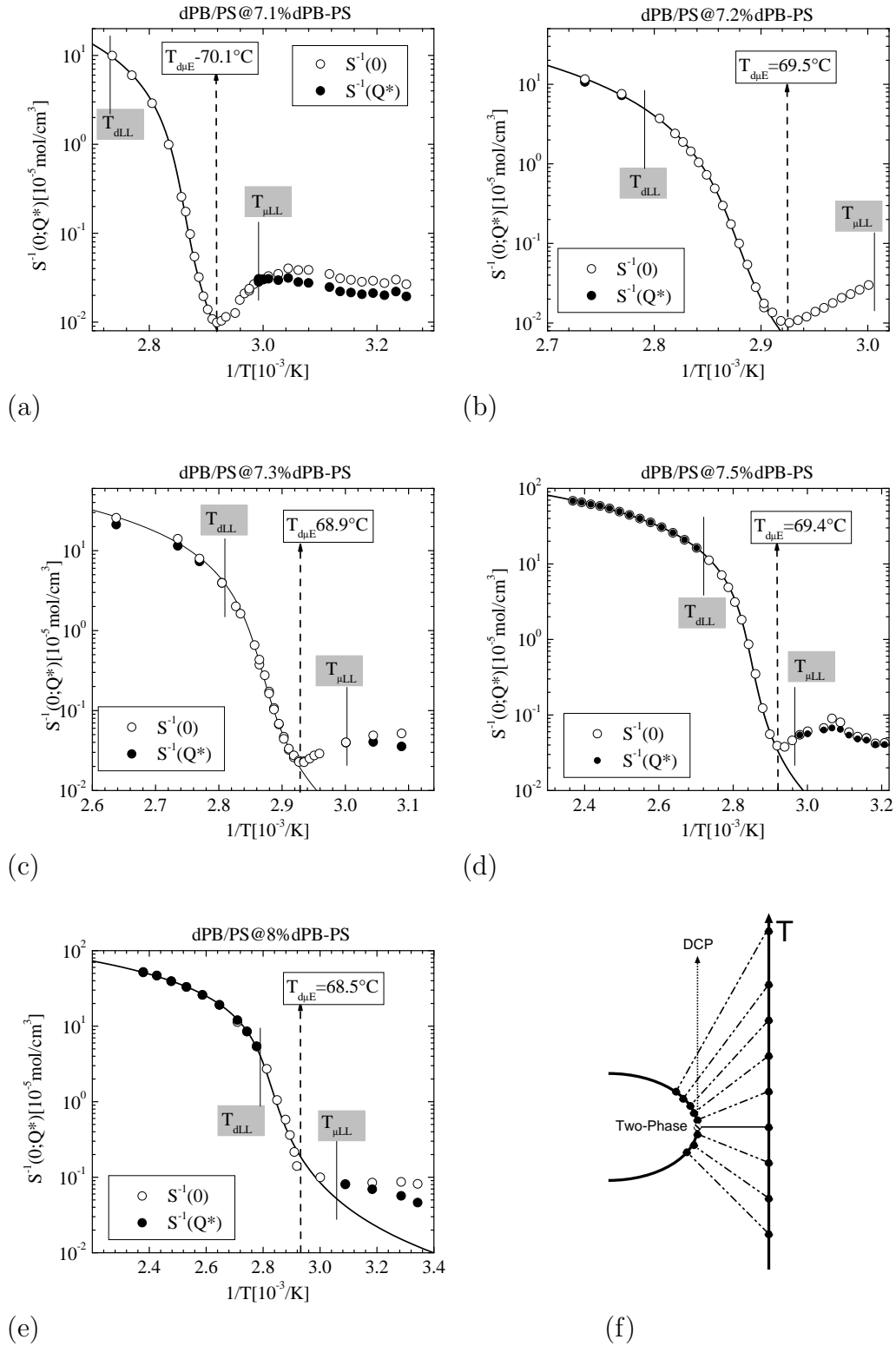


Figure 5.4: The inverse susceptibility $S^{-1}(Q^*)$ vs. inverse temperature $1/T$: Near the LL

$S^{-1}(0)$ relatively strong increases up to maximum at $T = 50^\circ\text{C}$. The temperature gap between the microemulsion boundary and the microemulsion LL the morphology of microemulsion is a droplet one. The diblock copolymers stabilize the thermal fluctuations of homopolymer blend. Below the LL microemulsion particles are strongly correlated, and this correlation is reflected in the broad peak of the structure factor.

At maximum of the inverse susceptibility at $T = 50^\circ\text{C}$ the peak position has also a maximum.

Table 5.3: *Parameters of samples near LL*

$\Phi[\%]$	Γ_s $10^{-4}\text{mol}/\text{cm}^3$	Γ_σ $10^{-4}\text{mol}/\text{cm}^3$	Γ_h molK/cm^3	\tilde{G}_i
7.1	8.778	5.3 ± 0.8	0.50 ± 0.03	0.046 ± 0.008
7.2	8.782	6.6 ± 0.6	0.54 ± 0.02	0.052 ± 0.006
7.3	8.786	10.0 ± 0.6	0.66 ± 0.02	0.093 ± 0.011
7.5	8.793	20 ± 1	1.02 ± 0.04	0.091 ± 0.007
8.0	8.810	8.2 ± 0.3	0.61 ± 0.01	0.22 ± 0.02
9.0	8.836	7.1 ± 0.1	0.57 ± 0.01	0.36 ± 0.02
10.0	8.853	9.0 ± 0.2	0.63 ± 0.01	0.44 ± 0.02

Chapter 6

Discussion

6.1 Critical Exponents and Double Critical Point within Lifshitz Universality Class. Comparison of Field Variables for Critical Phenomena Description

In Section 4.2 the crossover from the Ising to Lifshitz universality class near the Lifshitz line is shown. The critical exponent of the susceptibility ($\gamma_{\tau_U} = 3.24$) and correlation length ($\nu_{\tau_U} = 1.8$) within the Lifshitz universality class is determined by considering scaling with the conventional reduced temperature $\tau_U = |T - T_{UCST}|/T$. Near the Lifshitz line the reentrance behavior is terminated by a double critical point. The strong curvature of the Scott line in the temperature-diblock content plane near DCP arises a question about the relevant field variable for critical phenomena description. In Fig. 6.1 the orthogonal approaches, namely the critical isochor and critical isotherm, to the conventional critical point and double point are shown schematically for comparison. In the binary system any approach to the critical point is a critical path, and along it a property, for example compressibility, follows the scaling law $R^{\gamma_{Ising}}$, where R measures the distance from the critical point at the temperature-concentration plane. Thus along the critical isochor and isotherm one gets the critical exponents.

A double critical point is one of the points on the Scott line. In this case the critical path is perpendicular to the Scott line. In the vicinity of DCP an isopleth approach to the Scott line does not follow the maximum of the thermal fluctuations. On the other hand the isotherm at double critical point is critical path.

As one can see in Fig. 6.1 the closed-loop phase diagram shrinks to a point (DCP) with varying diblock copolymer content. Experimentally, one can approach the DCP both along the isopleth ($\Phi = \Phi_{DCP}$) or along the isotherm ($T = T_{DCP}$). The approach to the DCP is characterized by a so-called isopleth

and isotherm reduced field, τ_U and $\tau_\Phi = |\Phi - \Phi_{DCP}|/\Phi$. The susceptibility $S^{-1}(0)$ follows the scaling law along the isopleth

$$S^{-1}(0) \propto \tau_U^{\gamma_{isopleth}}, \quad (6.1)$$

with the critical exponent of the susceptibility $\gamma_{isopleth} = 3.24 \pm 0.05$. On the other hand the isothermal scaling law:

$$S^{-1}(0) \propto \tau_\Phi^{\gamma_{isotherm}}, \quad (6.2)$$

has an another dependence with $\gamma_{isotherm} = 1.55 \pm 0.15$ the ‘‘isothermal’’ critical exponent of the susceptibility. In Fig. 6.2 the horizontal arrow depicts the isothermal approach to the double critical point. The susceptibility along this line (between DCP and LL) is presented in Fig. 6.3. The measurement of the critical exponent along the isotherm shows a relatively large error bar due to the small variation of temperature and the limited number of points. Approaching to

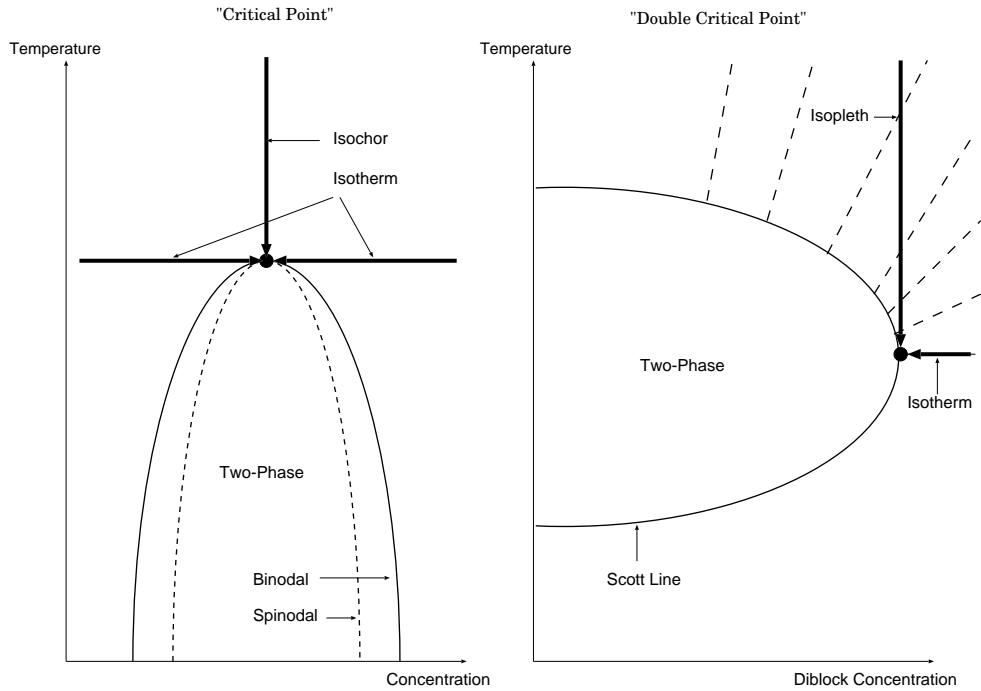
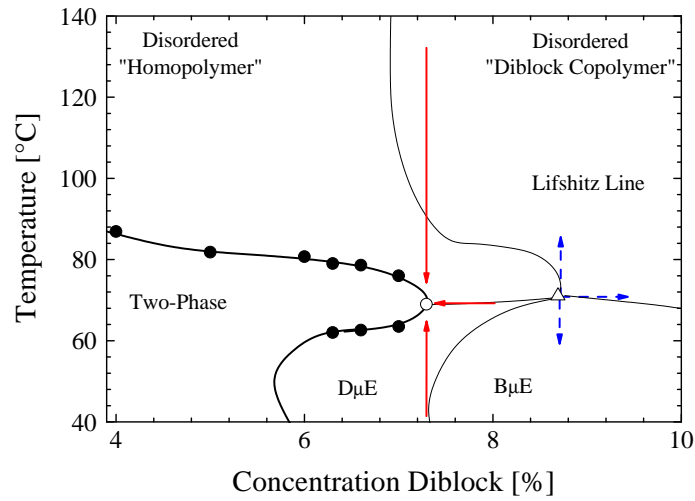
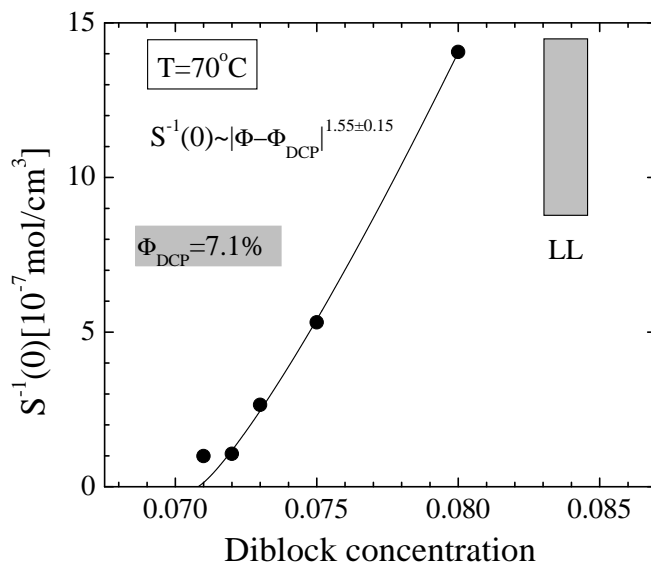


Figure 6.1: *Comparison of a conventional critical point (binary system) with a double critical point (ternary system). In a binary system any approach (f.e. isochor and isotherm) to the critical point is the relevant critical path. In a ternary system with a double critical point only orthogonal direction to the Scott line is the relevant critical path. Therefore in DCP the isopleth is not relevant critical path*

Figure 6.2: *Enlarged phase diagram near the double critical point*Figure 6.3: *The susceptibility vs. diblock content Φ . Concentration approach (isotherm) to the double critical point*

DCP along the isotherm is a critical path, therefore $\gamma = 1.55 \pm 0.15$ is the critical exponent of the susceptibility within the Lifshitz universality class. Arrows in the Fig. 6.2 reflects the approach to the double critical point along the isopleth and isotherm. In case of a conventional critical point (a liquid-liquid or a liquid-gas transition) the isothermal and isochor susceptibility follows a scaling law with the same Ising critical exponent $\gamma = 1.24$ because the critical point is a singular point of the coexistence curve. In a ternary system with multi-critical points the variation of one component changes the critical temperatures. A concentration dependence of the critical temperature (Scott line) changes the critical path in the temperature-concentration plane. Such critical behavior of the coexistence curve [78], the shear viscosity [79], the susceptibility [75, 80] and the correlation length [75, 81] near the double critical point has been studied within the Ising universality class. The respective critical exponents show a doubling in DCP. Considering with respect to the DCP the shape of the coexistence curve Prafulla et al. [76] offered a newly defined reduced temperature $\tau_{UL} = |(T - T_{UCST})(T - T_{LCST})|/T^2$ to describe a tangential approach to the Scott line along an isopleth. The critical exponents are affected by tangential approach to the Scott line only when the immiscibility gap $\Delta = T_{UCST} - T_{LCST}$ is less 20K.

The concentration dependence of critical exponents determined with conventional τ_U and “corrected” τ_{UL} are plotted in Fig. 4.24. The value of the “corrected” critical exponent $\gamma_{isopleth} = 1.62 \pm 0.03$ is half of the conventional exponent. This is the first measurement of critical exponents doubling within Lifshitz universality class.

In frame of the error bar the critical exponents of the susceptibility along the isopleth and the isotherm are found to be the same. The critical exponent of the susceptibility within the Lifshitz universality class is found to be 1.62 ± 0.03 .

The occurrence of a DCP seems to be universal in these polymer mixtures as a reentrance two phase regime are already reported in the (PEE/PDMS/PEE-PDMS) blend but not further worked out [57]. The reentrance range was invisible due to very narrow range of it.

Conclusion: Closed-loop phased diagram and its termination to DCP is seems to be universal behavior in A/B/A-B ternary polymer blends. The Lifshitz universality class is characterized by the critical exponents of the susceptibility: $\gamma = 1.62 \pm 0.03$ and for the correlation length: $\nu = 0.90 \pm 0.05$.

6.2 Disordered and Microemulsion Lifshitz Line. Bicontinuous and Droplet Microemulsion

The Lifshitz lines of the “disordered” and “microemulsion” regions were described in Section 4.1.1 and are depicted in the phase diagram Fig. 4.1. On the right side of LL the peak position Q^* of the structure factor $S(Q)$ follows the scaling

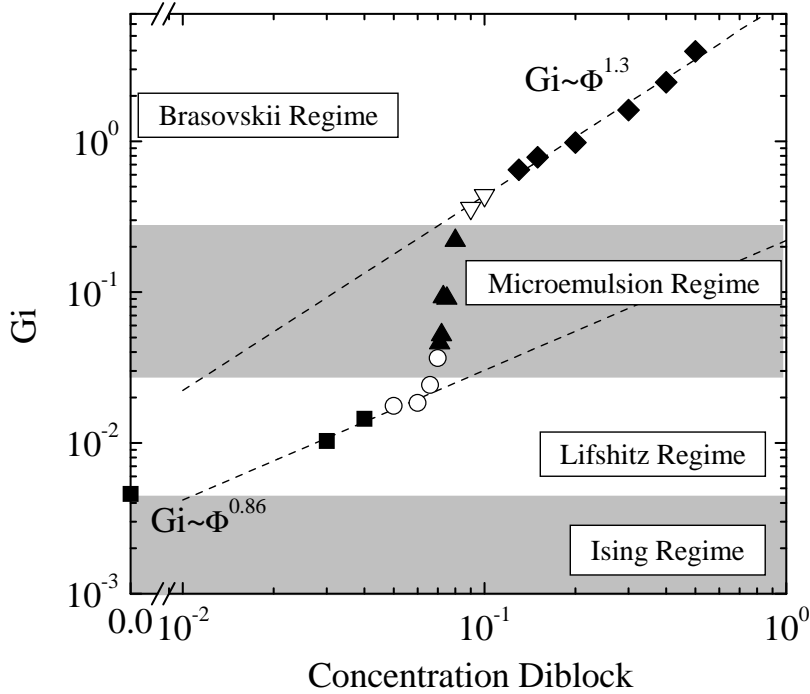


Figure 6.4: *Ginzburg number in whole concentration range*

law $Q^* |\Phi - \Phi_{LL}|^{\beta_Q}$ with different exponent β_Q in disordered and microemulsion phases, $\beta_Q = 0.4$ and $\beta_Q = 0.3$, respectively. The two different Lifshitz lines come into contact in one point at the disorder-microemulsion interface (opened triangle in Fig. 6.2). At this point four phases coexist, namely the droplet and bicontinuous microemulsion, the blend- and diblock-like disordered phase. A shift from a “multi-critical” point (Fig. 6.2) in direction of the dashed arrows leads to an appearing of a peak in the structure factor. The “fourth” orthogonal direction (in direction to DCP) is a critical path, as mentioned above.

Conclusion: Strong thermal fluctuations near the double critical point are responsible for the bend-like shape of the Lifshitz line and destruction of the spatial order of the diblock copolymers.

6.3 Microemulsion Phase, the Phase between Ising and Brasovskii Universality Classes

The concentration dependence of the Ginzburg number versus the diblock copolymer content is plotted in Fig. 6.4 in double logarithmic scale. A Ginzburg number

gives information about the temperature range, where fluctuations play an important role and consequently mean field theory does not work. The Ginzburg number and Flory-Huggins parameter were always adjustable parameters of the fits of the temperature dependence of the susceptibility in the regime of Ising, Lifshitz and Brasovskii universality classes (Chapter 5). As was mentioned in the theoretical part the Ginzburg number follows different scaling laws as a function of the degree of polymerization in the Ising, Lifshitz and Brasovskii regimes, namely N^{-1} , $N^{-2/3}$ and $N^{-1/3}$, respectively.

In Fig. 6.4 two characteristic regimes were found by applying scaling laws and which correspond to the blend-like and diblock-like parts of the phase diagram. The values of the Ginzburg number of the polymer blend and diblock copolymer differ by more than two order of magnitude. An approach to LL from both directions reduces this difference, but does not match at the LL. The Ginzburg number at 7% and 13% (last points of disorder- two-phase and disorder-lamellar transitions) is 0.02 and 0.8, respectively. This huge difference (40 times) of Gi on a narrow interval of the diblock content destroys the conditions of the Lifshitz critical point. A step-like change of the Ginzburg number is impossible due to a smooth character of the meanfield - fluctuation crossover. We suppose that the formation of the microemulsion phase between the two-phase and lamellar phase is a reaction of the large difference of Gi in the Ising and Brasovskii universality classes. Due to this fact no “recipe” exists to get a “real” Lifshitz critical point.

Conclusion: An isotropic Lifshitz critical point cannot exist in A/B/A-B polymer blends, due to the different degree of thermal fluctuations in Ising and Brasovskii universality classes.

6.4 Flory-Huggins Parameter

Thermodynamic properties of two linear homopolymers are different when they are mixed in a melt or in case of covalently connected to a single diblock copolymer. The ordered phases show different length scales in a binary homopolymer blend and a diblock copolymer melt. As mentioned above thermal composition fluctuations are more relevant in diblock copolymers.

In the limit of mean field theory ($\tau \gg Gi$) the Flory-Huggins parameters Γ of a blend Γ^{Blend} and a symmetric diblock copolymer Γ^{Block} is equal $\Gamma^{Blend} = \Gamma^{Block}$. In more sophisticated theory proposed by Dudowicz and Freed by Lattice Cluster Theory calculations [82] Γ^{Blend} and Γ^{Block} is connected by the following relationship:

$$\Gamma^{Block} = (\Gamma_h^{Blend} - A_h/V)/T - (\Gamma_\sigma^{Blend} - A_\sigma/V). \quad (6.3)$$

Only in the limit of large polymer chains the same FH-parameter is expected in blends and diblock copolymers. In Ref. [71] the pressure dependence of FH-

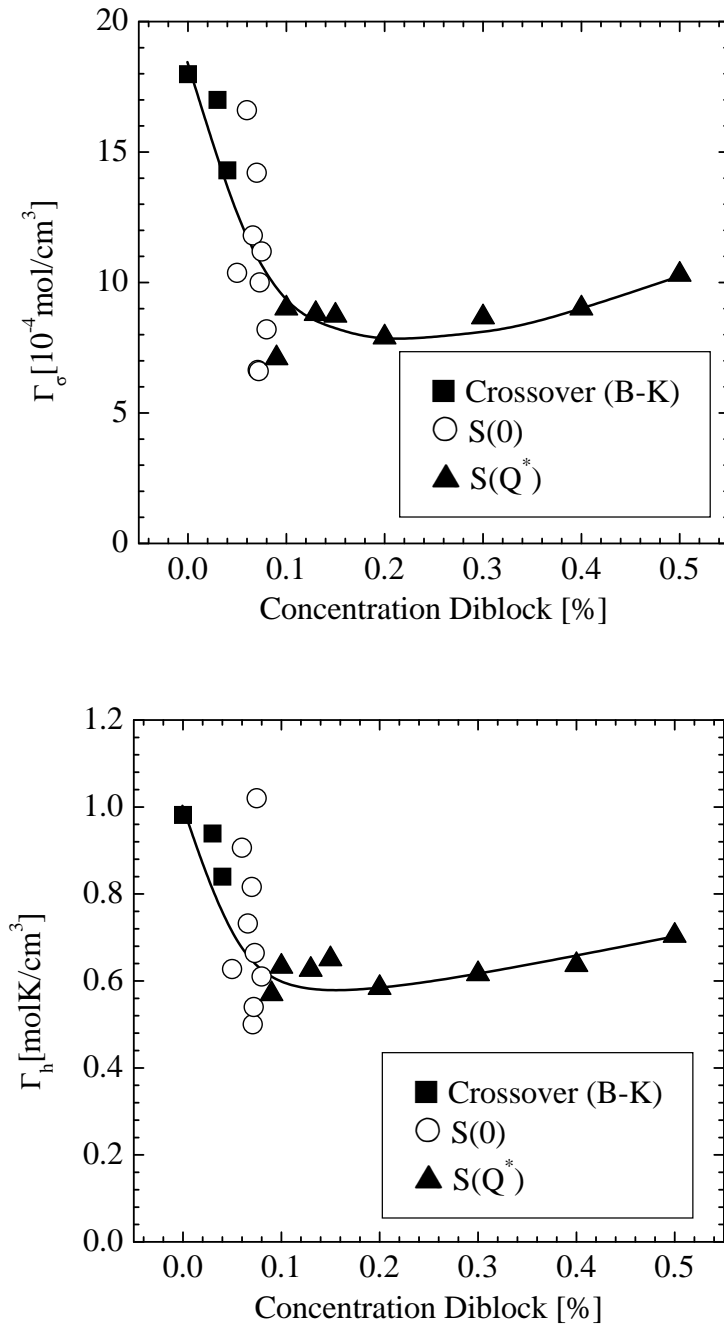


Figure 6.5: *Enthalpic and entropic terms of the Flory-Huggins parameter vs. diblock content*

parameter and Ginsburg number of dPB/PS blend and dPB-PS diblock copolymer is compared. They found $A_h = 6775K$ and $A_\sigma = 19.3$.

The FH-parameter for all investigated samples in this work are shown in Fig. 6.5. The FH-parameter of the homopolymer blend ($\Phi = 0$) and diblock copolymer melt ($\Phi = 1$) corresponds to the result of [71]. The homopolymer blend additive to the diblock copolymer melt and the diblock copolymer melt additive to the homopolymer blend decrease the enthalpic and entropic terms of the Flory-Huggins parameter. The terms of the Flory-Huggins parameter have a minimum near the microemulsion-lamellar boundary ($\Phi = 13\%$).

Chapter 7

Conclusions

SANS experiments on a three component mixture composed of a near critical polymer blend PS/dPB and a corresponding diblock copolymer are presented in this study. The ratio of the molar volumes between the homopolymer and diblock copolymer is $\alpha = 0.158$. From measurements of the static structure factor $S(Q)$ the phase boundaries between the disordered states at high temperatures and, respectively, the micro- and the macrophase separated states at low temperatures were determined for the dPB/PS/dPB-PS system. These results are summarized in the phase diagram in Fig. 4.1. The phase diagram of the investigated blend shows phases which were already observed in a similar blend [19,18], namely, two disordered phase at high temperatures, a two-phase coexistence, and microemulsion and lamellar phases. In the present system we additionally observed a double critical point, droplet and bicontinuous microemulsion region and could perform a detailed analysis of the critical exponents and the Ginzburg number.

Phase Diagram

Macrophase separation in the low diblock copolymer limit ($\Phi \leq 7.2\%$) is realized as a usual second order phase transition. For higher copolymer content, microphase separation appears as a first order phase transition to a lamellar ordered state above 13% diblock content with a periodicity determined by the size of the diblock copolymer and to a microemulsion phase between roughly 7% and 13% diblock concentration.

In the disordered regime, the fluctuations are reflected through the structure factor maximum, $S(0)$ and $S(Q^*)$, which represents the susceptibility and the maximum amplitude of the thermal fluctuation modes. The fluctuations resulting macro and microphase separation is occurring for a maximum in $S(Q)$ at $Q = 0$ and $Q = Q^*$ (Q^* being finite) respectively.

The disordered Lifshitz line separating these two disordered ranges was identified experimentally and shown in the phase diagram in Fig. 4.1. According to the

mean field theory the Lifshitz line should be at a constant block copolymer content in contrast to the observation.

The phase diagram of the dPB/PS/dPB-PS blend has the following characteristic features:

(a) In the narrow diblock concentration interval between 6% and 7.2% the ternary polymer blend shows closed-loop coexistence curve with upper and lower critical solution temperatures. The two phase gap was detected both by eye and SANS. Below the lower critical temperature and above the upper critical temperature of the two-phase gap the blend is transparent, on the other hand inside of the closed-loop it is turbid and white. The transition into the two-phase regime from both high and low temperature is detected by SANS; crossing the boundary and entering the two-phase regime the inverse susceptibility $S^{-1}(0)$ becomes negative and gives a signal which corresponds to an early stage of spinodal decomposition.

(b) The gap between upper and lower critical temperatures becomes zero at the double critical point ($T_{DCP} = 70^{\circ}C, \Phi_{DCP} = 7.2\%$). To our knowledge this is the first observation of a double critical point in polymer blends and within the Lifshitz universality class.

(c) The microemulsion phase is divided by a Lifshitz line into a droplet and bicontinuous microemulsion phase. In oil/water [83] and polymeric [57] microemulsion the Lifshitz line is referred as a transition from weakly to bicontinuous structured mixtures. But, we have here a scenario of a droplet microemulsion phase below a two-phase reentrance regime which must represent a more ordered state than the two-phase regime as the corresponding phase transition can only be an entropy driven process. Theoretical descriptions of reentrance two-phase diagrams have to consider distinct modes of interaction as van der Waals or hydrogen bonds. They are represented by an effective Flory-Huggins free energy parameter arising from an average over orientational degrees of freedom [77]. In the present polymeric melt the structural difference of homopolymers and diblock copolymers may lead to the necessary distinctive interactions, as the ordering of the diblock copolymer in the droplet phase shows a lower "orientational" entropy in comparison to the two-phase system.

(d) The "disordered" and "microemulsion" Lifshitz lines meet at the disorder - microemulsion boundary.

Mean field theory predicts a Lifshitz critical point where the disordered phases, the two-phase and lamellar phase coexists. But due to thermal fluctuations no Lifshitz critical point can exist. Instead a the microemulsion channel is found. This is because of the different Ginzburg numbers of blend-like and diblock-like behavior.

It seems that the formation of the microemulsion channel is caused by the two order of magnitude difference of the Ginzburg number as one can see in Fig. 6.4 in homopolymer blend and diblock copolymer. The huge difference in the Ginzburg number interpolates in the microemulsion channel. Comparing this value within Ising and Brasovskii parts of the phase diagram the small variation of the diblock

component change the Ginzburg number dramatically near the Lifshitz line. Beyond the characteristic border lines presented in the phase diagram in Fig. 4.1 the “critical” characteristics of the thermal composition fluctuations in the disordered regime were determined, including the identification of the crossover behavior from the universality classes of 3d-Ising to the isotropic Lifshitz. In the ternary PB/PS/PB-PS system the mean field approximation can, however, only be a rather poor approximation. In particular, critical fluctuations will become strong near the isotropic Lifshitz critical point since the stabilizing effects from the surface energy, expressed by the c_2 and L_2 term in Eqs. (2.1) and (2.3), respectively, becomes small. This effect is expressed by an upper critical dimension, which is derived as $d_U = 8$ at the Lifshitz line. Below the upper critical dimension, fluctuation effects are important near the critical point and the exponents differ from their classical values. The Lifshitz point, however, is destroyed by these thermal composition fluctuations as discussed before.

On the other hand in the ternary system of PE/PEP/PE-PEP, where the appearance of a microemulsion phase was first established [16] the observed critical exponents remained the mean field values. This situation is different from the present system and must be related to the order of magnitude smaller molar volume of the polymers in the PB/PS system, relative to the PE/PEP system. At the Lifshitz point the Ginzburg number scales with $N^{-2/5}$ in comparison with blends where a N^{-1} is proposed, which means an appreciably stronger sensitivity of G_i with molar volume.

Critical Behavior

Ising Critical Behavior: below $\Phi = 5\%$

At the low diblock content, below $\Phi = 5\%$, the macrophase separation is realized as a usual second order phase transition. The crossover from mean field, at high temperatures, to 3D-Ising behavior, near T_c , is described by the Belyakov-Kiselev crossover model. In this model the correlation length of the thermal fluctuation is the only relevant length. The temperature change of the crossover behavior is ruled by the Ginzburg number. The diblock additive strongly increases the Ginzburg number, thereby extending the temperature range where thermal fluctuations are important.

Lifshitz Critical Behavior

The critical behavior in the concentration range between $\Phi = 5\%$ and 7.3% is affected by the approach to the Lifshitz line and shows a crossover to the critical universality class of the isotropic Lifshitz case. Diblock copolymers further reinforce thermal fluctuations when the correlation length becomes comparable with the diblock radius of gyration. But very near the critical point the diblock copolymers confine a further growth of the thermal fluctuations as is visible from maximum of the L_2 a few degree before the critical temperature. Due to the

vanishing of the Q^2 -term of the inverse structure factor $S^{-1}(0)$ at LL two correlation lengths, namely ξ_{Q^2} and ξ_{Q^4} , have to be considered. Below 5% the ξ_{Q^2} correlation length dominates in the whole temperature range, $\xi_{Q^2} \gg \xi_{Q^4}$, and the structure factor follows the Ornstein-Zernike approximation. Above 5% diblock content at high temperatures ξ_{Q^4} is dominant, due to the reduction of the Q^2 -term. By the decrease of the temperature the system crosses the disorder line, where the oscillations of the correlation function vanish. At the DL the two correlation lengths become equal, and below the DL thermal fluctuations are ordered somehow by the diblock copolymer. Below DL thermal fluctuations rearrange the diblock copolymers by accumulating them at their interface. Few degrees above the critical temperature the L_2 coefficient of the structure factor shows a maximum, but the L_4 term increases continuously.

Reentrance Behavior and the Double Critical Point

A reentrance one phase regime is found between 6% and 7.2% of copolymer concentration. At the double critical point ($\Phi = 7.2\%$, $T = 70^\circ\text{C}$) the close-looped coexistence curve collapses to a point. The critical exponent in this range is affected by the tangential approach to the double critical point and gives a twice as large number.

Critical exponents above $\Phi = 5\%$ were determined accordingly to scaling laws with the reduced temperature τ_{UL} taking into account proximation to DCP. From 5% to 7.2% critical exponents continuously increase. At the DCP the critical exponent of the susceptibility γ is found to be 1.61, of the correlation length ($\nu_{\xi_{Q^2}}$) 0.9, and ($\nu_{\xi_{Q^4}}$) 0.4.

The critical path is perpendicular to the Scott line. Therefore at the DCP the critical path is only an isotherm, contrary to homopolymer blend, where any approach to critical point is a critical path. The critical exponent of the susceptibility obtained along the isotherm at DCP found to be $\gamma = 1.55 \pm 0.15$.

Order-Disorder Transition: above $\Phi = 13\%$

Above $\Phi = 13\%$ the ternary blend shows a first order disorder-order transition. The indication of the ordering transition is the second order peak at $Q = 2Q^*$ and the jump of the susceptibility.

Between $\Phi = 7\%$ and 13% a microemulsion phase is located; no indications of a two-phase regime are found, as the blend was optically transparent.

At the point where the two Lifshitz lines touches ($\Phi = 8.8\%$ and $T = 70^\circ\text{C}$) the peak position is at zero. A decrease or an increase of the temperature leads to a move of Q^* . At this point the disorder-microemulsion boundary is crossed. On the right side of the LL the disorder-bicontinuous boundary is depicted at points where Q^* vs T has a minimum. This boundary also seems to be the homopolymer-homopolymer Lifshitz line. On the left from LL the disorder-bicontinuous boundary is depicted in the phase diagram at points where the susceptibility has a maximum. Therefore the disorder-bicontinuous boundary on the left side of LL connects the double critical point and the Lifshitz meeting point.

The lower critical solution temperature represents an entropy driven phase separation process. Film contrast measurements have shown a continuous increase of copolymer content at the homopolymer-homopolymer interface with a decrease of temperature. Some diblock copolymers are randomly distributed in volume and another part at the homopolymer-homopolymer interface. The relation between “bulk” and “film” block copolymers seems to be a crucial parameter or characteristic in the phase behavior near the Lifshitz line.

The enthalpic and entropic terms of the FH-parameter demonstrate similar concentration dependence. Within the Ising universality class ($\Phi < 5\%$) the enthalpic and entropic terms of the FH-parameter are nearly constant. Above 13% they slowly increase. Within the microemulsion channel the enthalpic and entropic terms of the FH-parameter sharply decrease by a factor of two. The apparent differences of the FH-parameter of binary polymer blends and the corresponding diblock copolymers have been discussed in Refs. [71, 82, 84]. The conclusion of Refs. [71, 84, 18] was that the absolute values of the FH-parameters are always smaller in diblock copolymers which is consistent with the data of the present work.

The values for the segment length are plotted in Fig. 5.1 for the 13% sample. At high temperature the statistical segment length approaches the value given in literature for the corresponding linear polymer components. The polymers become increasingly stretched with decreasing temperature. A slight shrinkage of the chains is observed by passing the order-disorder temperature.

List of Figures

2.1	Mean field phase diagram	10
2.2	Polymer blends: Classification of phase diagrams	13
2.3	$F(x)$: Inverse form factor	20
2.4	$\Gamma_s, Q^*R_g, N\Gamma'_2(0), N\Gamma''_2(0)$ and $N\Gamma_4(0, 0)$: the concentration dependence	23
2.5	(1): 3D-numerical calculations of final configuration of bicontinuous microemulsion at $\alpha = 0.1$ [55]. (2): Transmission electron microscopy from the symmetric PE/PEP/PE-PEP blend:(a) lamellar,(b) and (c) bicontinuous microemulsion, (d) a two-phase state	26
2.6	(a): Phase prism for a three-component system. (b): “Fish-cut” isopleth for water-oil microemulsion. (c): “Fish”-cut isopleth for an A/B/A-B mixture	27
3.1	Cell for SANS	32
3.2	General layout of a scattering experiment	35
3.3	Aperture configuration	38
4.1	Phase diagram	42
4.2	Concentration scaling $Q^* \sim \Phi - \Phi_{LL} ^{\beta_Q}$	43
4.3	The concentration dependence of the β_Q exponent	43
4.4	The temperature dependence of Q^* -value near the LL: 7.3%	44
4.5	The temperature dependence of Q^* -value near the LL: 7.5%	44

4.6	The temperature dependence of Q^* -value near the LL: 8%	45
4.7	The temperature dependence of Q^* -value near the LL: 9%	45
4.8	The temperature dependence of the different length scale parameters λ_{TS} , ξ_{TS} , ξ_{L_2} and ξ_{L_4} of the sample with $\phi = 6.6\%$ diblock content. Dashed lines limit the two-phase range. Lines are the disorder lines of this sample	47
4.9	Q^* -scaling vs. the reduced copolymer concentration: film, block and bulk contrasts	48
4.10	The temperature dependence of Q^* for the 8% sample in the bulk and block contrast	48
4.11	B09%: Temperature induced bicontinuous microemulsion formation. The structure factor	50
4.12	B09%: Temperature induced bicontinuous microemulsion formation. TS-analysis	51
4.13	The scattering profile of the 10% and 13% samples at $T = 40^\circ C$.	54
4.14	T=40C: Two-phase, droplet, bicontinuous, lamellar transition . .	54
4.15	The position of the maximum intensity Q^* vs. temperature: dPB-PS(\circ) and dPB-PB-dPS (\star), the filled circles (\bullet) being the twice large position of maximum of diblock copolymer (\circ) corrected to the different volume of diblock and triblock copolymers.	55
4.16	The scattering profile of the 50% sample at different temperatures. The solid lines represents a fit of the structure factor by Eq. 2.44 .	56
4.17	The susceptibility $S^{-1}(Q^*)$ and the peak position Q^* vs. inverse temperature $1/T$	56
4.18	Phase Diagram: the bulk and film contrast	57
4.19	Structure factor in Zimm representation: below LL	60

4.20	The inverse susceptibility $S^{-1}(0)$ and the correlation length ξ_{Q^2} vs. inverse temperature $1/T$ in Ising regime of the critical behavior. (a): 0% (homopolymer blend); (b): 3%; (c): 4%. Lines are fits of $S^{-1}(0)$ and ξ_{Q^2} by Belyakov-Kiselev crossover model and simple scaling law $t^{-\nu}$, respectively	61
4.21	The inverse susceptibility $S^{-1}(0)$, the correlation lengths ξ_{Q^2} and ξ_{Q^4} vs. inverse temperature $1/T$. (a): 5% ; (b): 6%; (c): 6.6%; (d) 7%.	62
4.22	The inverse susceptibility $S^{-1}(0)$ and the correlation length ξ vs. temperature T . (a): B0% (binary blend); (b): B3%. Lines are simultaneous fits of ξ and $S^{-1}(0)$ by Anisimov crossover model . . .	63
4.23	(a): The temperature dependence of the susceptibility: 3%, 6.6% and 7.5% diblock copolymer content. (b): A schematic explanation of the tangential approach to the double critical point	64
4.24	The critical exponents of the susceptibility γ and the correlation length ν	65
4.25	The scattering profile of the dPB-PB-dPS melt	68
4.26	The temperature dependence of the scattering profile for 3% of the triblock copolymers dPB-PB-dPS (film contrast)	70
4.27	The temperature dependence of the scattering profile for 7% of the triblock copolymers dPB-PB-dPS (film contrast)	70
4.28	The temperature dependence of the scattering profile for 3% of the triblock copolymers dPB-PB-dPS (film contrast)	71
4.29	Scattering profile of the 7% sample at disordered ($145^\circ C$) and droplet microemulsion ($25^\circ C$) phases Scaling of the peak position with PB-block volume fraction	71
4.30	Scaling of the peak position with PB-block volume fraction	72
5.1	Temperature dependence of the segmental length at $\Phi = 13\%$. . .	75

5.2	The inverse susceptibility $S(Q^*)$ vs. the inverse temperature: above LL	77
5.3	Q^* vs. T: 50%, 40%, 30%, 20%, 15% and 13% samples	78
5.4	The inverse susceptibility vs. inverse temperature: near LL	80
6.1	Comparison of a conventional critical point (binary system) with a double critical point (ternary system). In a binary system any approach (f.e. isochor and isotherm) to the critical point is the relevant critical path. In a ternary system with a double critical point only orthogonal direction to the Scott line is the relevant critical path. Therefore in DCP the isopleth is not relevant critical path	84
6.2	Enlarged phase diagram near the double critical point	85
6.3	The susceptibility vs. diblock content Φ . Concentration approach (isotherm) to the double critical point	85
6.4	Ginzburg number in whole concentration range	87
6.5	Enthalpic and entropic terms of the Flory-Huggins parameter vs. diblock content	89

List of Tables

2.1	Mean field definitions of characteristic points. The parameters of the second column will be defined later	6
2.2	Theoretical critical exponents near the Lifshitz critical point . . .	12
2.3	Theoretical predictions for the critical exponents: Ising [47] and mean field [20]	15
3.1	Sample characteristics: Bulk contrast	30
3.2	Sample characteristics: Film contrast	30
3.3	Investigated samples	31
3.4	Instruments details	34
3.5	The coherent and incoherent scattering lengths of some isotopes .	37
3.6	Contrast factor	37
3.7	Incoherent background	37
4.1	Fitting results of the temperature dependence of the susceptibility and correlation length in quasi-binary system (“blend-like” range of phase diagram) by Belyakov-Kiselev and Anisimov crossover function	67
4.2	Critical parameters of the isotropic Lifshitz critical range. Exponents are listed corrected to DCP	67

5.1	Parameters of the samples with diblock content less than the Lifshitz line, but above “blend-like” regime, evaluated from the susceptibility $S(0)$ using Eq. 2.51 and the BK-crossover function. The 0%, 3% and 4% samples could not be appropriately described by Eq. 2.51. $\bar{N} = 1070$ was evaluated assuming $\sigma = 6.5\text{\AA}$	75
5.2	Parameters of approximation of the susceptibility of samples above LL	76
5.3	Parameters of samples near LL	81

Bibliography

- [1] Binder K., *Adv. Polym. Sci.* **112**, 181 (1994).
- [2] D. Schwahn, K. Mortensen, and H. Yee-Madeira, *Phys. Rev. Lett.* **58**, 1544 (1987).
- [3] F.S. Bates and G.H. Fredrickson, *Annual Rev. Phys. Chem.* **41**, 525 (1990).
- [4] P.G. de Gennes, *Scaling Concepts in Polymer Physics*, Cornell University Press, Ithaca, 1979 .
- [5] A. Sariban, K. Binder, and D.W. Heermann, *Phys. Rev. B* **35**, 6873 (1987).
- [6] M.Y. Belyakov and S.B. Kiselev, *Physica A* **190**, 75 (1992).
- [7] M.A. Anisimov, A.A. Povodyrev, V.D. Kulikov, and J.V. Sengers, *Phys. Rev. Lett.* **75**, 3146 (1995).
- [8] H. Frielinghaus, D. Schwahn, J. Dudowicz, K.F. Freed, and K.W. Foreman, *J. Chem. Phys.* **114**, 5016 (2001).
- [9] D. Schwahn, H. Frielinghaus, and L. Willner, *J. Chem. Phys.* **116**, 2229 (2002).
- [10] H. Frielinghaus, D. Schwahn, L. Willner, and K.F. Freed, *J. Chem. Phys.* **116**, 2241 (2002).
- [11] L. Leibler, *Macromolecules* **13**, 1602 (1980).

- [12] G.H. Fredrickson and E. Helfand, *J. Chem. Phys.* **87**, 697 (1987).
- [13] M. E. Fisher, *Phys. Rev.* **176**, 257 (1968).
- [14] M. E. Fisher and P. E. Scesney, *Phys. Rev. A* **2**, 825 (1970).
- [15] R. Holyst and M. Schick, *J. Chem. Phys.* **96**, 7728 (1992).
- [16] F.S. Bates, W. Maurer, T.P. Lodge, M.F. Schulz, M.W. Matsen, K. Almdal, and K. Mortensen, *Phys. Rev. Lett.* **75**, 4429 (1995).
- [17] D. Schwahn, K. Mortensen, H. Frielinghaus, and K. Almdal, *Phys. Rev. Lett.* **82**, 5056 (1999).
- [18] D. Schwahn, K. Mortensen, H. Frielinghaus, K. Almdal, and L. Kielhorn, *J. Chem. Phys.* **112**, (2000).
- [19] F.S. Bates, W.W. Maurer, P.M. Lipic, M.A. Hillmyer, K. Almdal, K. Mortensen, G.H. Frederickson, and T.P. Lodge, *Phys. Rev. Lett.* **79**, 849 (1997).
- [20] L. D. Landau and E. M. Lifshits, *Statistical physics*, Nauka, Moscow, 1976 .
- [21] W. Selke, in *Phase Transitions and Critical Phenomena*, edited by C. Domb and J. L. Lebowitz, Academic, New York, 1992 .
- [22] Y. Shapira, C.C. Becerra, Jr. Oliveira, N.F., and T.S. Chang, *Phys. Rev. B* **24**, 2780 (1981).
- [23] C.C. Becerra, Y. Shapira, Jr. Oliveira, N.F., and T.S. Chang, *Phys. Rev. Lett.* **44**, 1692 (1980).
- [24] R.M. Hornreich, M. Luban, and S. Shtrikman, *Phys. Lett. A* **55A**, 269 (1975).
- [25] J.H. Chen and T.C. Lubensky, *Phys. Rev. A* **14**, 1202 (1976).

- [26] V. Borue and I. Ya. Erukhimovich, *Macromolecules* **21**, 3240 (1988).
- [27] J.F. Joanny and L. Leibler, *J. de Physique* **51**, 545 (1990).
- [28] G. Gompper and M. Schick, *Self-Assembling Amphiphilic System*, Academic Press, London, New York, 1994 .
- [29] G.H. Fredrickson and S.T. Milner, *Phys. Rev. Lett.* **67**, 835 (1991).
- [30] A.V. Dobrynin and L. Leibler, *Europhys. Lett.* **36**, 283 (1996).
- [31] D. Broseta and G.H. Fredrickson, *J. Chem. Phys.* **93**, 2927 (1990).
- [32] A. Kudlay and S. Stepanow, *Macromol. Theory Simul.* **11**, 16 (2002).
- [33] M. Teubner and R. Strey, *J. Chem. Phys.* **87**, 3195 (1987).
- [34] S.-H. Chen, S.L. Chang, R. Strey, J. Samseth, and K. Mortensen, *J. Phys. Chem* **98**, 7427 (1991).
- [35] K.-V. Schubert and R. Strey, *J. Chem. Phys.* **95**, 8532 (1991).
- [36] K.-V. Schubert, R. Strey, S.R. Kline, and E.W. Kaler, *J. Chem. Phys.* **101**, 5343 (1994).
- [37] R.D. Koehler, K.-V. Schubert, R. Strey, S.R. Kline, and E.W. Kaler, *J. Chem. Phys.* **101**, 10843 (1994).
- [38] J.F. Nicoll, G.F. Tuthill, T.S. Chang, and H.E. Stanley, *Phys. Lett. A* **58**, 1 (1976).
- [39] J.F. Nicoll, G.F. Tuthill, T.S. Chang, and H.E. Stanley, *Phys. B* **88**, 618 (1977).
- [40] M.L. Huggins, *J. Chem. Phys.* **9**, 440 (1941).
- [41] P.J. Flory, *J. Chem. Phys.* **9**, 660 (1941).

- [42] R.L. Scott, *J. Polym. Phys.* **9**, 423 (1952).
- [43] J.S. Higgins and H. Benoit, *Polymers and Neutron Scattering*, Oxford University Press, New York, 1994 .
- [44] J.V. Sengers, in *Supercritical Fluids: Fundamentals for Application*, edited by E.Kiran and J.M.H.Levelt Sengers, Kluwer Academic, Dordrecht, 1994 .
- [45] D.R. Paul and S. Newman, *Polymer Blends*, Academic Press, Amsterdam, 1979 , Part. 1 and 2.
- [46] L.A. Utracki, *Polymer Alloys and Blends: Thermodynamics and Rheology*, Hanser, Munich, Viena, New York, 1989 .
- [47] R. Guida and J. Zinn-Justin, *J. Phys. A* **31**, 8103 (1993).
- [48] S. Janssen, D. Schwahn, and T. Springer, *Phys. Rev. Lett.* **68**, 3180 (1992).
- [49] G. Meier, D. Schwahn, K. Mortensen, and S. Janssen, *Europhys. Lett.* **22**, 577 (1993).
- [50] D. Schwahn, K. Mortensen, and S. Janssen, *Phys. Rev. Lett.* **73**, 1452 (1994).
- [51] D. Schwahn, G. Meier, K. Mortensen, and S. Janssen, *J. de Physique II* **4**, 837 (1994).
- [52] D. I. Uzunov, *Theory of Critical Phenomena*, World Scientific, Singapore, 1993 .
- [53] Helfand E. and Wasserman Z.R., *Developments in Block Copolymers*, Elsevier, London, 1982 .
- [54] L. Kielhorn and M. Muthukumar, *J. Chem. Phys.* **107**, 5588 (1997).
- [55] S. Komura, H. Kodama, and K. Tamura, *J. Chem. Phys* **117**, 9903 (2002).

- [56] M.A. Hillmyer, W.W. Maurer, T.P. Lodge, F.S. Bates, and K. Almdal, *J. Phys. Chem. B* **103**, 4814 (1999).
- [57] T.L. Morkved, P. Stepanek, K. Krishnan, F.S. Bates, and T.P. Lodge, *J. Chem. Phys.* **114**, 7247 (2001).
- [58] K. Krishnan, K. Almdal, W.R. Burghardt, T.P. Lodge, and F.S. Bates, *Phys. Rev. Lett.* **87**, 098301 (2001).
- [59] F.E. Caputo, W.R. Burghardt, K. Krishnan, F.S. Bates, and T.P. Lodge, *Phys. Rev. E* **66**, 41401 (2002).
- [60] M.W. Matsen, *J. Chem. Phys.* **110**, 4658 (1999).
- [61] R.B. Thompson and M.W. Matsen, *Phys. Rev. Lett.* **85**, 670 (2000).
- [62] M. Morton and L.J. Fetters, *Rubber Chem. Technol.* **48**, 359 (1975).
- [63] M. Morton, *Anionic Polymerization: Principles and Practice*, Academic press, New York, London, 1983 .
- [64] L.J. Fetters, N. Hadjichristidis, J.S. Lindner, and J.W. Mays, *Phys. Chem. Ref. Data* **23**, 619 (1994).
- [65] H. Frielinghaus, PhD thesis, Aachen, 1999.
- [66] *Neutronenstreuexperimente am FRJ-2 in Jülich*, Institut für Festkörperforschung, Forschungszentrum Jülich GmbH.
- [67] J.S. Pedersen, *J. Phys. IV* **3**, 491 (1993).
- [68] J.G. Barker and J.S. Pedersen, *J. App. Cryst.* **28**, 105 (1995).
- [69] J.S. Pedersen, D. Posselt, and K. Mortensen, *J. App. Cryst.* **29**, 321 (1996).
- [70] S.A. Brazovskii, *Sov. Phys. JETP* **41**, 85 (1975).

- [71] H. Frielinghaus, B. Abbas, D. Schwahn, and L. Willner, *Europhys. Lett.* **44**, 606 (1998).
- [72] D. Schwahn, H. Frielinghaus, K. Mortensen, and K. Almdal, Pressure dependence of the order-disorder transition in several diblock copolymers studied with SANS, 1997.
- [73] B. Abbas, PhD thesis, Münster, 2000.
- [74] L. Kielhorn and M. Muthukumar, *J. Chem. Phys.* **111**, 2259 (1999).
- [75] R. Johnston, N. Clark, P. Wiltzius, and D. Cannell, *Phys. Rev. Lett.* **54**, 49 (1985).
- [76] B.V. Prafulla, T. Narayanan, and A. Kumar, *Phys. Rev. A* **46**, 7456 (1992).
- [77] R. Goldstein and J. Walker, *J. Chem. Phys.* **78**, 1492 (1983).
- [78] S. Deerenberg, J.A. Schouten, and N.J. Trappeniers, *Physica* **103**, 183 (1980).
- [79] G. A. Larsen and C. M. Sorensen, *Phys. Rev. Lett.* **54**, 343 (1985).
- [80] R.J.Tufeu, P.H. Keyes, and W.B. Daniels, *Phys. Rev. Lett.* **35**, 1004 (1975).
- [81] C. M. Sorensen and G. A. Larsen, *J. Chem. Phys.* **83**, 1835 (1985).
- [82] J. Dudowicz and K. F. Freed, *Macromolecules* **26**, 213 (1993).
- [83] K.-V. Schubert, R. Strey, S.R. Kline, and E.W. Kaler, *J. Chem. Phys.* **101**, 5343 (1994).
- [84] W.W. Maurer, F.S. Bates, T.P. Lodge, K. Almdal, K. Mortensen, and G.H. Fredrickson, *J. Chem. Phys.* **108**, 2989 (1998).

Acknowledgments

I would like to thank Prof. Dr. Dieter Richter for giving me possibility to work at Institut für Festkörperforschung of Forschungszentrum Jülich.

I am grateful to Dr. Dietmar Schwahn, whom I worked more closely with. I profited strongly from his supervision and his knowledge and experience in the field of critical phenomena, polymers and neutron scattering. His contribution to this work cannot be appreciated highly enough.

I would like to thank Dr. L. Willner for the polymers synthesis and the general assistance of the samples preparation.

I am grateful to Dr. Hitoshi Endo for illuminating discussions.

I would like to thank Dr. Manfred Heiderich for technical support at the SANS spectrometers during measurements.

I would like to thank Dr. Basil Abbas for his help and support at the first stage of my stay in Institut für Festkörperforschung.

A lot of thanks to Reidar Lund for the help in the final stage of the writing of this manuscript.

Last, but not least, I thank my Family: my wife and my children; for strong support and for them patience of my long absence.

Lebenslauf

Vitaliy Pipich,

geboren am 1. April 1975 in Chmelnytskyi, Ukraine;

verheiratet, 2 Kinder;

Vater: Anatoliy D. Pipich;

Mutter: Kateryna S. Pipich, geb.Iwanischina.

Schulbildung: 09/1982 - 07/1992 Mittelschule für Allgemeinbildungs №4
der Stadt Chmelnytskyi.

Hochschulreife: 7/1992 Abitur.

Studium: 09/1992 - 07/1997 Studium der Physik an der
Schewtschenko-Universität in Kiew, Ukraine.

Diplomarbeit: 09/1996 - 07/1997 Thema: "Influence of ionic impurities on the
critical anomaly of the shear viscosity near lower critical solution
point";
Schewtschenko-Universität in Kiew.

Prüfungen: 30/06/1997 Diplom im Fach Physik an der
Schewtschenko-Universität in Kiew.

Promotionsstudium: seit 10/2002 an der Westfälischen Wilhelms-Universität Münster.

Dissertation: seit dem 01/05/2000 am Institut für Festkörperforschung,
Forschungszentrum Jülich;
Betreuer: Prof. Dr. Dieter Richter;
Mitbetreuer: Dr. Dietmar Schwahn.

Jülich, 10. October 2003

